

# NORTHWEST GEOLOGY

Volume 31, 2002

A Journal Serving the Northern Rocky Mountain Region

Published by the Department of Earth Sciences  
Montana State University, Bozeman, MT 59717

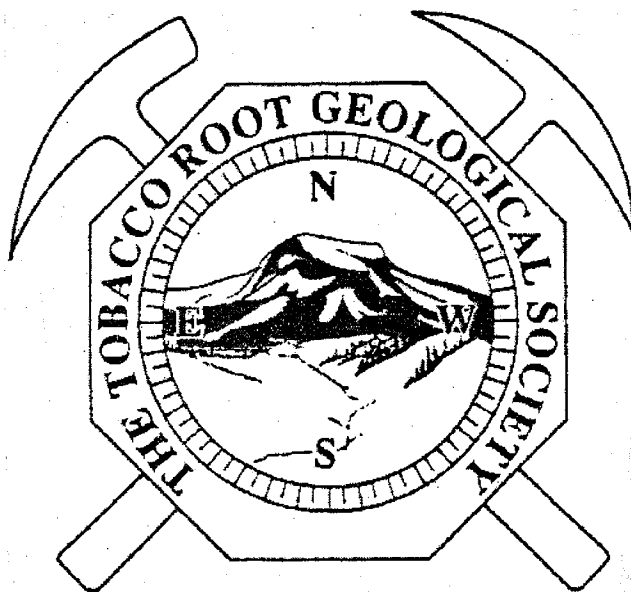


Editor: David R. Lageson  
Assistant Editor: Vickie Perryman



# The Tobacco Root Geological Society, Inc.

P.O. Box 2734  
Missoula MT 59806



## Officers

President: Larry Smith, Butte, Montana, lsmith@mtech.edu  
Vice President: Phyllis Hargrave, Butte, Montana, PHargrave@mtech.edu  
Secretary/Treasurer: George Furniss, Butte, Montana, gfurniss@state.mt.us  
Corresponding Secretary: Ann Marie Gooden, Bozeman, Montana, agooden@libby.org

## Directors

Dean Kleinkopf  
Marie Marshall Garsjo  
Bruce Cox  
Dick Gibson  
Rob Thomas

## Conference Organizers

Larry Smith  
Dave Lageson  
Ann Marie Gooden

# Northwest Geology Volume 31

Tobacco Root Geological Society  
27th Annual TRGS Field Conference

*Virginia City Here We Come!*

Virginia City, Montana  
Elks Lodge  
August 15-18, 2002

## CONFERENCE SCHEDULE

August 15:	Officers and Board Members Meeting Registration and Social hour Poster Presentations on display
August 16:	Oral Presentations (am) Poster Presentations on display Field Trips (Afternoon) Barbeque at Brewery Park
August 17-18:	All - Day Field Trips

Cover: TRGS Logo (or location of photo and who submitted it)

Northwest Geology  
v. 31

ISSN: 0096-7769

© Tobacco Root Geological Society Inc.  
P.O. Box 2734  
Missoula, Montana 59806  
<http://trgs.org>

First printing: August 2002  
Second printing: December 2006

---

Cover: Virginia City, Montana. Photo by David R. Lageson (Summer, 2002)

# U-Pb Zircon Geochronology of the Eastern Pioneer Igneous Complex, SW Montana: Magmatism in the Foreland of the Cordilleran Fold and Thrust Belt

Julia G. Murphy<sup>a\*</sup>, David A. Foster<sup>a</sup>, Thomas J. Kalakay<sup>b</sup>, Barbara E. John<sup>c</sup>, and Michael Hamilton<sup>d</sup>

<sup>a</sup>Department of Geological Sciences, PO Box 112120, University of Florida, Gainesville, Florida 32611

\*now at: Department of Geophysical Sciences, The University of Chicago, 5730 S. Ellis Ave., Chicago, IL 60637

<sup>b</sup>Department of Earth Sciences, Montana State University, Bozeman, Montana 59717-2470

<sup>c</sup>Department of Geology and Geophysics, University of Wyoming, Laramie, WY 82071-3006

<sup>d</sup>Geological Survey Canada, 601 Booth St., Room 689, Ottawa, Ont., Canada K1A 0EA

## INTRODUCTION

The presence of magma within an actively deforming orogenic belt has the potential to alter the thermal and mechanical properties of the lithosphere, as well as effect the gravitational stability of an orogenic wedge or plateau (for example, Armstrong and Ward, 1991; Nelson et al., 1996; Crawford et al., 1999; Vanderhaeghe and Teyssier, 2001; Foster et al., 2001; Kalakay et al., 2001; Lageson et al., 2001). The effects of magmatism spatially and temporally associated with deformation in extensional settings (e.g., Armstrong and Ward, 1991; Gans et al., 1989; Hutton, 1998) and in transpressional settings (e.g., Druget and Hutton, 1998; Crawford et al. 1999) are relatively well documented. However, the role that magmatism plays in contractional settings when magma is present in the crust has been more elusive (e.g., Hyndman et al., 1988; Lageson et al., 2001). It can be difficult to temporally constrain episodes of magmatic activity and the ages of associated thrusting because it is rare to find shortening structures and magmatic intrusions exposed over a sufficiently large area so that both may be independently dated. This is because in most orogenic belts magmatism is concentrated in the hinterland while thrust and fold structures that can be accurately dated are most common in the foreland.

This paper is focused on the timing of emplacement of the Pioneer igneous complex (Figure 1), which intruded the Cordilleran foreland fold and thrust belt in southwest Montana (Snee, 1982; Zen, 1988). In this unique area there is a close spatial relationship between epizonal plutons and contractional structures (Hyndman et al., 1988; Sears et al., 1988; Kalakay, 2001; Kalakay et al., 2001). Late Cretaceous-Paleocene deformation in this region is typical of the thin-skinned, Sevier-style fold and thrust belt. Magmatism is broadly contemporaneous with the latest stages of thrusting in SW Montana, based on the presence of andesitic and rhyolitic volcanic rocks interstratified with syntectonic gravels (Snee, 1982; Johnson and Sears, 1988; Kalakay et al., 2000; Kalakay, 2001), magmatic foliation in the plutons, and locally deformed contact metamorphic assemblages (Kalakay, 2001; Kalakay et al., 2000, 2001). Many of the intrusions were emplaced at the tops of thrust ramps and along thrusts and do not show post-crystallization deformation so they are relatively late in the shortening history (Kalakay, 2001; Kalakay et al., 2000; 2001).

We report herein, preliminary U-Pb zircon ages for selected rocks within the Pioneer intrusive complex. Our data complement previous geochronological constraints on these rocks from K-Ar and Ar-Ar studies. The magmatic ages obtained in this study provide information on the timing and duration of plutonism and volcanism in the eastern Pioneer

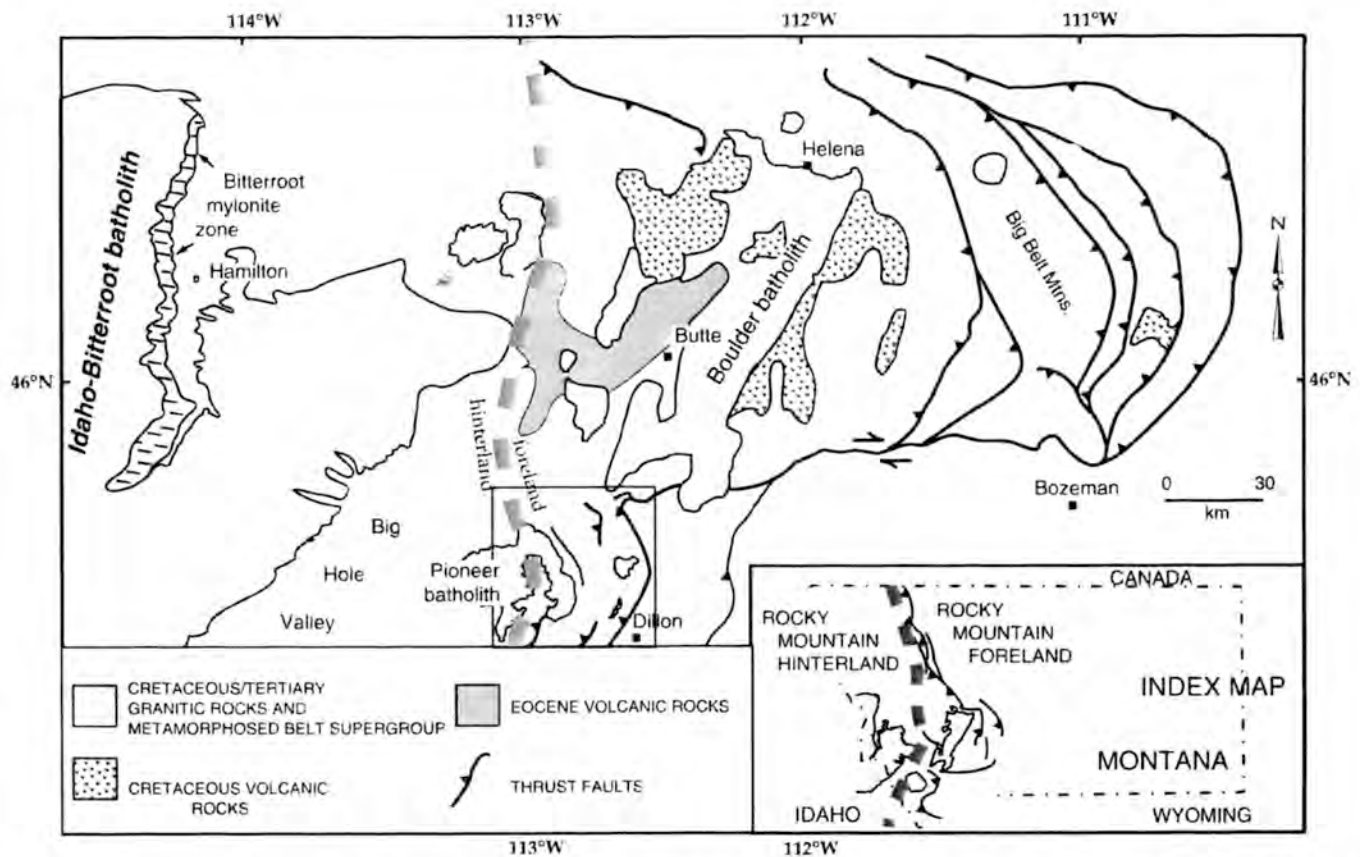


Figure 1. Tectonic elements map of southwest Montana with Late Cretaceous-Eocene plutons and major thrusts. Modified from Kalakay et al., 2000.

igneous complex. Additional information from analyses of premagmatic zircons provides constraints on the age of the source rocks beneath the batholith.

### Pioneer Igneous Complex

The calc-alkaline Pioneer igneous complex (Figure 2), consisting of the Pioneer batholith and the McCartney Mountain, Bighole Canyon, and Bannack plutons (Snee, 1982; Zen, 1988; 1996). The Pioneer batholith is exposed over an area of ~800 km<sup>2</sup>, and has been divided by Zen (1988) into five major intrusive phases. The plutons vary in composition as a function of cooling age from hornblende gabbro (~80 Ma), to hornblende-biotite quartz diorite (~76 Ma), to hornblende-biotite tonalite (~74 Ma), to biotite-hornblende granodiorite and biotite granite (~72 Ma), and biotite granodiorite and 2-mica granite (~67-65 Ma) (Snee, 1982; Marvin and others, 1983; Zen, 1988). Snee (1982) showed that most of the Ar-Ar and K-Ar dates from

the Pioneer batholith were cooling ages, especially those from the deeper western part of the batholith. Accurate emplacement ages, therefore, do not exist for all of these plutons, and will best be determined from U-Pb zircon studies. The largest pluton, the Uphill Creek granodiorite, makes up over 75% of the exposed batholith and is considered to have been emplaced ~75 Ma based on projecting the rate of cooling through hornblende and biotite Ar-Ar ages (Snee, 1982). The Pioneer igneous complex intrudes sedimentary rocks as old as the Proterozoic Belt Supergroup in the west, and as young as the Late Cretaceous Colorado Group in the east.

The relationships between magmatism and thrust faults are best displayed along the margins of the Pioneer igneous complex where the intrusions are smaller in size. To the south of the Pioneer batholith fine-grained granodiorite dikes, sills, and stocks in the Bannack area (Figure 2) intrude deformed Paleozoic strata along thrust ramps and flats beneath and within the Ermont thrust (e.g., Kalakay et al.,

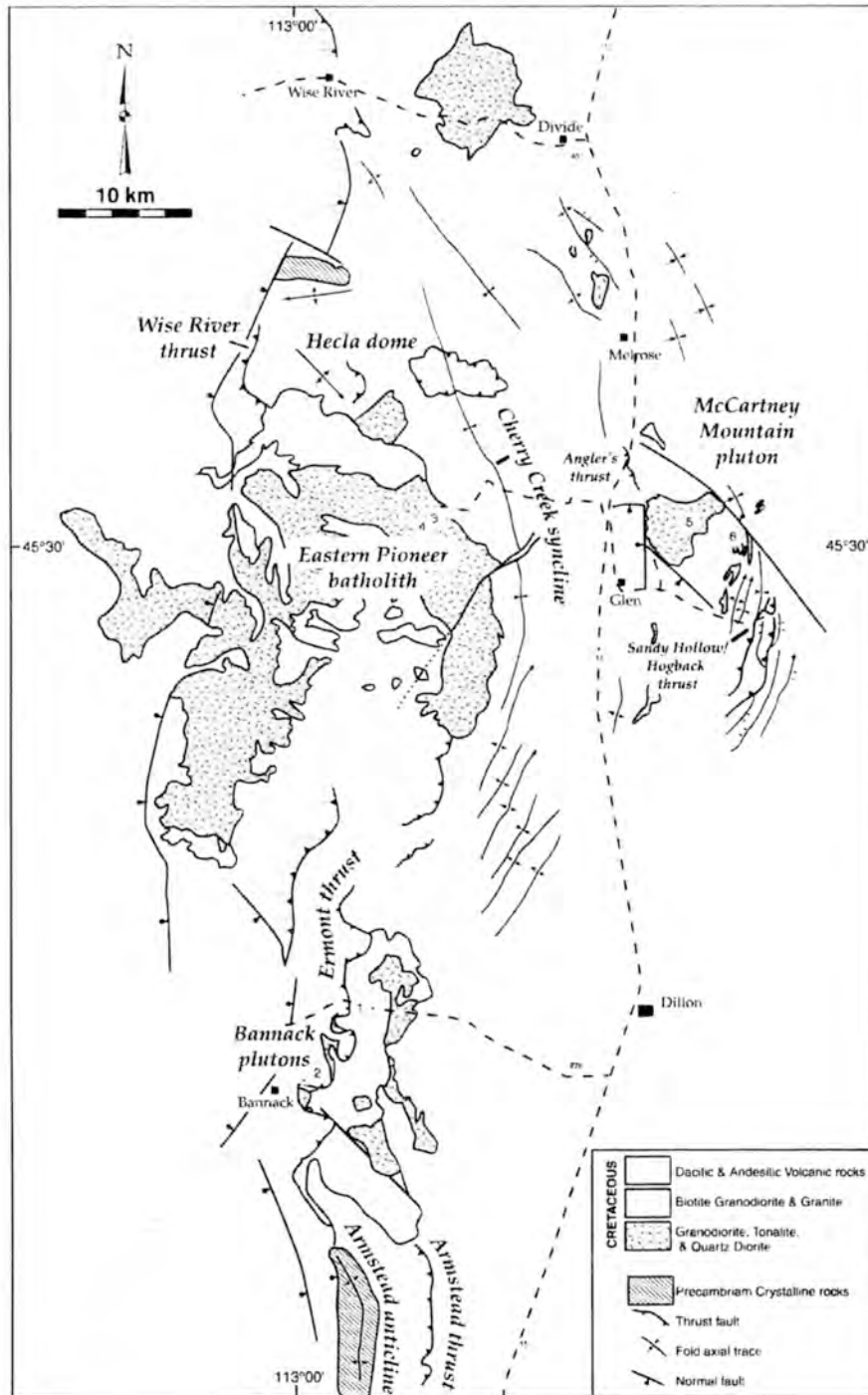


Figure 2. Generalized geologic map of the eastern Pioneer batholith and the McCartney Mountain thrust salient. Horizontal line pattern denotes the eastern boundary of allochthonous Middle Proterozoic Belt sedimentary rocks. Sample locations: DF98-067 is from location 1; DF98-069 and DF98-070 are from location 2; DF 98-071 is from location 6; DF98-072 is from location 5; DF98-074 is from location 3; and DF98-076 is from location 4. From Kalakay et al., 2000.

2001). Cretaceous rhyolite and andesite also associated with the Pioneer complex overlie the deformed Paleozoic and Mesozoic strata at Bannack. The two larger granodiorite plutons in this area are the Anniversary stock and Bannack stock. The McCartney Mountain stock and a swarm of associated sills define the easternmost boundary of the Pioneer igneous complex (Figure 2). Kalakay (2001) identified a magmatic foliation that is axial planar to folds in country rock, suggesting that the pluton was emplaced, at least in part, synkinematically.

### U-Pb Analysis

U-Pb analyses of individual zircon grains were performed with a Sensitive High Resolution Ion Microprobe (SHRIMP-II) at the Geological Survey of Canada (Williams, 1998; Stern, 1997). Single-grain, spot analyses were performed because of the large fraction of premagmatic zircon in these rocks. With SHRIMP-II ~20-30 micron spots were targeted on the magmatic rims of zircon crystals. A summary table of the results for the magmatic zircons from each sample is given in Table 1. Complete analytical data are tabulated in Murphy (2000) and can also be obtained from the authors. A concordia plot of the premagmatic zircon data is given in Figure 3. It should be noted that the crystallization ages for most of the samples should be treated as preliminary because more grains should be analyzed to improve the statistical calculations of the data. It is unlikely that with more data the crystallization ages will change beyond the two-sigma error limits quoted in Table 1, but the uncertainties would be reduced. Enough magmatic grains were analyzed from sample 98-074 to give a precise crystallization age for the Uphill Creek granodiorite (Figure 4).

We analyzed zircons from seven samples, five of which are intrusive and two are volcanic rocks. The two volcanic rocks are from syntectonic Beaverhead Group the Bannack area (Figure 2). One sample is from an andesite at the base of the Grasshopper Creek growth syncline, which is related to the Madigan Gulch anticline, and the other a rhyolite from the Grasshopper Creek tuff (see Johnson and Sears, 1988; Kalakay, 2001; Kalakay et al., 2000, 2001). The third sample from the Bannack area is a granodiorite from the Anniversary stock. Two

samples are from the McCartney Mountain area: one a granodiorite from the McCartney Mountain stock, and the other from a granodiorite sill east of the stock. The remaining two samples are from the Uphill Creek granodiorite and Grayling Lake granite plutons of the Pioneer batholith.

The  $^{206}\text{Pb}/^{238}\text{U}$  ages of magmatic zircons range from 75 +/- 1 Ma to 72.2 +/- 0.6 Ma, except for the andesite, which gave a preliminary age of 77.1 +/- 8.1 Ma from only three analyses (Table 1). The Grasshopper Creek tuff and two samples from the McCartney Mountain plutons gave ages of about 75 Ma with errors of 1 or 2 Ma. The Anniversary stock gave an age of 73.4 +/- 1.3 Ma. These last three ages are based on four grains each and more analyses will reduce the errors. Finally, the two Pioneer batholith samples gave ages of 72.2 +/- 0.6 Ma and 72.2 +/- 1.7 Ma for the Uphill Creek and Grayling Lake plutons, respectively.

Nine premagmatic zircon grains gave relatively well defined  $^{207}\text{Pb}/^{206}\text{Pb}$  ages (Table 2; Figure 3). Three of the grains gave ages of about 1690 to 1760 Ma. One grain each gave concordant ages of about 1890 and 1469 Ma, and two other grains gave discordant ages of ~2647 and ~418 Ma.

## DISCUSSION AND CONCLUSIONS

### Chronology of Magmatism and Thrusting

These data indicate that 1) the satellite plutons in the McCartney Mountain stock and the Grasshopper Creek crystallized within error of 75 Ma, 2) the main mass of the Pioneer batholith crystallized at about 72 Ma, and 3) the Anniversary stock was emplaced within error of both of the other groups of dates. These U-Pb data suggest that the greatest volume of the Pioneer igneous complex was emplaced within about 2-6 million years. The phases of the complex sampled in this study include two of the most voluminous phases of the batholith, but do not include any of the earliest or latest phases (such as the early hornblende gabbro or late stage pegmatite). The Ar-Ar data suggests that the total span of intrusion ages is closer to 10 million years or more (Snee, 1982). Clearly a more comprehensive U-Pb zircon study would be helpful for constraining the full duration of emplacement for the entire complex.



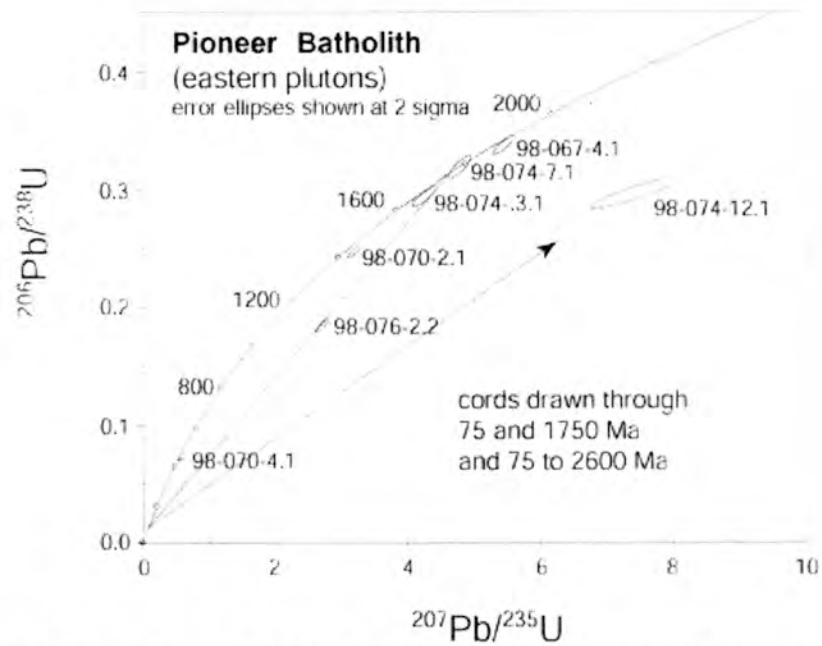


Figure 3. Concordia diagram showing the U-Pb data from premagmatic zircons.

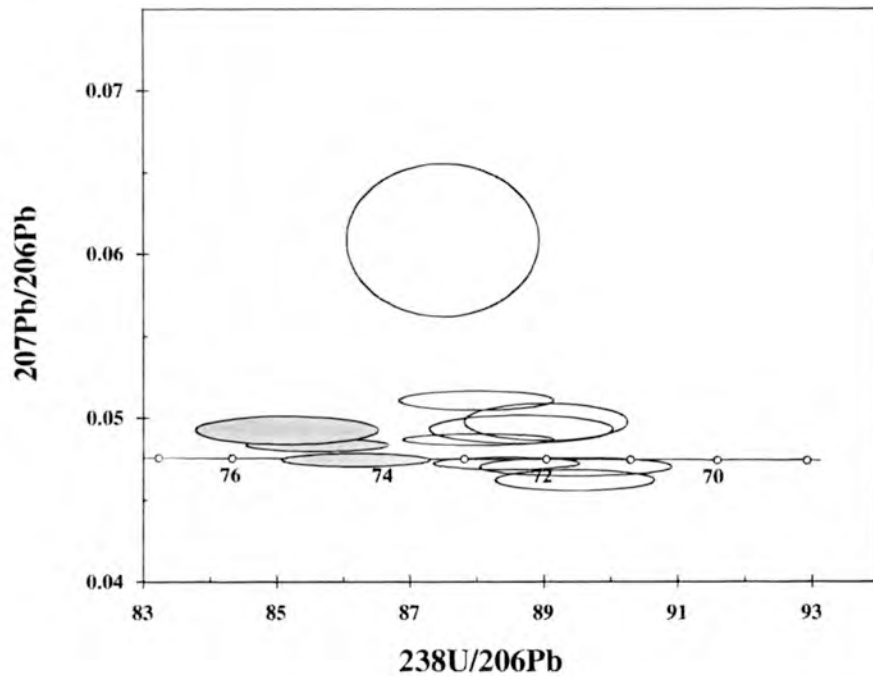


Figure 4. Tera-Wasserburg concordia plot for magmatic zircon from sample DF98-074 from the Uphill Creek granodiorite. The open ellipses are interpreted to be the magmatic population and the shaded ellipses are zircon inherited from earlier Pioneer batholith magmas.

Table 1. Summary of U-Pb zircon data from the Pioneer igneous complex. U-Pb crystallization ages are weighted mean  $^{206}\text{Pb}/^{238}\text{U}$  ages. Raw data and sample details are in Murphy (2000).

Sample	Unit and Location	Rock Type	$^{206}\text{Pb}/^{238}\text{U}$ Age (Ma)	+/- 2 $\sigma$	No. of analyses
DF98-067	Grasshopper Creek tuff, Bannack	Rhyolite tuff	75.1	1.1	7
DF98-069	Anniversary stock, Bannack	Granodiorite	73.42	1.3	4
DF98-070	Lower Beaverhead andesite, Bannack	Andesite tuff	77.1	8.1	3
DF98-071	McCartney Mountain sill	Micro- granodiorite	75	1.4	4
DF98-072	McCartney Mountain stock	Granodiorite	75.5	2.2	4
DF98-074	Uphill Creek granodiorite, Pioneer batholith	Granodiorite	72.20	0.57	8
DF98-076	Grayling Lake granite, Pioneer batholith	Granite	72.17	1.7	5

Table 2. Summary of premagmatic U-Pb zircon ages. Asterisk (\*) indicates concordant age.

Sample-Grain.Spot	$^{207}\text{Pb}/^{206}\text{Pb}$ Age (Ma)	+/- 1 $\sigma$
DF98-067-4.1	1890.6*	13.1
DF98-070-2.1	1469.1*	10.1
DF98-071-4.1	417.5	15.3
DF98-074-3.1	1689.9*	17.0
DF98-074-7.1	1760.4*	12.6
DF98-074-12.1	2647.4	48.2
DF98-076-2.2	1715.1	6.7

The results from the Bannack area have implications for the timing of thrusting in the Armstead-Bannack area. The age of the Grasshopper Creek growth syncline is constrained by dating the Grasshopper Creek rhyolite tuff and the lower Beaverhead andesite tuff, which together form upper and lower stratigraphic bounding units within the growth structure. The difference between zircon ages for the lower Beaverhead andesite and Grasshopper Creek rhyolite spans a period of 0 to 12 million years, if errors are applied to minimize or maximize their age difference. This time period encompasses the entire rotational and depositional history for the Grasshopper Creek growth syncline, so that an important constrain on the slip rate of the Madigan Gulch thrust will be determined when more analyses are completed on the andesite to reduce the errors (see Kalakay, 2001).

Further refinements on the age of the Ermont thrust have been made by the date of the Anniversary stock, which intruded the thrust. The stock contains a well-developed high-temperature magmatic foliation. However, where the pluton margin intersects contractional faults there is no evidence of solid-state deformation. The field relationships indicate that magmatic emplacement was either synchronous with final stages of thrusting or that it post-dated thrusting altogether (Kalakay, 2001; Kalakay et al., 2000, 2001). The U-Pb zircon age of 73.4 +/- 0.82 Ma from Anniversary stock places a lower age limit on the time of thrusting. There is an overlap in age of the Grasshopper Creek tuff and Anniversary stock if errors are applied to minimize their difference. However, the Ermont thrust cuts the Grasshopper Creek tuff and is intruded by the Anniversary stock (Kalakay, 2001). The Ermont thrust truncates the Madigan Gulch anticline and accompanying Grasshopper Creek syncline and is therefore, younger than these structures. The late phase of thrust motion is bracketed between the ages of the Grasshopper Creek tuff (75.1 +/- 1.1 Ma) and the Anniversary stock (73.4 +/- 0.8 Ma). The McCartney Mountain stock and associated sills intruded thrusts at the eastern edge of the McCartney Mountain thrust salient (Brumbaugh and Dresser, 1976; Sears et al., 1988; Kalakay

et al., 2000). Mineral lineations within contact metamorphic rocks adjacent to the McCartney Mountain stock suggests that deformation (shortening) within the thrust salient continued during intrusion, but the lack of post-magmatic deformation within the margins of the pluton indicates that shortening ended by the time intrusion was completed. The ca. 75 Ma age for the stock, which is concordant with a previous 74 +/- 1 Ma K-Ar biotite age (Brumbaugh and Hendrix, 1981), dates the end of shortening in the thrust salient.

### **Zircon Inheritance and Age of the Basement**

Strontium and lead isotopic data from the Pioneer batholith suggest that the magmas were primarily derived from Paleoproterozoic crust. Initial Sr isotopic values for the Pioneer batholith range from 0.7110 to 0.7160 (Arth et al., 1986; Ann Heatherington, personal communication to DAF, 2000), and Pb isotopes give a model age of 1.9 +/- 0.2 Ga (Doe et al., 1968; Zen, 1992). These results can be interpreted as being derived primarily from a Proterozoic source or some mixing between partial melts of Archean crust and younger (Cretaceous) mantle derived magma. The premagmatic zircon ages indicate a significant Paleoproterozoic component in the crustal source region of the batholith. The most common age of premagmatic zircon found in this study is about 1.7 to 1.9 Ga. The concordance between the secondary isotopic model ages and the ages of the premagmatic zircons suggests that the Paleoproterozoic crust formed from the mantle during the Paleoproterozoic and is not simply reworked Archean material.

The three remaining inherited grains suggest that other components exist within the crust beneath the batholith as well. A discordant Archean grain from the Uphill Creek granodiorite could indicate that Late Archean Wyoming province crust is interleaved with the Paleoproterozoic crust. Alternatively, this zircon could have been recycled either through sedimentary or magmatic reworking of Archean crust. The ~1.47 Ga zircon is similar in age to mafic and alkaline igneous rocks that intruded the base of

the Mesoproterozoic Belt basin (e.g., Sears et al., 1998), and its presence in the andesite could either indicate that similar igneous rocks exist beneath the Pioneer batholith, or result from surface contamination of detrital zircon during eruption and deposition.

The Pioneer igneous complex lies within the Great Falls tectonic zone as defined by (O'Neil, 1998). The basement within the Great Falls tectonic zone is thought to be Paleoproterozoic in age and includes primitive rocks with ages of ~1.86 Ga that were involved in collisional orogenies between 1.8 and 1.7 Ga (O'Neil, 1998; Mueller et al., 2002). The presence of the Paleoproterozoic premagmatic zircons in the Pioneer igneous complex rocks, along with published Paleoproterozoic U-Pb zircon data from outcropping basement in the northern Pioneer Mountains, confirms that this area is northwest of the boundary between the Archean Wyoming province and accreted Proterozoic basement terranes.

The premagmatic zircon population in the Pioneer batholith differs from that in the Cretaceous Tobacco Root batholith, which intrudes Archean rocks. The Tobacco Root batholith inherited zircon population includes a large component of Archean grains with ages of 2.6 to 3.0 Ga (Mueller et al., 1996). On the other hand, the Pioneer batholith data are consistent with the ages of premagmatic zircons and Nd depleted mantle isotopic model ages in the Idaho batholith that also show that the basement west of the Wyoming province is dominated by 1.7-1.8 Ga crust (Bickford et al., 1981; Fleck, 1990; Toth and Stacey, 1992; Mueller et al., 1995; Foster and Fanning, 1997).

This Paleoproterozoic crust is similar in age and Nd isotopic composition to the Mojave province (Bennett and DePaolo, 1987) and may be part of a continuous Paleoproterozoic accretionary orogen that once existed along the western margin of the Wyoming province (e.g., Mueller et al., 1995; Bennett and DePaolo, 1987). The age and character of the Paleoproterozoic basement west and northwest of the Wyoming province also has implications for any proposed Precambrian continental reconstruction, because rocks of similar Paleoproterozoic age should exist on the

rifted edge of the continent that was once jointed to Laurentia (e.g., Moores, 1991; Hoffman, 1991; Karlstrom et al., 1999; Burrett and Berry, 2000; Brookfield, 1993; Sears and Price, 2000; Li et al., 1995; Piper, 2000; Dalziel, 1991, 1992, Ross et al., 1992; Borg and DePaolo, 1994; Powell et al., 1994; Foster and Ehlers, 1998, Googe et al., 2001

### Acknowledgments

This research was supported by a grant from the Tobacco Root Geological Society to Julia Murphy, and by grants from NASA/Wyoming Space Grant Consortium, Geological Society of America, Society of Sedimentary Geology, Colorado Scientific Society, and Tobacco Root Geological Society to Tom Kalakay.

### REFERENCES

- Armstrong, R.L., and Ward, P., 1991, Evolving geographic patterns of Cenozoic magmatism in the North American Cordillera: The temporal and spatial association of magmatism and metamorphic core complexes: *Journal of Geophysical Research*, v. 96, p. 13, 201-13, 224.
- Armstrong, R.L., Taubeneck, W.H., and Hales, P.O., 1977, Rb-Sr and K-Ar geochronometry of Mesozoic granitic rocks and their Sr isotopic composition, Oregon, Washington, and Idaho: *Geological Society of America Bulletin*, v. 88, p. 397-411.
- Arth, J.G., Zen, E., Sellers, G., and Hammarstrom, J., 1986, High initial Sr isotopic ratios and evidence for magma mixing in the Pioneer batholith of southwest Montana: *Journal of Geology*, v. 94, p. 419-439.
- Bennett, V., and DePaolo, D., 1987, Proterozoic crustal history of the western United States as determined by neodymium isotope mapping: *Geological Society of America Bulletin*, v. 99, p. 647-685.
- Bickford, M.E., Chase, R.B., Nelson, B.K., Shuster, R.D., and Arruda, E.C., 1981, U-Pb studies of zircon cores and overgrowths, and monazite: Implications for age and petrogenesis of the northeastern Idaho batholith: *Journal of Geology*, v. 89, p. 433-457.
- Brookfield, M.E., 1993, Neoproterozoic Laurentia-Australia fit: *Geology*, v. 21, p. 683-686.
- Borg, S. and DePaolo, D., 1994, Laurentia, Australia, and Antarctica as a Late Proterozoic

- supercontinent: Constraints from isotope mapping: *Geology*, v. 22, p. 307-310.
- Brumbaugh, D.S. and Dresser, H.W., 1976, Exposed step in Laramide thrust fault, southwest Montana: American Association of Petroleum Geologists Bulletin, v. 60, p. 2142-2149.
- Brumbaugh, D.S. and Hendrix, T.E., 1981, The McCartney Mountain structural salient, southwestern Montana: Montana Geological Society Field Conference and Symposium to SW Montana, p. 201-209.
- Burrett, C., and Berry, R., 2000, Proterozoic Australia-Western United States (AUSWUS) fit between Laurentia and Australia: *Geology*, v. 28, p. 103-106.
- Crawford, M.L., Klepeis, K.A., Gehrels, G., and Isachsen, C., 1999, Batholith emplacement at mid-crustal levels and its exhumation within an obliquely convergent margin: *Tectonophysics*, v. 312, p. 57-78.
- Dalziel, I.W.D., 1991, Pacific margins of Laurentia and East Antarctica-Australia as a conjugate rift pair: evidence and implications for an Eocambrian supercontinent: *Geology*, v. 19, p. 598-601.
- Dalziel, I.W.D., 1992, On the organization of American Plates in the Neoproterozoic and the Breakout of Laurentia: *GSA Today*, v. 237, p. 240-241.
- Doe, B.R., Tilling, R.I., Hedge, C.E., and Klepper, M.R., 1968, Lead and strontium isotope studies of the Boulder batholith, southwestern Montana: *Economic Geology*, v. 63, p. 884-906.
- Druguët, E. and Hutton, D.H.W., 1998, Syntectonic anatexis and magmatism in a mid-crustal transpressional shear zone: An example from the Hercynian rocks of the eastern Pyrenees: *Journal of Structural Geology*, v. 20, p. 905-916.
- Fleck, R.J., 1990, Neodymium, strontium, and trace-element evidence of crustal anatexis and magma mixing in the Idaho batholith, in Anderson, J.L., ed., *The nature and origin of Cordilleran magmatism*: Geological Society of America Memoir 174, p. 359-373.
- Foster, D.A., and Ehlers, K., 1998,  $^{40}\text{Ar}$ - $^{39}\text{Ar}$  thermochronology of the southern Gawler Craton, Australia; implications for Mesoproterozoic and Neoproterozoic tectonics of East Gondwana and Rodinia: *Journal of Geophysical Research*, v. 103, p. 10,177-10,193.
- Foster, D.A. and Fanning, C.M., 1997, Geochronology of the northern Idaho batholith and the Bitterroot metamorphic core complex: Magmatism preceding and contemporaneous with extension: *Geological Society of America Bulletin*, v. 109, p. 379-394.
- Foster, D.A., Schafer, C., Hyndman, D.W., and Fanning, C.M., 2001, Relationships between crustal partial melting, plutonism, orogeny, and exhumation: Idaho-Bitterroot batholith: *Tectonophysics*, v. 342, p. 313-350.
- Gans, P.B., Mahood, G.A., and Schermer, E., 1989, Synextensional magmatism in the Basin and Range Province; A case study from the eastern Great Basin: *Geological Society of America Special Paper* 233, 53 p.
- Googe, J.W., Fanning, C.M., Bennett, V.C., 2001, U-Pb evidence of ~1.7 Ga crustal tectonism during the Nimrod Orogeny in the Transantarctic Mountains, Antarctica: implications for Proterozoic plate reconstructions: *Precambrian Research*, v. 112, p. 261-288.
- Hoffman, P.F., 1991, Did the breakout of Laurentia turn Gondwanaland inside-out?: *Science*, v. 252, p. 1409-1412.
- Hutton, D.H.W., 1988, Granite emplacement mechanisms and tectonic controls: Inferences from deformation studies: *Transactions of the Royal Society of Edinburgh: Earth Sciences*, v. 79, p. 245-255.
- Hyndman, D.W., Alt, D., and Sears, J.W., 1988, Post-Archean metamorphic and tectonic evolution of western Montana and northern Idaho, in Ernst, W.G., (ed.), *Metamorphic and Crustal Evolution of the Western United States*, Ruby volume VII: Englewood Cliffs, NJ: Prentice Hall, p. 333-361.
- Johnson, L.M. and Sears, J.W., 1988, Cordilleran thrust belt-Rocky Mountain foreland interactions near Bannack, Montana, in Schmidt, C.J., and Perry, W.J., eds., *Interaction of the Rocky Mountain foreland and the Cordilleran thrust belt*: Geological Society of America Memoir 171, p., 229-236.
- Kalakay, T.J., 2001, The role of magmatism during crustal shortening in the retro-arc Sevier fold and thrust belt of southwest Montana: unpublished PhD dissertation, University of Wyoming, Department of Geology and Geophysics, Laramie, WY, 238 p.
- Kalakay, T.J., John, B.E., and Foster, D.A., 2000, Granite emplacement during contemporaneous thrust faulting in the Sevier fold and thrust belt of southwest Montana. in Roberts, S. and Winston, D. (eds.), *Geologic field trips, western Montana and adjacent areas: Rocky Mountain Section of the Geological Society of America*. University of Montana, Missoula, p. 157-177.
- Kalakay, T.J., John, B.E., and Lageson, R.J., 2001, Fault-controlled pluton emplacement in the Sevier fold-and-thrust belt of southwest Montana, USA, *Journal of Structural Geology*, v. 23, p. 1151-1165.

- Karlstrom, K.E., Harlan, S.S., Williams, M.L., McLelland, J., Geissman, J.W., Ahall, K-I., 1999. Refining Rodinia: Geologic evidence for the Australia-Western U.S. connection in the Proterozoic: *GSA Today*, v. 9, p. 1-7.
- Lageson, D.R., Schmitt, J.G., Kalakay, T.J., Horton, B.K., Burton, B.R., and 2001. Influence of late Cretaceous magmatism on the Sevier orogenic wedge, western Montana: *Geology*, v. 29, p. 723-726.
- Li, Z.X., Zhang, L., and Powell, C. McA., 1995. South China in Rodinia: part of the missing link between Australia-East Antarctica and Laurentia: *Geology*, v. 23, p. 407-410.
- Moore, E.M., 1991. Southwest U.S.- East Antarctic (SWEAT) connection: a hypothesis: *Geology*, v. 19, p. 425-428.
- Mueller, P.A., Wooden, J.L., Nutman, A.P., and Mogk, D.W., 1998. Early Archean crust in the northern Wyoming province; Evidence from U-Pb ages of detrital zircons: *Precambrian Research*, v. 91, n. 3-4, p. 295-307.
- Mueller, P.A., Heatherington, A.L., D'Arcy, K.A., Wooden, J.L., and Nutman, A.P., 1996. Contrasts between Sm-Nd whole-rock and U-Pb zircon systematics in the Tobacco Root batholith, Montana: Implications for the determination of crustal age provinces: *Tectonophysics*, v. 265 p. 169-179.
- Mueller, P.A., Shuster, R.D., D'Arcy, K.A., Heatherington, A.L., Nutman, A.P., and Williams, I.S., 1995. Source of the northeastern Idaho batholith: Isotopic evidence for a Paleoproterozoic terrane in the northwestern U.S.: *Journal of Geology*, v. 103, p. 63-72.
- Mueller, P., Heatherington, A., Kelley, D., Wooden, J., and Mogk, D., 2002. Paleoproterozoic crust within the Great Falls tectonic zone: Implications for the assembly of southern Laurentia: *Geology*, v. 30, p. 127-130.
- Murphy, J.G., 2000. Geochronology of Late Synkinematic Plutons in the Sevier Fold and Thrust Belt, SW Montana (M.S. thesis): University of Florida, 146 p.
- Nelson, K.D. et al., 1996. Partially molten middle crust beneath southern Tibet: synthesis of Project INDEPTH results: *Science*, v. 274, p. 1684-1688.
- O'Neill, J.M., 1998. The Great Falls tectonic zone, Montana-Idaho:-- An early Proterozoic collisional orogen beneath and south of the Belt Basin, *in* Berg, R.B., ed., *Belt Symposium III - 1993: Montana Bureau of Mines and Geology Special Publication 112*, p. 222-228.
- Piper, J., 2000. The Neoproterozoic supercontinent: Rodinia or Paleopangea?: *Earth and Planetary Science Letters*, v. 176, p. 131-146.
- Powell, C.McA., Preiss, W.V., Gatehouse, C.G., Krapez, B., and Li, Z.X., 1994. South Australia record of a Rodinian epicontinental basin and its mid-Neoproterozoic breakup (~700 Ma) to form the Palaeo-Pacific Ocean: *Tectonophysics*, v. 237, p. 113-140.
- Ross, G., Parrish, R., and Winston, D., 1992. Provenance and U-Pb geochronology of the Mesoproterozoic Belt supergroup (northwestern United States): Implications for age of deposition and pre-Panthalassa plate reconstructions: *Earth and Planetary Science Letters*, v. 113, p. 57-76.
- Sears, J.W., and Price, R.A., 2000. New look at the Siberian connection: No SWEAT: *Geology*, v. 28, p. 423-426.
- Sears, J.W., Chamberlain, K.R., and Buckley, S.N., 1998. Structural and U-Pb geochronological evidence for 1.47 Ga rifting in the Belt basin, western Montana: *Canadian Journal of Earth Sciences*, v. 35, p. 467-475.
- Sears, J.W., Johnson, L.M., Geiger, B.C., and Brandon, W.C., 1988. Southwest Montana thrust belt: Bannack to Melrose, *in* Link, P.K., and Hackett, W.R. (eds.), *Guidebook to the Rocky Mountain Thrust Belt Geology of central and southern Idaho: Idaho Geological Survey Bulletin*, v. 27, p.305-319.
- Snee, L.W., 1982. Emplacement and cooling of the Pioneer Batholith, southwestern Montana: unpublished Ph.D. dissertation, The Ohio State University, 320 p.
- Stern, R. A., 1997. The GCS Sensitive High Resolution Ion Microprobe (SHRIMP): analytical techniques of zircon U-Th-Pb age determinations and performance evaluation: *Radiogenic Age and Isotopic Studies: Report 10: Geological Survey of Canada, Current Research 1997-F*, p. 1-31.
- Toth, M.L., and Stacey, J.S., 1992. Constraints on the formation of the Bitterroot lobe of the Idaho batholith, Idaho and Montana, from U-Pb zircon geochronology and feldspar Pb isotopic data: *U. S. Geological Survey Bulletin* 2008, 14 p.
- Vanderhaeghe, O., and Teyssier, C., 2001. Partial melting and flow of orogens, *Tectonophysics*, v. 342, p. 41-472.
- Williams, I.S., 1998. U-TH-Pb geochronology by ion microprobe: *Reviews in Economic Geology*, v. 7, p. 1-35.
- Zen, E-an, 1988. Bedrock Geology of the Vipond Park 15-Minute, Stine Mountain 7 1/2-Minute, and Maurice Mountain 7 1/2-Minute Quadrangles, Pioneer Mountains, Beaverhead County, Montana: *U.S. Geological Survey Bulletin* 1625, 49 p.
- Zen, E-an, 1992. Using granite to image the thermal state of the source terrane: *Transactions of the*

Royal Society of Edinburgh, Earth Sciences, v. 8.  
p. 107-114.

Zen, E., 1996. Plutons in the eastern part of the  
Pioneer batholith: field relations and petrographic  
descriptions: U.S. Geological Survey Open-File  
Report 96-97, 62 p.

# Gold-Bearing Quartz Veins in the Virginia City Mining District, Madison County, Montana

Jane M. Hammarstrom - U.S. Geological Survey, 954 National Center, Reston, VA 20192

Bradley S. Van Gosen - U.S. Geological Survey, MS 905, Box 25046, Denver Federal Center, Denver CO 80225

Michael J. Kunk - U.S. Geological Survey, MS 963, Box 25046, Denver Federal Center, Denver CO 80225

James R. Herring - U.S. Geological Survey, MS 973, Box 25046, Denver Federal Center, Denver CO 80225

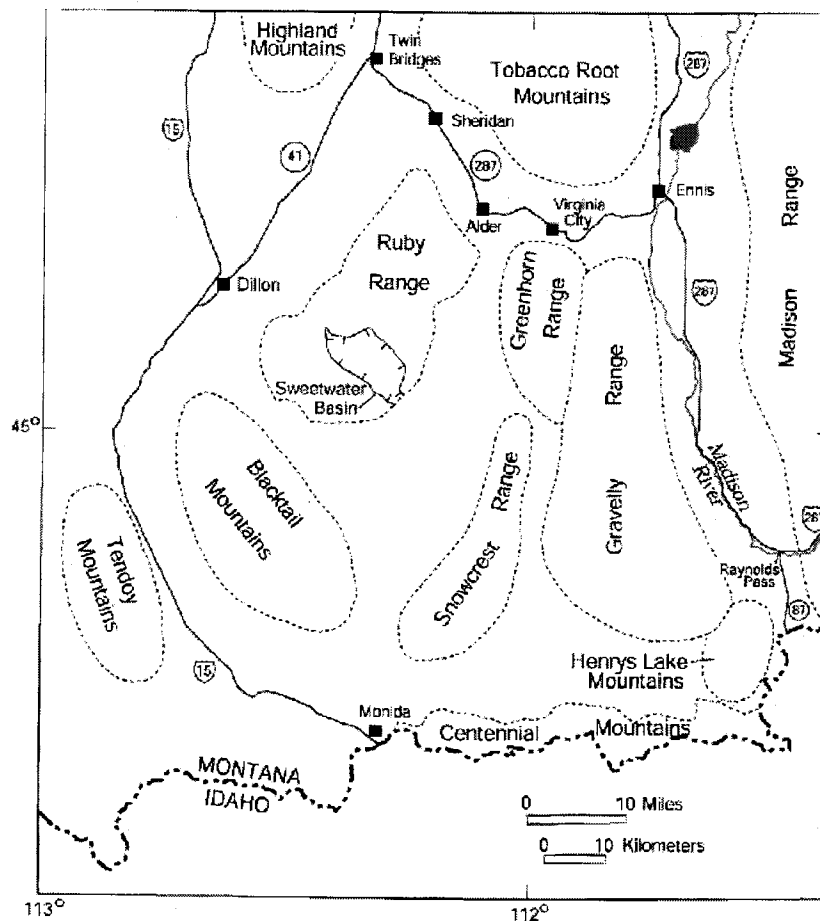


Figure 1. Location map

## INTRODUCTION

The Virginia City mining district is one of the most significant historic placer gold districts in the United States. More than 2.5 million ounces\* of gold were produced from the 1890's until the 1940's, mainly from placer workings in

Quaternary alluvial deposits along a 25-km long stretch of Alder Gulch between the towns of Alder and Virginia City in southwestern Montana (Fig. 1). The lode source of the placer gold has been the subject of considerable scientific debate for more than 100 years (Shawe and Wier, 1989; Barnard, 1993). Historic lode mines along several drainages to the south of Virginia City have been considered the most

\* Troy ounces; 1 troy ounce = 31.103 g



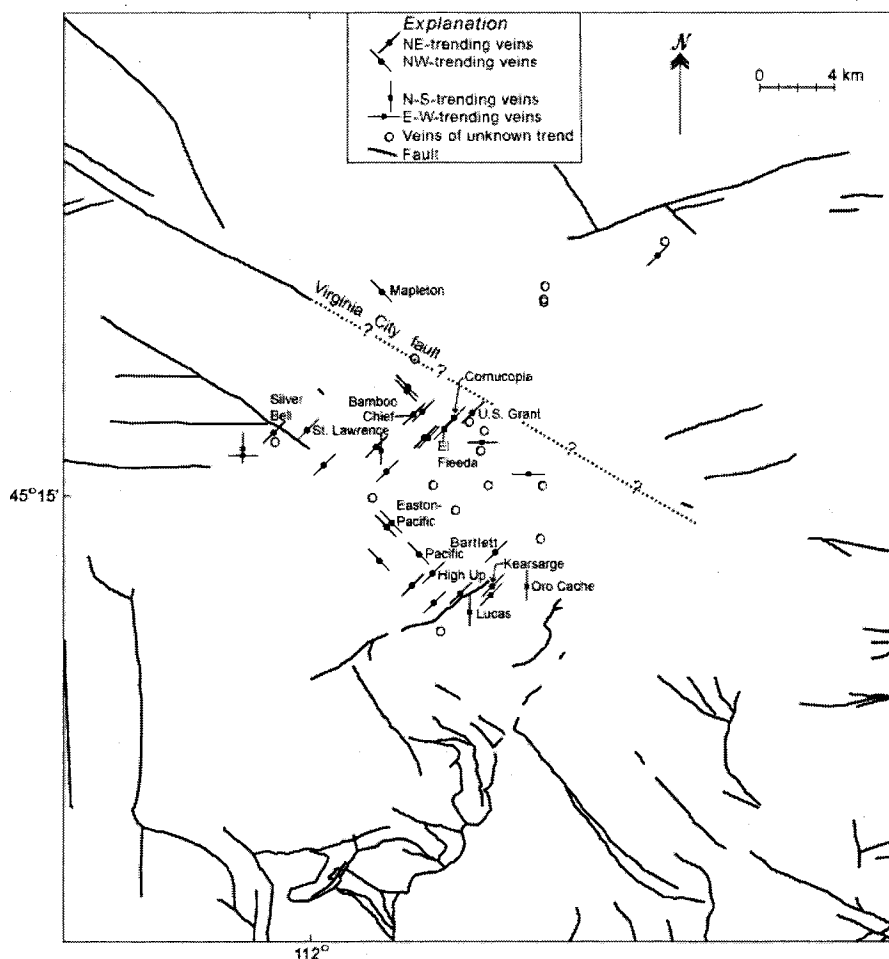


**Figure 2.** Map showing major faults and locations of mines and prospects in the Virginia City mining district. Faults are from Ruppel et al. (1993) and Kellogg and Williams (2000). Mines are plotted in terms of major vein orientations, where known. Mine locations and vein orientations are from Ruppel and Liu (in press), McFaul et al. (2000), Lockwood (1990), and this study. Mines and prospects sampled for this study are named on the map.

likely sources of the rich placer deposits. More than 60 properties (Fig. 2) were active in the district in the early 1900's (Lorain, 1937). Lode gold mining peaked in the late 19<sup>th</sup> century, although some mining continued until World War II. Tansley et al. (1933) noted that secondary enrichment by near-surface oxidation developed high-grade ores that were exploited during early periods of lode gold mining. Interest in the district revived in the late 1980's when a number of mining companies conducted exploration and minor development.

From 1994 to 1998, the USGS collected samples throughout the district as part of a reconnaissance study conducted to provide federal land managers with a perspective on the mineral resources in the Dillon BLM Resource

Area and intervening areas of the Beaverhead National Forest, Madison and Beaverhead Counties, southwest Montana. A number of gold districts in the northern part of the Dillon Resource Area (Virginia City, Pony, Red Bluff, Sheridan, Revenue) have been explored more or less continuously during the past 20 years, although little development has been attempted. Federal lands border many of the mining claims. Should a favorable economic climate for gold mining develop in the future, many of the historic gold mining districts in the northern part of the Dillon BLM Resource Area may become more attractive to industry. Although the existence of a lode gold resource in the district has been established by exploration, the nature of the lode mineralization has been difficult to ascertain. A variety of different mineral deposit

types have been proposed for the lode veins, the age of mineralization has not been firmly established, and a genetic association with igneous intrusions as a source of hydrothermal fluids has been debated. In this paper, we summarize published studies and proposed models for the district, present new geochemical, mineral chemistry, and age data for representative lode gold deposits in the district, and discuss the geoenvironmental signature of the deposits.

## OVERVIEW OF THE VIRGINIA CITY MINING DISTRICT

The Virginia City mining district (Fig. 3) is also known partly or wholly as the Browns Gulch, Barton Gulch, Granite Creek, Williams Gulch, Fairweather, and Alder Gulch district. Recent exploration activities focused on the historic lode mines along the upper reaches of the main drainage of Alder Gulch (U.S. Grant, Kearsarge, and Garrison mine areas), and drainages to the west along Hungry Hollow Gulch and Browns Gulch (Easton-Pacific mine). The area of most recent exploration activity falls within the Virginia City and Cirque Lake 7.5' topographic quadrangles. The historic lode mines of the district were developed as underground mines that followed quartz veins and lenses in highly fractured shear zones in Archean quartzofeldspathic gneiss. Although the details vary from mine to mine, most of the veins were a few cm to a meter wide, or occurred as zones of closely spaced veins <7 m wide, or lenses with pockets of high-grade ore; some ore is disseminated in wallrock adjacent to veins. The predominant vein orientations in the district are northwest and northeast (Fig. 2). North-south and east-west trends appear to represent second-order structures. Numerous mines and prospects were developed along some vein systems. Prominent vein orientations are N70E (Kearsarge, Bamboo Chief), N50E to N65E (Silver Bell, St. Lawrence), and N35W to N60W (Mapleton, Easton-Pacific). Table 1 lists characteristics of the major vein types in the district. Descriptions of individual deposits, mining history and production, and comparisons with other lode gold districts in the region are summarized in a number of thesis studies

(Lockwood, 1990; Cole, 1983, Despotovic, 2000). Ruppel and Liu (in press) prepared a comprehensive account of the mining history of the district and descriptions of individual deposits.

All veins share some of the characteristics of low-sulfide (Motherlode-type) gold quartz veins (Berger, 1986; Groves and others, 1998). Most of the veins are continuous over distances of 100 m or less; the exception is the Kearsarge-Oro Cache sheeted vein system at the head of Alder Gulch, which is over 1 km long (Lockwood, 1990). The overall percentage of sulfide minerals is low (2 to 3 volume percent). Pyrite is the most abundant sulfide mineral. Alteration styles vary with host rock lithology. Potassic alteration is widespread in granitic gneisses. Chlorite is especially well developed along northwest-trending structures and is most predominant in more mafic rocks. In the vicinity of the Kearsarge mine, the dominant alteration assemblage associated with veins is quartz-sericite-carbonate-graphite (Bill Neal, personal commun., 1998).

In the 1990's, a number of mining companies (BHP, Billiton, Kennecott, Hanover, King of Kings) conducted exploration in the area of historic lode mines along the upper reaches of Alder Gulch, as well as to the west along Hungry Hollow Gulch and Browns Gulch (Fig. 3). From 1992 until 1998, Hanover Gold acquired 125 unpatented and 41 patented mining claims in the Alder Gulch area after negotiating land consolidation agreements with other parties. Exploration by Hanover Gold included surface mapping, geophysical surveys, diamond drilling, metallurgical testing, and limited underground development. Declining precious-metal prices and the passage of Montana initiative I-137 (banning the use of cyanide in precious-metal extraction) led the company to curtail activities in the district. With the termination of leases with Hanover Gold, the Moen family regained control of previously held mining claims in Alder Gulch and continued small-scale mining. Under the auspices of Moen Builders, Inc., the Apex Gold Development LLC was formed in 1999 as a joint venture to develop and mine the Apex portion of

the Apex-Kearsarge lode in the southern part of the district. Ore was mined from an open pit and stockpiled for processing at the M & W mill near Virginia City, where plans were underway (as of

2000) to process ore by gravity, flotation, and cyanide in the recently upgraded mill.

**Table 1.** Vein types in the Virginia City mining district.

Type	NW-trending veins		NE-trending veins	
		<u>Bartlett type</u>	<u>Kearsarge type</u>	
Host rock	Archean metamorphic rocks	Silicified dolomitic marbles in Archean rocks	Archean metamorphic rocks	
Ore Mineralogy	Acanthite, gold, auriferous pyrite, argentite, galena, chalcopyrite, tetrahedrite, sphalerite, stibnite	Gold, pyrite, chalcopyrite, tetrahedrite	Gold, pyrite, chalcopyrite, sphalerite, galena, tetrahedrite, minor arsenopyrite, tellurides	
Supergene minerals	Goethite, hematite, malachite, chalcocite, chrysocolla, Mn-oxides, clays, cerussite, hemimorphite			
Gangue	Quartz, K-feldspar	Quartz, ankerite	Quartz, K-feldspar, calcite, ankerite, graphite, barite	
Dominant alteration style	Argillic alteration	Carbonate, graphite	K-feldspar, carbonate, <u>+</u> chlorite, graphite, sericite	
Mines, prospects, and named vein systems	Easton-Pacific, Prospect, Alhambra, Winnetka, Bell, Prospect, Mapleton, Kid vein (Brown's Gulch adit), Pearl vein (Hungry Hollow Gulch)	Bartlett, General Shafter	U.S. Grant, El Fleeda, St. Lawrence, Silver Bell, Cornucopia, Black Rock, Fork, High-Up, Irene, Kearsarge, Big vein, Oro Cache, Garrison, Lucas-Atlas	

### Geologic setting

All of the lode deposits of the Virginia City mining district are hosted by Archean metamorphic rocks (Fig. 3). To the east of Alder Gulch, Tertiary volcanic rocks cover Archean rocks. An allocthonous assemblage of folded Paleozoic sedimentary rocks and landslide deposits form the head of Alder Gulch. A few Tertiary volcanic plugs are present in the area of some mines. A number of geologic maps at different scales cover parts of the district. Tansley et al. (1933) provided a geologic sketch map of the district. Wier (1982) prepared an outcrop map of the Virginia City 7.5' quadrangle, which shows individual

pegmatite and granite dikes as well as mine dumps. Most of the pegmatites and dikes strike northwest-southeast. Cole (1983) included a bedrock map of the northern part of the district in his thesis, based on his own mapping and a compilation of existing maps. Hadley (1969) mapped the Varney 15' quadrangle, which covers the southern parts of the district in the Cirque Lake 7.5' quadrangle. Most of the mining district lies within the Ennis 30' x 60' quadrangle (Kellogg and Williams, 2000). The western edge of the district lies within the Dillon 1° x 2° quadrangle, which is included in the Dillon 1:250,000-scale geologic map (Ruppel et al., 1993).

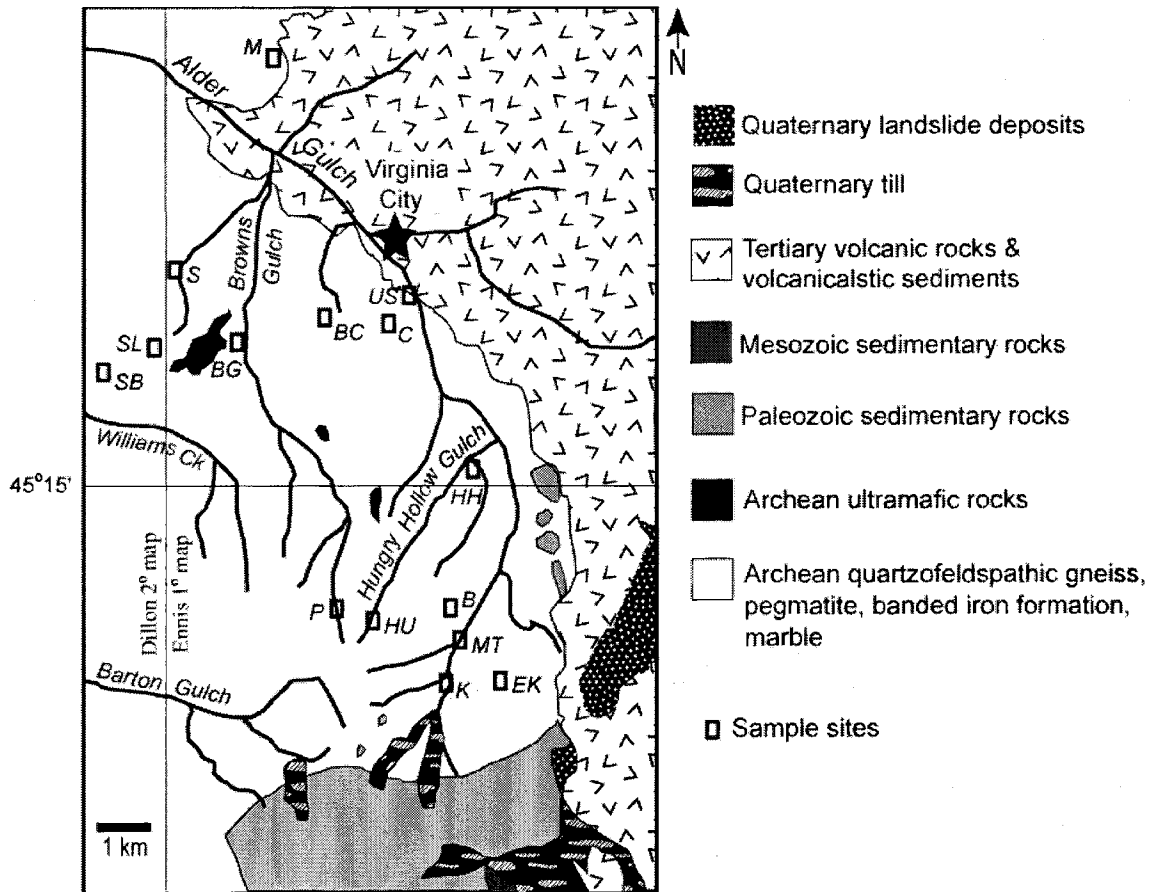


**Figure 3.** Simplified geologic map of the Virginia City district based on Kellogg and Williams (2000) and Ruppel et al. (1993). Sample localities are as follows: US, U.S. Grant mine; C, Cornucopia mine; BC, Bamboo Chief mine; M, Mapleton mine; S, Sampson mine; SL, St. Lawrence mine; SB, Silver Bell mine; BG, unnamed adit along Browns Gulch; HH, unnamed adit along Hungry Hollow gulch; HU, High Up-Irene vein; P, Pacific mine; B, Bartlett mine; MT, Millard tunnel; K, Kearsarge mine; EK, shafts and prospects east of the Kearsarge mine along the Oro Cache vein.

Tansley et al. (1933) and Cole (1983) show an ovoid intrusive body, elongate in a northwest-southeast direction, in the areas of the Easton and Pacific mines, west of Browns Gulch. Tansley et al. (1933) called this rock a quartz monzonite aplite. Cole (1983) called it the "late Cretaceous granitic Browns Gulch stock". The rationale for the late Cretaceous age assigned to the stock is not apparent. Winchell (1914) described the host rock for the vein system at the Easton and the Pacific mines as a feldspar-rich, lenticular mass of quartz monzonite aplite that crosscuts gneiss. He described the mineralogy of the aplite as quartz, microcline, orthoclase, sericitized plagioclase, and rare muscovite. Aplites, by definition, are fine-grained white rocks composed of quartz, albite, potassium feldspar, and muscovite. The presence of two potassium feldspars in the rock suggests that this rock has undergone potassic alteration. On Hadley's (1969) geologic map, the area of the "stock" near the Easton mine (northwest end) is not shown separately; it lies within an area mapped as Precambrian granite and migmatite. The area near the Pacific mine (southeast end) is shown within biotite and hornblende gneiss of the Cherry Creek Group. The Cherry Creek package of rocks includes beds of dolomitic marble, schist, and quartzite. Wier (1982) mapped at a much larger scale than Hadley (1:12,000 versus 1:62,500) and used different map units. Wier (1982) described the predominant rock type in the area as non-foliated to foliated quartz-feldspar gneiss; individual outcrops of amphibolite, marble, and pegmatite were mapped separately. Eimon (1997) based the outline of his proposed Garrison igneous complex at the head of Alder Gulch on drill core. He described the complex as a 900 m by 450 m complex of granite, granodiorite, quartz monzonite, and gneiss. The complex is elongate in a northeast direction and intrudes Precambrian gneiss. Large-scale (1:6,000) mapping of the southern part of the district was done as part of Hanover Gold's exploration during the 1990's. Despotovic (2000) mapped a 5.5 km<sup>2</sup> area along the southeastern side of Alder Gulch at a scale of 1:1,200; this study included logging of Hanover core from several of the northeast-trending veins in that part of the district and analysis of the

nature of the host rock. Lithologies encountered in surface and drill core included granitic gneiss with and without magnetite, tonalitic gneiss, and hornblende-plagioclase gneiss and amphibolite. Within Despotovic's map area, map patterns indicate that the granitic gneisses are complexly folded and faulted, but individual lithologic units and fold axes trend northeast-southwest, parallel to Alder Gulch. Granitic gneisses are weakly to moderately foliated and locally migmatitic; those with magnetite (and high magnetic susceptibility) comprise the most abundant unit. More mafic units are moderately to strongly foliated, and interleaved with felsic and garnetiferous lithologies. Dolomitic marbles, mafic gneiss, and small plugs of Archean ultramafic rocks appear to be confined to the western side of southern Alder Gulch. Despotovic (2000) suggested that Alder Gulch represents a major lithostratigraphic contact between metasedimentary rocks (marbles, metaquartzites, iron formation) to the west and metaigneous rocks (granitic gneiss) to the east. However, Wier's (1982) outcrop map shows patches of marble on the eastern side of Alder Gulch, to the north of the area mapped by Despotovic. Archean marbles in the Ruby Mountains to the west (Fig. 1) host massive metasomatic talc deposits; none of the marbles exposed in the Virginia City mining district are altered to talc.

The geologic maps of Hadley (1969) and Wier (1982) each show small ultramafic bodies scattered throughout the district. Wier's map shows an unusually dense concentration of pegmatite, mainly narrow dikes of coarse quartz-feldspar pegmatite oriented in a northwesterly direction. Wier (1982) mapped a localized swarm of northwest-trending, medium-grained granitic dikes north of Williams Creek (Fig. 3). He reported a preliminary K/Ar date of 1.9 Ga for one of these dikes, and concluded that these granite bodies are probably genetically related to the pegmatites. The only report of an intrusive rock in the northern part of the district is a description of porphyritic granite dikes and sills encountered in drill core that crossed the third level of the U.S. Grant vein system (Sheets, 1980). Although these granites were interpreted as Cretaceous in age, the description of high

concentrations of pink potassic feldspar suggests that these rocks may also represent Proterozoic(?) intrusions related to the pegmatites.

A number of workers have considered the lode deposits of the district to be related to the Cretaceous Tobacco Root batholith, which is flanked by lode gold vein deposits. However, the main mass of the batholith is located about 15 miles (24 km) north of the northern end of the Virginia City district. The Tobacco Root batholith is a composite body that ranges in composition from hornblende diorite to monzonite. No satellite plutons of these compositions are recognized in the Virginia City district, such as those present near Copper Mountain in the Sheridan district to the north (Fig. 1). Lockwood (1990) interpreted the vein deposits at the Easton-Pacific mine as epithermal to mesothermal deposits genetically related to the Tobacco Root batholith. The stock in this area appears to be an aplitic facies within, or intrusive into, Precambrian granitic gneiss. The unfoliated, aplitic rocks in the Virginia City district (the Brown's Gulch aplite stock and the unexposed proposed Garrison igneous complex) may be Early Proterozoic in age. O'Neill et al. (1996) describe leucocratic granitic aplite and pegmatite sills of Early Proterozoic age in the southern part of the nearby Highland Mountains (Fig. 1). We consider it unlikely to have genetically-related, homogeneous aplitic plutons so far removed from the main mass of the Cretaceous Tobacco Root batholith. Although marginal-facies pegmatites of the Tobacco Root batholith occur within the batholith and in adjacent rocks, Cretaceous pegmatites related to the batholith contain sulfide minerals, whereas Precambrian pegmatites lack sulfides (Vitaliano and Cordua, 1979). The pegmatites of the Virginia City district are probably related to the late stages of cooling of the large mass of granite that appears to be younger than the Cherry Creek package of rocks (Hadley, 1969). We know of no reports of sulfide minerals in the pegmatite bodies in the Virginia City district, such as are observed for Cretaceous pegmatites near the Tobacco Root batholith.

The NW-striking Virginia City fault zone is a major boundary (Fig. 2) between the Tobacco Root batholith and the lode gold deposits south of Virginia City, and may have offset parts of the district (Ruppel, 1993). The left-lateral strike-slip fault zone cuts Archean crystalline metamorphic rocks as well as younger rocks and surficial deposits, controls the NW-trending segment of Alder Gulch near Virginia City, and displaces the Tobacco Root mountain front north of Alder a minimum of 4 to 5 km to the northwest since middle Cenozoic time and as much as 10 km in the last 34 Ma (Ruppel, 1993). On regional-scale geophysical maps, the Tobacco Root batholith is a prominent magnetic high anomaly that coincides with a gravity low anomaly; this pattern reflects the density contrast between the rocks of the batholith and the Archean metamorphic rocks they intrude (Hanna et al., 1993). No similar pattern suggestive of a large, buried intrusion is apparent in the regional-scale geophysics for the Virginia City area (Pinckney et al., 1980). Barnard (1993) noted the contrast in geophysical properties between the Tobacco Root and Virginia City areas. He suggested that although existing geophysical data for the area are too generalized to clearly indicate a felsic intrusion in the Virginia City district, the weak magnetic and gravity lows observed there are permissive for a granitic intrusion with relatively low-magnetic and low-density properties.

#### **Previous district- and mine-scale studies**

The lode gold veins of the district are structurally controlled quartz veins. Intersections of vein systems have been proposed as the most attractive exploration targets (Eimon, 1997), and discontinuities and offsets of vein systems are likely to be the limiting factor in defining mineable ore reserves. Much of the debate over the nature of the lode gold deposits revolves around the age (Archean, Proterozoic, Cretaceous, or Tertiary) and relation of the veins to one or more postulated, but unexposed, intrusive center(s). The models proposed to date vary in detail, but generally espouse two different end-member mineral deposit types: (1) Archean lode gold deposits, such as those found in Archean greenstone-

sedimentary belts elsewhere (Boyle, 1991); and (2) veins related to a Cretaceous age or younger intrusive center(s). The lack of a detailed geologic framework on a district-wide scale has hindered interpretation of existing data. Studies that espoused different models are summarized below.

Eimon (1997) reviewed proposed models for the genesis of the lode veins in the district and defined additional exploration targets near the head of Alder Gulch, which he based on projected fault zone intersections. Both Barnard (1993) and Lockwood (1990) cited mineral zoning in the central part of the district and in the Easton-Pacific area as evidence for an unexposed hydrothermal source (intrusion). Barnard (1993) plotted available mineralogic data from the literature for all of the workings in the district. He defined mineral zones based on computed galena to pyrite ratios and argued that these "zones" define a buried intrusion or heat source responsible for mineralization. Shawe and Wier (1989) also defined zones based on silver to gold ratios from vein production. They showed a relatively low Ag: Au zone (2:1 to 10:1) just south of Virginia City in the area of the U.S. Grant mine, and also just north of Baldy Mountain in the Garrison mine area, near the head of Alder Gulch. In between these two zones is a wide area of veins characterized by silver to gold ratios ranging from 10:1 to 50:1. The silver-rich zone generally coincides with Barnard's (1993) barren zone and surrounding pyrite-galena zone, whereas the more gold-rich zone of Shawe and Wier (1989) overlaps Barnard's galena zone. Previously, Lorain (1937) suggested that the variation in the metallogeny with respect to copper:silver:gold ratios of mining districts in the entire region reflected zonation around the Tobacco Root batholith. Franklin (1994) used field observations to relate the lode gold deposits to northeast- and northwest-striking high angle faults. He bracketed the mineralization as post-Proterozoic pegmatite dike intrusion and pre-Tertiary basaltic volcanism, possibly related to an unexposed Late Cretaceous-Early Tertiary satellite pluton of the Tobacco Root batholith. Godfrey (1995) proposed a cordilleran vein model and suggested Tertiary batholiths and

volcanics exposed in the Gravelly Range as a heat source for generating hydrothermal fluids. Others have suggested that the lode gold deposits represent metamorphic low-sulfide gold quartz veins, which formed in the Archean or were remobilized during subsequent metamorphism. None of the veins in the district are observed cutting rocks thought to be younger in age than Precambrian. Anecdotal reports of gold-bearing Cambrian Flathead conglomerate in upper Alder Gulch suggest that some gold may be present in paleoplacers that developed during the Cambrian on Archean or Proterozoic bedrock.

Lockwood (1990) studied the Easton-Pacific vein system at the head of Brown's Gulch (Figs. 2 and 3). He used VLF (very-low-frequency electromagnetic) anomalies to demonstrate that the Easton and Pacific mines lie on the same NW-trending curvilinear structure. Argillic alteration is pervasive in the vicinity of the Pacific mine. Illite:smectite ratios increase proximal to the veins; illite proximal to the veins records a temperature of approximately  $250 \pm 40$  °C. Fluid inclusion and stable isotope data for the Pacific veins indicate that the veins formed from fluids that evolved from moderate temperature, low-salinity (275 °C, 3 to 6 eq. wt. % NaCl) solutions to lower temperature, higher salinity fluids (175 °C, 10 to 12 eq. wt. % NaCl). High-grade ores are associated with high temperature, low salinity, high  $\delta^{18}\text{O}$  fluids (Lockwood et al., 1991).

Loen (1992) used mass balance calculations to test the hypothesis that the lode gold deposits in upper Alder Gulch provided the placer gold. The largest gold nugget (32 oz) found in Alder Gulch apparently came from the upper part of the Gulch near the Kearsarge mine (Loen, 1997). Previous studies suggested that the lode deposits were of insufficient size and grade to provide the large amounts (>77 tons) of gold produced from the placer deposits. Mass balance calculations indicated that this volume of placer gold requires a volume of eroded source rocks on the order of 10 to 24 km<sup>3</sup> with a mean gold content of 2.4 to 29 parts per billion (ppb) Au. Erosion of unusually rich source rocks could account for the placer gold, but such volumes of gold-rich

rocks are no longer exposed in the district. Preconcentration of gold from Archean source rocks prior to the Quaternary, possibly beginning as early as middle Miocene time, provides a more likely explanation for the placer gold. Erosion of source rocks containing 0.65 to 9.69 ppb Au (essentially crustal abundance) over a prolonged period (15 Ma) of fluvial erosion is sufficient to derive the rich Virginia City placers (Loen, 1992). Crustal abundance for gold is on the order of 1 to 4 ppb (Rickwood, 1983).

On the basis of structure, Despotovich (2000) related mineralization in the district to uplift of metamorphic core complexes and interactions of thrust belt structures and NW-trending left-lateral strike-slip faults that developed positive flower structures. Low-sulfide, meso-to epithermal vein deposits were emplaced along subsidiary shears that develop at small angles to the main strike-slip fault; structures that host the veins were likely reactivated over time.

A number of other reports describing properties in the district have been prepared by consultants (Sheets, 1980) and mining companies as internal documents for evaluating the viability of developing mines. Drill core intercept data are included in press releases and annual reports of mining companies that were active in the district in the past (Hanover Gold Company, Inc., 1997).

### Age

The relevance of any Proterozoic hydrothermal activity to lode gold deposition is unknown at present. Brecciation of early pyrite and cataclastic textures in quartz veins indicate that at least some of the veins systems were fractured and healed repeatedly. Archean or Proterozoic vein systems may have been reactivated during Laramide-age tectonism. Presumably on the basis of observed cross-cutting relationships, Franklin (1994) bracketed the timing of vein formation as post-intrusion of Proterozoic pegmatite dikes and prior to the extrusion of overlying Tertiary basalts. Wier (1982) reported a preliminary age of 1.9 Ga for a northwest-trending granite dike located 1.9 km northwest of the Silver Bell mine (Figs. 2 and 3). Cole

(1983) reported two K-Ar mineral dates from the area of the U.S. Grant mine, in the northern part of the district: (1) an age of  $1,572 \pm 51$  Ma for a biotite from a pegmatite exposed in underground workings and; (2) an age of  $311 \pm 11$  Ma for an impure potassium feldspar sample from altered wallrock at the same mine level where the pegmatite was sampled. The biotite age from pegmatite is consistent with the 1.6 Ga age of the last regional metamorphic event. The feldspar age is problematic and sheds little light on the age of mineralization in the district. Cole (1983) noted that the feldspar population of the wallrock represented a mixture of hydrothermal microcline and sericitized "Precambrian" feldspar. Thus, he interpreted the age of the sample is probably a composite age representing a mixture of hydrothermal microcline and older feldspar. Sericite could have formed as an alteration product at any time; any sericite present in the sample will contribute to the age, and the sericite, as well as the two different generations of potassium feldspar, complicate any interpretation of the age of this sample.

An andesite plug dated at  $51.1 \pm 1.2$  Ma (whole rock K-Ar date by Marvin and Dobson, 1979) cuts the El Fleeda vein system. This age at the El Fleeda mine, located about a mile (1.5 km) south of Virginia City, on the west side of Alder Gulch in the northern part of the district, suggests that at least some of the mineralization is older than Eocene (Cole, 1983).

## STUDY METHODS AND RESULTS

### Methods

Quartz veins, brecciated ores, gossan and host rock were sampled at localities throughout the district (Fig. 3). Some samples represent composites of 30 or more chip samples from a single vein system. Samples were analyzed for geochemistry by a variety of techniques. Samples collected prior to 1997 were analyzed by ACTLABS, Inc. of Wheat Ridge, Colorado. Samples collected in 1997 and 1998 were analyzed by XRAL Laboratories of Don Mills, Ontario, Canada. Analytical techniques included multi-element instrumental neutron activation (INAA), acid digestion followed by



inductively coupled plasma- atomic emission spectrometry (ICP-AES), hydride ICP analysis for selected elements (Bi, Ge, Se, Te), x-ray fluorescence (XRF), and lead fire assay inductively coupled plasma - mass spectrometry (ICP-MS) for determination of platinum-group elements. For most samples, multi-element analytical packages were selected that are suitable for gold and base metal exploration, supplemented with special analytical techniques for elements of particular interest, such as tellurium. Methods and detection limits are described in detail in Hammarstrom and Van Gosen (1998), Arbogast (1996), and Hammarstrom et al. (2002, Appendix B).

Polished thin sections of 30 selected samples from different vein systems were prepared for petrography. Selected samples were analyzed by electron probe microanalysis to determine compositions of sulfide and silicate minerals. Analyses were done on a JEOL JXA-8900 instrument at USGS laboratories in Reston, Virginia. The microprobe, equipped with 5 fully automated, wavelength-dispersive spectrometers, was operated at 15 kV for silicate mineral analysis and at 20 kV for analysis of sulfide minerals. Natural and synthetic minerals were used as primary and secondary standards.

Hanover Gold, Inc. provided samples of drill core from the Oro Cache vein system for mineralogical analysis. Green sericite from a typical sample of altered rock associated with the Kearsarge vein system was separated and dated by the  $^{40}\text{Ar}/^{39}\text{Ar}$  technique in USGS laboratories. The sericite sample was prepared using standard mineral separation techniques and then irradiated in the USGS TRIGA reactor (Dalrymple et al., 1981) in Denver, Colorado. We used MMhb-1 hornblende, with an age of  $519.4 \pm 2.5$  Ma (Alexander et al., 1978; Dalrymple et al., 1981) as the neutron flux monitor. Corrections for the production of interfering argon isotopes during the irradiation are the values reported by Dalrymple et al. (1981), and Roddick (1983). Corrections for mass spectrometer discrimination were determined using repeat measurements of atmospheric argon. The decay constants used were those reported by Steiger and Jäger

(1977). Details of the  $^{40}\text{Ar}/^{39}\text{Ar}$  age spectrum dating technique that was used for the sericite can be found in Haugerud and Kunk (1988) and Kunk et al. (2001).

Composited ore samples from the Pacific, Bamboo Chief, and U.S. Grant mines were subjected to a leach experiment to determine the most readily soluble metals present in the ores. The analytical protocol for the water leachate experiments used 2.5-g aliquots of the <100 mesh samples used for whole-rock geochemistry, as received, mixed with 18 M $\Omega$  deionized water in a water:rock ratio of 20:1 by mass. After equilibration with the atmosphere, the pH of the deionized water typically reached 5.5. Leaching was passive, with no continuous agitation or shaking other than an initial gentle shake to ensure wetting of all ground rock and a second gentle shake to repeat the re-suspension of solids after one hour. The samples were allowed to react at room temperature for 24 hours. After the reaction time, samples were centrifuged to separate most of the solids, then the solutions were decanted into rinsed syringes and filtered through a rinsed, 0.45  $\mu\text{m}$  pore-size, cellulose nitrate filter. Immediately after filtration, the pH and conductivity (for total dissolved solids—TDS) of the filtrates were measured. Filtrate samples for metals analysis by ICP-MS were acidified with Ultrex  $\text{HNO}_3$  to a pH between 1 and 2, and those for anion analysis by ion chromatography (IC) were left untreated until analysis.

## Geochemistry

Past studies relied on vein production data to examine district- and regional-scale zoning trends and did not address the trace element signature of the deposits. Such data were collected as part of the exploration efforts in the 1990's. With the exception of samples described by Despotovic (2000), these data are not publicly available. Multi-element geochemical data for selected elements from 17 mines and mineralized vein systems in the Virginia City district are listed in Table 2, grouped by vein type and subarea within the district. Elements that are below detection limits for all samples included in a particular table are

omitted. Gold concentrations in individual samples are subject to nugget effects. We attempted to avoid this problem by collecting multiple samples from each locality, and in some cases, by compositing a minimum of 30 randomly selected chip samples from quartz veins or dump materials. Selected X-ray fluorescence data reported by Despotovic (2000)

for drill core samples from the northeast-trending Atlas and Lucas veins systems in the area north and east of the Kearsarge mine (EK on Fig. 3) are summarized in Table 2B for comparison with our samples from upper Alder Gulch. Complete geochemical data and sample location information for most samples are given in Hammarstrom and Van Gosen (1998).

**Table 2.** Geochemical data.\*  
A. NE-trending veins in N. Alder Gulch

Mine	Bamboo Chief			U.S. Grant			Cornucopia			
Sample	E9516	V9521A	V9521B	E9517	V9522	009V94	95JH118	95JH119	95JH120	E9518
Ag ppm	360	42	1,200	78	1,100	7	<5	51	53	210
As ppm	1.6	210	41	4.5	27	0.6	<0.5	2.8	27.0	11
Au ppb	6,280	238	90,400	2,980	27,300	340	<2	9,670	491	10,300
Ba ppm	<50	<50	110	<50	440	210	1,500	230	480	<50
Ca %	<1	0.6	0.04	<1	<0.02	<0.01	<1	<1	<1	<1
Co ppm	66	<1	2	220	14	1	11	65	21	98
Cr ppm	<5	10	17	<5	11	8	2	<1	230	<5
Cu ppm	n.d.	5,670	158	n.d.	166	54	n.d.	n.d.	n.d.	n.d.
Fe %	0.24	1.26	23.1	0.93	12	0.96	2.8	2.7	24.0	0.69
Hg ppm	<1	<1	4	<1	<1	<1	<1	<1	<1	<1
Mo ppm	62	34	2,000	30	127	14	<1	28	140	27
Na %	0.01	0.02	0.03	0.02	0.03	0.02	1.39	0.02	0.25	0.02
Pb ppm	n.d.	17,670	29,900	n.d.	1,640	221	n.d.	n.d.	n.d.	n.d.
Sb ppm	0.7	100	19	2.6	6.9	1.1	<0.1	1.7	2.7	8.7
Se ppm	0.6	0.8	8.7	0.5	0.7	0.8	<3	<3	<3	0.7
Te ppm	1.9	0.7	5.5	1.5	0.2	0.6	n.d.	n.d.	n.d.	1.2
Zn ppm	95	631	2,000	290	543	30	152	<50	3,300	<50
Ag/Au	57	176	13	26	40	21	n.d.	5	108	20

Bamboo Chief mine: Ore stockpile at Moen's mill; SW¼ of sec. 27, T.6S., R.3W.

E9516: Siliceous gneiss "ore" with abundant iron oxide mineral staining

V9521A: Copper-stained, limonitic quartz-rich rock

V9521B: Ore - quartz vein with abundant iron oxide minerals

U.S. Grant mine: Ore stockpile from the lower adit; SW¼ of NW¼ of sec. 26, T.6S., R.3W

E9517: Pyrite-rich quartz vein ore

V9522: Quartz vein gossan with pyrite clots

Cornucopia mine: SE¼ of sec. 27, T.6S., R.3W

009V94: Iron oxide mineral-stained quartz vein with clots of pyrite

95JH118: Amphibolite, garnet-rich, iron oxide mineral stained

95JH119: Ore - quartz vein with pyrite

95JH120: Red gossan

E9518: Iron oxide mineral-stained quartz vein with clots of pyrite

\* n.d., not determined; dl, detection limit

**Table 2**—Continued.

B. NE-trending veins in S. Alder Gulch.

Mine or vein	High-Up Irene	Millard tunnel	Kearsarge	Oro Cache	Atlas	Lucas	
Sample	96JH62	95JH055	97BV01	012V94	KS13-1	KS13-2	KS11,KS12,KS14
Ag ppm	6.4	<5	11	<0.4	5	5.7	1.0 to 6.8
As ppm	9.9	25.0	16.3	11	14	47	13 to 52
Au ppb	1450	3800	6,550	398	n.d.	n.d.	4,000 <sup>†</sup>
Ba ppm	290	280	406	2200	894	1,040	557 to 1,419
Ca %	4.97	10	0.69	<1	0.04	0.27	0.26 to 1.7
Cd ppm	<0.5	n.d.	17	<0.5	4	5.2	1.0 to 8.6
Co ppm	25	33	4.26	2	n.d.	n.d.	n.d.
Cr ppm	250	330	3	5	16	17	7 to 31
Cu ppm	122	n.d.	110	69	18	6	3 to 72
Fe %	4.94	6.4	1.25	1.11	2.24	2.06	0.8 to 3.3
K %	3.9	n.d.	1.6	5.47	4.9	5.7	2.8 to 6.4
Mg %	3.4	n.d.	0.31	0.51	0.05	0.12	0.46 to 1.84
Mn ppm	961	n.d.	96	154	0.04	0.03	0.03 to 0.06
Mo ppm	8	5	151	2	16	3.9	<dl to 12
Na %	0.46	0.22	0.0281	0.65	0.22	1.5	0.8 to 1.6
Ni ppm	101	<28	16	3	14	6	7.0 to 15.9
Pb ppm	39	n.d.	305	20	50	14	11 to 42
S %	n.d.	n.d.	1.14	n.d.	<dl	<dl	<dl to 0.4
Sb ppm	4.1	2.0	35.6	0.6	4.4	1.4	<dl to 2.3
Se ppm	0.5	<3	<0.01	<0.2	0.3	<dl	<dl to 0.1
Te ppm	2.3	n.d.	1	0.2	n.d.	n.d.	n.d.
Tl ppm	n.d.	n.d.	0.7	n.d.	<dl	0.3	<dl to 1.0
V ppm	145	n.d.	26	59	36	56	8 to 135
Zn ppm	92	252	2,570	19	33	50	7 to 69
Ag/Au	4	-	2	-	-	-	0.25 to 17

Mined area in High Up - Irene vein system; NE¼ of sec. 15, T.7S., R.3W.

96JH62: Gneiss with sulfide mineral-bearing quartz veins.

Millard tunnel- 0.8 mi N-NE of Kearsarge mine; NW¼ of SE¼ of sec. 14, T.7S., R.3W

95JH55: Quartz-sulfide "ore".

Kearsarge 7000' level mine dump; NW¼ of NE¼ of sec. 23, T.7S., R.3W

97BV01: Quartz vein with finely disseminated pyrite.

Shaft & prospects east of Kearsarge mine along the Oro Cache vein; NW¼ of NW¼ of sec. 24, T.7S., R.3W

012V94: Highly fractured, limonitic K-feldspar gneiss from dump.

Atlas vein. Diamond drill core data from Despotovic (2000, Appendix 5)

KS13-1: Gold-bearing, altered granitic gneiss without magnetite at 196'. Fine to medium-grained pinkish rock with mm- to cm-wide quartz veins. K-feldspar and weak chloritic alteration.

KS13-2: Gold-bearing, altered granitic gneiss without magnetite at 318'. Fine to medium-grained pinkish-white rock with mm- to cm-wide quartz veins. K-feldspar alteration.

Lucas vein. Diamond drill core data from Despotovic (2000, Appendix 5). Range of data reported for mineralized intervals from 3 cores: KS11 (444', 491', and 525'); KS12 (263', 270'); and KS14 (409', 471'). All were logged as granitic gneiss without, or with, magnetite. All samples exhibit K-feldspar + chlorite + carbonate alteration. <sup>†</sup> Au value based on typical assay grades for the vein system.

**Table 2**—Continued.

C. NE-trending veins west of Alder Gulch.

Sample		Sampson	Silver Bell	St. Lawrence	Bartlett (in Archean dolomitic marble)			
		98JH12	98JH15	98JH14A	96JH21	96JH23	96JH24	97JH09
Ag	ppm	26	39	55	<0.4	0.6	0.8	24
As	ppm	66.2	4.8	20.7	<0.5	8.4	45	36
Au	ppb	0.298	1.04	0.636	<2	70	109	14,600
Ba	ppm	86	1,680	671	65	320	220	156
Ca	%	0.767	1.581	0.124	20.14	0.7	0.04	0.02
Cd	ppm	12	3	<2	<0.5	<0.5	<0.5	<2
Co	ppm	4	5	<2	1	38	3	7.72
Cr	ppm	<2	2	<2	8	210	12	19
Cu	ppm	1,160	55	72	2	125	54	110
Fe	%	1.87	1.32	0.51	1.04	4.03	4.15	2.24
Hg	ppm	0.98	0.73	0.52	<1	<1	<1	n.d.
K	%	0.39	0.74	0.45	0.08	3.3	5.16	2
Mg	%	0.24	0.055	0.01	11.22	0.49	0.03	0.03
Mn	ppm	456	316	46	4543	649	34	29
Mo	ppm	6	18	29	<2	3	26	87
Na	%	0.019	0.489	0.181	0.03	1.9	0.94	0.0222
Ni	ppm	9	12	4	2	109	10	38
Pb	ppm	1,680	724	1,800	20	19	584	898
S	%	<0.05	0.06	0.06	n.d.	n.d.	n.d.	<0.05
Sb	ppm	8	5.6	1.4	0.5	2.9	6.4	26.7
Se	ppm	0.5	0.2	0.3	0.8	0.7	1.4	1.3
Te	ppm	1.1	1.5	5.1	0.2	<0.2	0.3	3.9
Tl	ppm	<0.1	<0.1	<0.1	n.d.	n.d.	n.d.	0.6
V	ppm	48	16	4	3	194	14	104
Zn	ppm	930	164	120	132	219	315	780
Ag/Au		87,250	37,500	86,500	-	9	7	2

Sampson mine (?); about 1.5 mi SW of Nevada City; NE¼ of NW¼ of sec. 29, T.6S., R.3W.

98JH12: Brecciated quartz vein with Fe-oxide staining. Chip samples (n=31) from adit entrance and waste piles.

Silver Bell mine; SW¼ of NE¼ of sec. 31, T.6S., R.3W.

98JH15: Fractured, hematitic quartz vein. Chip samples (n=30) from waste piles.

St. Lawrence Au-Ag mine; NW¼ of NE¼ of NW¼ of sec. 32, T.6S., R.3W

98JH14A: Brecciated quartz vein with Fe-oxide staining. Chip samples (n=30) from waste piles.

Bartlett mine - upper adit; NW¼ of NE¼ of sec. 14, T.7S., R.3W

96JH21: Massive dolomite.

96JH23: Magnetite-bearing quartz-carbonate.

96JH24: Gossan float from dump at main adit.

97JH09: Ore. Brecciated quartz veins stained with Fe-oxides.

**Table 2**—Continued.

D. NW- and EW-trending veins.

Mine		Brown's Gulch adit				Mapleton	Pacific		Hungry Hollow Gulch adit	
Sample		007AV94	007BV94	95JH35	95JH38	E9520	008AV94	008BV94	96JH57	96JH58
Ag	ppm	7	9	9	<5	99	<0.4	<0.4	122.6	0.5
As	ppm	23	10	2.5	1.2	41	<0.5	1	61	<0.5
Au	ppb	434	5,050	9,890	2,730	18,000	31	56	24,000	40
Ba	ppm	620	2,100	700	17,000	520	220	190	5,800	920
Ca	%	5	4	<1	<1	<1	1.66	1.77	0.01	1.99
Cd	ppm	6.2	32.9	n.d	n.d	n.d	<0.5	<0.5	1.1	<0.5
Co	ppm	9	9	81	95	94	1	<1	5	22
Cr	ppm	130	42	19	7	<5	6	6	21	120
Cu	ppm	139	403	n.d	n.d	n.d	12	278	1,111	163
Fe	%	4.08	4.16	1.68	0.58	0.16	0.47	0.56	2.9	5.05
Hg	ppm	<1	<1	<1	<1	2	<1	<1	<1	<1
K	%	4.78	4.85	n.d	n.d	n.d	3.9	3.68	0.03	2.06
Mg	%	1.69	1.96	n.d	n.d	n.d	0.04	0.04	0.01	1.57
Mn	ppm	881	869	n.d	n.d	n.d	53	63	410	532
Mo	ppm	3	5	5	7	10	<1	2	15	<1
Na	%	0.06	0.06	0.02	0.02	0.02	2.6	2.81	0.01	2.8
Ni	ppm	<20	67	<20	<20	<20	2	2	10	73
Pb	ppm	112	1,442	n.d	n.d	n.d	28	26	5,080	22
Sb	ppm	15	14	1.2	1.3	17	0.2	<0.1	100	0.4
Se	ppm	<0.2	0.8	0.4	0.2	0.4	<0.2	<0.2	0.2	<0.2
Te	ppm	0.6	1.4	0.2	0.2	1.9	0.2	0.2	2.7	1.0
Zn	ppm	1,370	2,800	320	4,100	520	14	7	1072	128
Ag/Au		16	2	1	-	6	-	-	5	13

Browns Gulch unnamed adit; SW¼ of SW¼ of sec. 28, T.6S., R.3W. Vein sampled trends east-west.

007AV94, 007BV94: Brecciated gneiss at vein deposit with quartz veins and iron oxide minerals

95JH035: Quartz vein with sulfide minerals

95JH038: Quartz with pyrite, chalcopyrite, and tetrahedrite(?)

Mapleton mine; NW¼ of SE¼ of sec. 9, T.6S., R.3W

E9520: Limonitic quartz vein from ore bin (tetrahedrite?)

Pacific mine; NW¼ of sec. 15, T.7S., R.3W. SE end of NW-trending curvilinear vein that continues to the Easton mine.

008AV94, 008BV94: Limonitic, sheared gneiss

Hungry Hollow Gulch unnamed adit in Archean gneiss; NE¼ of SE¼ of sec. 2, T.7S., R.3W.

Adit probably accessed the NNW-trending Pearl vein.

96JH57: Quartz vein ore (brecciated, vuggy, iron oxide mineral-stained) at adit.

96JH58: Archean gneiss country rock with brown carbonate veinlets.

Gneiss is interlayered with amphibolite in the outcrop.

### **Mapleton mine**

The Mapleton mine, located north of Nevada City on the north side of Alder Gulch, explored a northwest-trending quartz vein for gold. Tansley et al. (1933) mention the Mapleton ore body as one of many mines in the district where surficial enrichment was an important factor in producing minable metals. In other words, the oxidized zone of the orebody was exploitable, whereas the sulfide zone was not economic at the time. The mine was developed in 1939 on 2 patented and 6 unpatented claims as an underground mine that opened 1,200 feet of drifts and 150 feet of raises and shipped about 20 tons of ore a day (Trauerman and Waldron, 1940).

A limonitic quartz vein sample ran in gold (18,000 ppb), silver (99 parts per million (ppm)), antimony (17 ppm), and tellurium (1.9 ppm) (Table 2D). Copper and lead were not determined; zinc was measured at 520 ppm. The relatively high antimony content reflects the presence of tetrahedrite in the sample. Relative to the mines south of Alder Gulch, the rocks at the Mapleton workings showed more evidence of copper staining and opaline silica.

### **Browns Gulch area**

Three samples were collected at an unnamed adit along the west side of Brown's Gulch. The adit explored a quartz vein that appears to be about 10 ft wide and strikes approximately east-west, parallel to the foliation in the host rock gneiss at the surface. Farther into the workings, the vein appears to cross-cut the foliation. The vein carries sulfide minerals (pyrite, chalcopyrite, and tetrahedrite), and has an adularia-rich margin. Brecciated, iron-stained gneiss with quartz veins comprises the wallrock at the adit. The gneiss at this locality is leucocratic and biotite appears to be the only ferromagnesian silicate mineral present. Garnet-rich amphibolite is present as float on the hill above the adit. The gneiss is locally sheared and iron-stained. Two gneiss samples contain elevated, but highly variable concentrations of gold, copper, lead, and zinc (Table 2D). Agreement between the two samples is excellent

for some elements (9 ppm Co for both); the discrepancies in the metal analyses are probably due to a nugget effect. Sulfide-bearing quartz veins contain more than 2,000 ppb gold. Gneiss is elevated in tellurium and antimony relative to quartz vein samples.

The Easton and Pacific mines are located farther south, near the head of Brown's Gulch. Both mines worked splays of the same vein system within the aplitic body previously described as the Brown's Gulch stock; the vein system strikes N55° W and dips 70° NE, and the two veins reportedly join off to the southeast of the workings (Winchell, 1914; Cole 1983). The Easton-Pacific mines produced the largest tonnage of ore in the district. From 1902 to 1935, the mines yielded more than 22,000 ounces of gold and more than 750,000 ounces of silver (Lorain, 1937). The Easton mine, located about 0.5 mi (0.80 km) northwest of the Pacific workings, was worked to a depth of about 700 feet. The mines are no longer accessible. According to Winchell (1914), (1) the ore minerals included argentite, auriferous pyrite, native silver, tetrahedrite, gold, sphalerite, and stibnite in a gangue of quartz, orthoclase, hematite, and limonite; (2) the ore shoot decreased in thickness with depth; (3) the vein thickness varied from 18 inches to 6 or 8 feet; and (4) a fault defined the footwall of the vein. We did not observe any rock that we would call a quartz monzonite aplite exposed at the surface or in the dump materials; we did observe a lot of pegmatite in the area.

The vein at the Pacific mine reportedly contained antimony- and gold-bearing silver sulfide minerals in a gangue of quartz and iron oxides (Winchell, 1914). Lockwood et al. (1991) noted that precious metals are generally restricted to the veins in this area, but a low-grade halo is present around some of the veins and argillic alteration is pervasive in the Pacific mine area. They also report the only published fluid inclusion data for the district (see above). BHP-Utah and Hanover Gold reported drill intercepts of 295 ft of 0.132 ounces per ton (opt) gold at the Pacific mine (Hanover Gold, 1997). Two samples of limonitic, sheared gneiss from the Pacific mine area contained gold (31 and 56

ppb); silver is below detection limits (<0.4 ppm) (Table 2D). Copper is variable (12 and 278 ppm), and lead and zinc values were relatively low (<30 ppm). Bismuth and selenium are below detection levels; both samples contained 0.2 ppm tellurium. Both samples are potassium-rich (>3 wt. % K).

### **Alameda-Cornucopia-U.S. Grant mine area**

A number of historic mines exploited a series of northeast-trending quartz veins on the west side of Alder Gulch. These veins have been described as shallow, epithermal fissure veins that contained quartz, pyrite, arsenopyrite, tetrahedrite, argentite, galena, sphalerite, chalcopyrite, and electrum (McLeod, 1986). The U.S. Grant produced about 800 ounces of gold and 46,000 ounces of silver between 1908 and 1926; the Alameda mine produced a small amount of oxidized ore in the early 1900's. Underground workings exploited the gold-rich, near-surface oxidized zone. Ore grades are not continuous at depth; veins are generally offset by faults. In the 1980's, companies examined the possibility of reworking dumps from these mines and pursuing underground exploration, but no new mines have been developed to date. We sampled ore from the Bamboo Chief (Alameda mine) vein system, a stockpile of ore from the lower level of the U.S. Grant workings, and a variety of rocks from the Cornucopia mine.

Three different samples from a stockpile of Bamboo Chief included iron-stained quartz veins and silicified gneiss. All three samples contained gold (238 to 90,400 ppb), silver (42 to 1200 ppm), tellurium (0.7 to 5.5 ppm), and antimony (0.7 to 100 ppm) (Table 2A). One of the quartz vein samples is also anomalous in mercury (4 ppm), molybdenum (2,000 ppm), lead (29,910 ppm), and zinc (2,000 ppm). Sheets (1980) identified accessible economic (at that time) ore at several mine dumps on patented claims in the northern part of the district.

Two samples of pyrite-rich quartz vein ore were collected from a stockpile of ore extracted from the lower adit of the U.S. Grant mine. Both samples contain anomalous gold (>2,000 ppb), silver (>70 ppm), as well as a minor

element signature that includes antimony>tellurium>selenium (Table 2A).

Samples from the Cornucopia mine include pyrite-bearing quartz vein, red gossan, and garnetiferous amphibolite wallrock. With the exception of the amphibolite, all samples contain gold (340 to 10,300 ppb) and silver (7 to 210 ppm) (Table 2A). Relative to the quartz vein samples, the gossan is enriched in arsenic and zinc. The gossan contains an element suite that suggests a mafic-ultramafic rock association (chromium, nickel, PGE), although these elements are not enriched in the amphibolite.

### **Hungry Hollow Gulch**

Hungry Hollow Gulch follows a southwest-trending creek that splits off along the west side of Alder Gulch about 2.5 miles (4.0 km) south of Virginia City. Three locations were sampled along Hungry Hollow Gulch. From north to south, these include (1) an unnamed adit driven along a quartz vein in brecciated gneiss in a side gulch to the east of the main gulch; (2) a chloritized diabase dike exposed at the Black Hawk workings on the west side of the gulch and (3) sulfide-bearing quartz veins in gneiss along the High-Up Irene vein system near the head of the gulch. The unnamed adit explored a north-trending quartz vein in gneiss interlayered with amphibolite. Some exploration drilling was conducted at this adit in the past, but the findings are unknown to us. Brecciated, iron-stained quartz vein is anomalous in gold (24,000 ppb), silver (>100 ppm), copper (1,111 ppm), lead (>5,000 ppm), and zinc (>1,000 ppm). Antimony (100 ppm) and tellurium (2.7 ppm) are also anomalous for this vein sample. Host rock gneiss contains this same suite of elements in measurable concentrations, but below the concentrations present in the vein. For example, the gold concentration in the gneiss is 40 ppb.

The High Up and Irene vein systems are two parallel, northeast-trending vein systems at the head of Hungry Hollow Gulch, about 1 mile (0.6 km) northeast of the Marietta mine. Workings include several adits. Hadley (1969) showed the rock in this area as Precambrian granite and migmatite. The quartz vein sample contains

1,450 ppb gold, 4.1 ppm antimony, 0.5 ppm selenium, and 2.3 ppm tellurium. Copper and zinc are present at about 100 ppm and lead concentration is low (39 ppm). A stream sediment sample adjacent to the adit contained a small (67 ppb) amount of gold (Hammarstrom and Van Gosen, 1998).

### **Alder Gulch**

A number of sites were sampled along Alder Gulch north and east of the Kearsarge mine. These include the Bartlett mine area, the Millard tunnel, and an area of historic shafts and prospects east of the old townsite of Summit and north of Bachelor Gulch. At the Bartlett mine, adits are driven along a northwest-trending quartz vein that may have followed the contact of a thick dolomite bed. The dolomite forms a prominent cliff above the workings; this particular bed of dolomite is not shown on Hadley's (1969) map. Hadley shows northwest-trending dolomite beds within the "Cherry Creek" Group rocks that crop out to the west in Barton Gulch and Wier (1982) mapped numerous, mainly northeast-trending marble beds to the north. Massive dolomite is calcium-rich (>20 weight percent Ca), moderately magnesian (11 wt. % Mg); with the exception of moderate zinc concentrations (about 130 ppm), the dolomite is barren of metals (Hammarstrom and Van Gosen, 1998). Samples of magnetite-bearing quartz-carbonate rock from the caved adit area and gossan float from the mine dump both contained gold (70, 109 ppb) and other metals. These altered rocks contain approximately twice as much zinc as the dolomite. The zinc in the dolomite could be primary, or could be an overprint from fluid infiltration related to mineralization.

Quartz-sulfide ore from the Millard tunnel, at adits on the east side of Alder Gulch 0.8 mile (0.48 km) north of the Kearsarge Mine, contains over 3,000 ppb gold, but no detectable silver. These workings were driven eastward from Alder Gulch, probably to intersect the Kearsarge vein system. Similarly, a dump sample of highly fractured, limonitic gneiss from prospects north of Bachelor Gulch contains gold (>300

ppb), but no other anomalous metal concentrations.

Hanover Gold Company (1997) identified a number of targets along Alder Gulch. They reported drill core intercepts of 190 ft of 0.210 opt Au for the northeast-trending Kearsarge-Apex vein system, and other high-grade intercepts along veins to the north and east of the Kearsarge,

### **Western part of the district**

The Silver Bell, St. Lawrence, and Sampson mines exploited northeast-trending veins in the western part of the mining district. Chip samples of fractured, iron-stained quartz were sampled at all three localities. Trace amounts of gold (0.3 to 1 ppb) were detected in all three of the chip samples. The St. Lawrence mine accessed tabular quartz bodies up to 2 m thick and quartz veinlets in two parallel vein systems in fractured quartzofeldspathic gneiss. Wallrocks show pervasive potassic and carbonate alteration. Ore minerals include pockets of pyrite with minor galena and chalcopyrite (Cole, 1983). All three of these deposits were mined for gold and silver, mainly in the early 1900's. Some exploration work was conducted in the 1960's. A small amount of ore (680 tons) was mined from the St. Lawrence in 1980; ore grades for milky-white quartz and what was described as porphyritic sulfide ore were reportedly 0.160 opt Au and 2.50 opt Ag (Sheets, 1980).

### **Summary of vein geochemistry**

Gold is detected in all of the quartz vein samples, and in many of the associated rocks. Gold concentrations range from 0.3 to over 20,000 ppb. The only two samples that lacked detectable gold are an amphibolite at the Cornucopia mine and the massive dolomitic marble host rock at the Bartlett mine. Silver:gold ratios are variable (5:1 to 176:1) among the samples from northeast-trending veins in northern Alder Gulch (Table 2A). Other northeast- and northwest-trending veins have similar low Ag:Au ratios, with the exception of the three northeast-trending vein



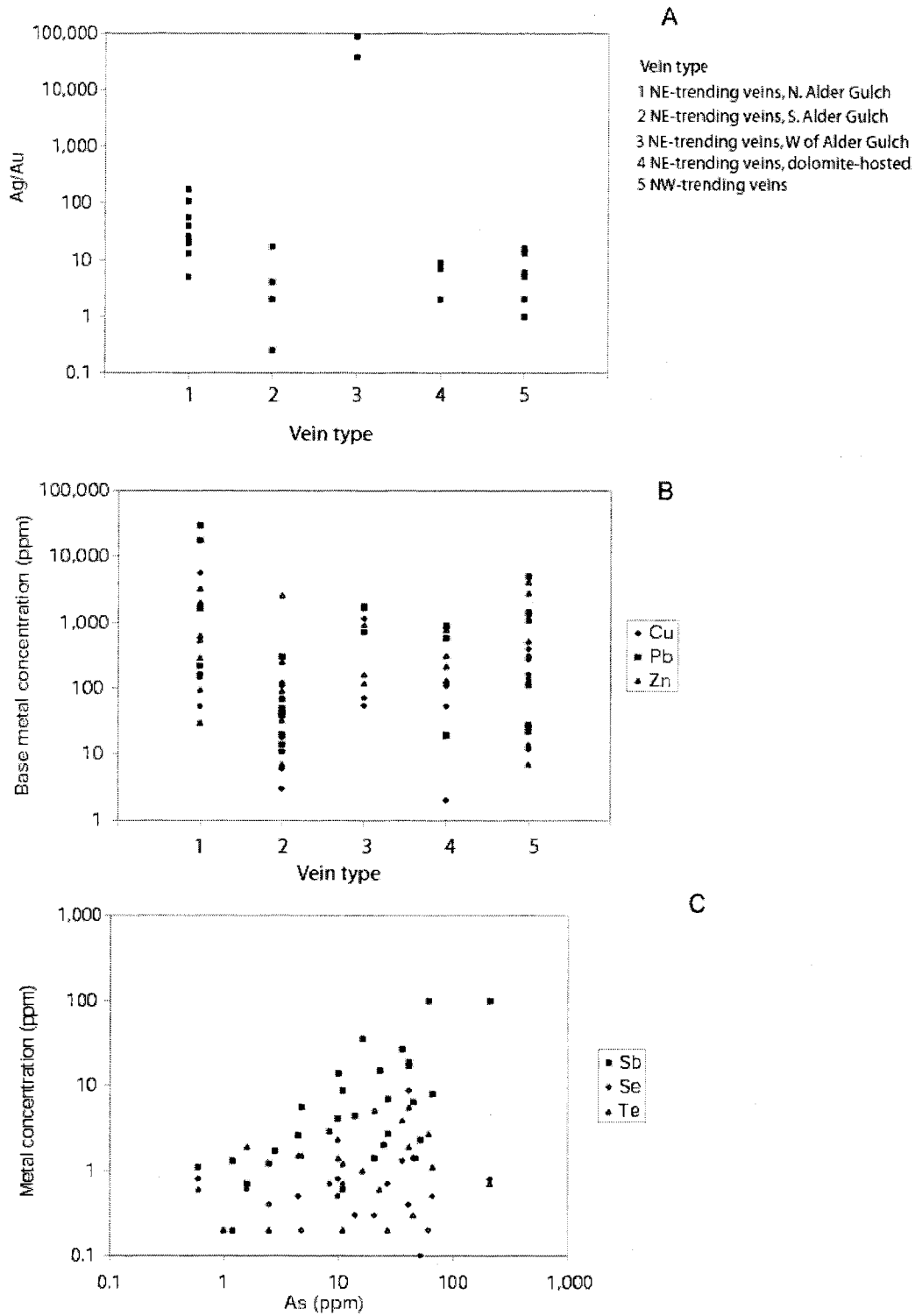


**Figure 4.** Geochemical data. A, Range of Ag:Au ratios plotted by vein subtype. B, Range of base-metal compositions plotted by vein subtype. C, Sb, Se, and Te concentrations plotted as a function of As content for all vein subtypes.

systems sampled in the westernmost part of the district, which all have Ag:Au>30,000:1 (Fig. 4A).

Base metal concentrations vary over several orders of magnitude (Fig. 4B). Zinc is the most reliable indicator of base metal occurrences because all samples were analyzed for zinc. Copper and lead are listed for some samples, but absence of a reported copper or lead value does not imply that the sample lacks these elements. Lead concentrations in northeast-trending veins in northern (N.) Alder Gulch range from 220 to over 10,000 ppm; northeast-trending veins in southern (S.) Alder Gulch contain <500 ppm lead (Fig. 4B). Maximum and minimum base-metal concentrations, as reported by Despotovic (2000) for drill core samples of northeast-trending veins in the southern part of Alder Gulch, are included in Figure 4B. Selenium and tellurium concentrations typically are less than 10 ppm. Antimony is positively correlated with arsenic (Fig. 4C). This trend in bulk vein composition reflects the fact that these two elements mainly are present in tetrahedrite-tennantite solid solutions.

Mercury is below detection limits for most samples. Samples from the ore bin at the Mapleton mine and from a stockpile of ore from the Bamboo Chief mine represent the most mercury-rich samples in our data set with values of 2 and 4 ppm Hg, respectively. Lockwood (1990) reported elevated mercury (2 ppm) in channel samples across the major veins in the Easton-Pacific; mercury was elevated in most gold-bearing samples.

### Leaching experiments

Passive leaching experiments simulate the behavior of mine materials exposed to precipitation and provide an indication of metal mobility and acid-generating versus acid-neutralizing characteristics of mine wastes. A variety of leach tests have been developed in recent years (Hageman and Briggs, 2000; U.S. Environmental Protection Agency, 1994). Our leach experiments are a modification of these methods. We used the same 20:1 liquid to solid ratio as other experiments with pure, rather than

acidified water, and performed the experiments on composites of ground (<100 mesh) material. The enhanced surface area on ground material promotes dissolution. Therefore, the dissolved metals analyzed for filtered leachates indicate a “worst case” scenario for the sample. Final leachate pH values (Table 3) for samples from the Bamboo Chief, Pacific, and U.S. Grant mine dumps are all neutral to alkaline. Low conductivity (SC) is compatible with observed low dissolved metal concentrations. Dissolved base-metal concentrations are elevated for the Bamboo Chief leachate relative to the other two samples. Elevated lead (5,611 ppb) probably reflects rapid dissolution of supergene minerals in the pile. Cerussite (PbCO<sub>3</sub>) occurs with goethite and quartz in oxidized Bamboo Chief ore. Cerussite is slightly soluble in neutral water (0.00011 g/cc). Dissolution of cerussite and other secondary minerals in oxidized ore on the dump may contribute very minor amounts of base metals to surface runoff.

**Table 3.** Leachate chemistry.

	Mine dump	Bamboo Chief	Pacific	U.S. Grant
pH		9.2	9.9	7.5
SC	uS/cm	59	65	46
Al	ppb	0	56	0
As	ppb	0.07	0.08	0.26
Ba	ppb	116	1.6	154
Ca	ppb	2,439	3,066	1,669
Cd	ppb	4.7	0.028	0.74
Co	ppb	122	0.087	299
Cu	ppb	544	0.73	0.16
Fe	ppb	15.5	47	21.7
Hg	ppb	<0.2	<0.2	<0.2
K	ppb	414	2,980	729
Mg	ppb	480	141	417
Mn	ppb	78	0.84	3.8
Na	ppb	596	1,051	664
Ni	ppb	1.6	0.28	1.3
Pb	ppb	5,611	<0.1	0.94
Sb	ppb	0.08	0.03	0.69
Se	ppb	4.9	<0.2	0.77
Si	ppb	289	566	528
Ti	ppb	0.28	0.56	0.56
Tl	ppb	0.012	0.011	0.009
W	ppb	<0.01	<0.01	68
Zn	ppb	355	<0.5	4.4

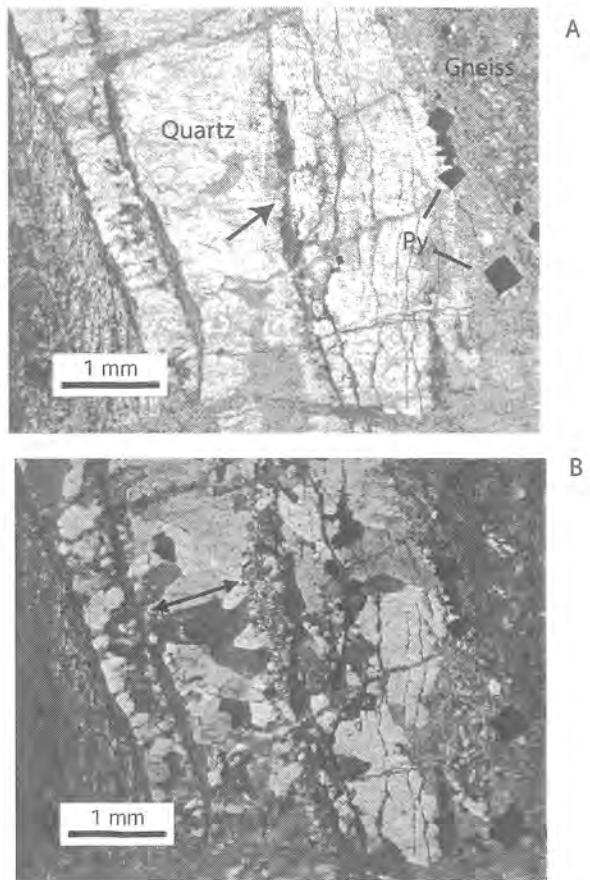


**Figure 5: Vein textures.** **A**, Comb-textured quartz veins cutting gneiss at an unnamed adit along Brown's Gulch, sample 96JH68. Note the euhedral pyrite cubes along vein selvages. Late ankerite stringers parallel and crosscut the quartz vein. The arrow points to an area of brecciated quartz adjacent to an ankerite vein. Plane polarized light. **B**, Same view in crossed nicols shows orientation of coarse quartz crystals perpendicular to the vein wall.

Many of the quartz veins observed on the surface and in dump materials show textures typical of epithermal to mesothermal vein systems, such as open-space growth, vugs, and doubly terminated euhedral quartz crystals, as well as evidence for brittle deformation such as brecciated pyrite grains. Masses of doubly terminated quartz crystals cemented by limonite and siderite are common on the dumps at the Easton mine and at workings along Hungry Hollow Gulch. Barnard (1993) referred to this texture as "candle-quartz". He noted that this texture is especially common in upper Alder

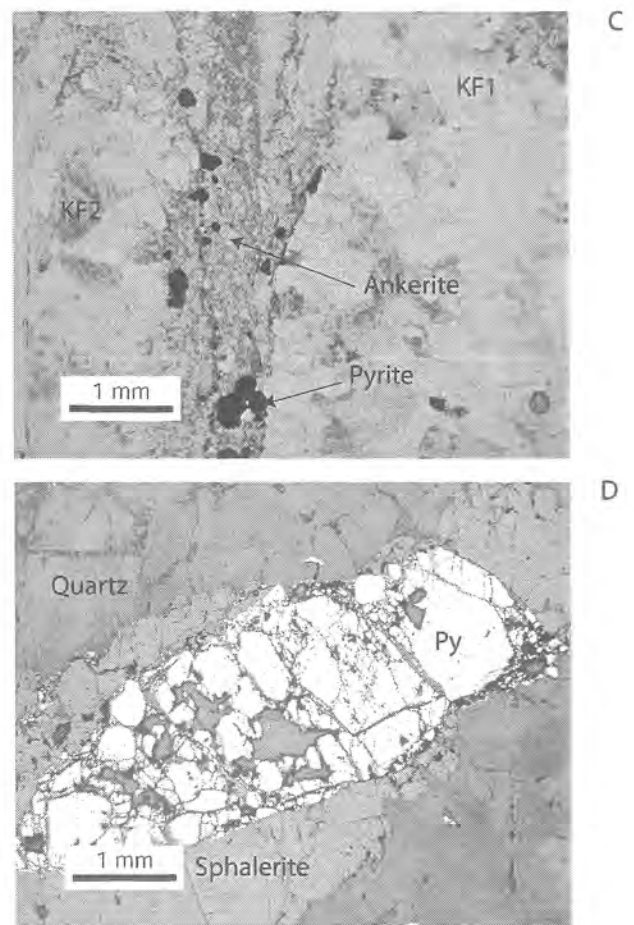


**Figure 5. C**, Pervasive potassic alteration in gneiss in drill core from the Oro Cache vein system. Note the two generations of potassium feldspars. KF1, cloudy, Fe-rich orthoclase that replaces plagioclase; KF2, microcline. **D**, Brecciated pyrite enclosed by unbroken sphalerite in a quartz vein from the Kearsarge 7,000-ft-level mine dump. Sample 96JH07, reflected light. Mineralogy

Gulch, associated with a distinct episode of mineralization that deposited gold, pyrite, and telluride minerals. Lockwood (1990) described three types of quartz veins in the district: (1) euhedral to subhedral syntaxial quartz crystals oriented perpendicular to vein walls; (2) narrow, sheeted white to gray quartz veins in gneiss with selvages of salmon pink potassium feldspar; and (3) bull quartz veins along northwest-trending fractures. Figure 5 illustrates typical vein textures.

Hydrothermal alteration associated with the veins includes pervasive potassic alteration in and along the veins. Alteration haloes are narrow due to the relative impermeability of the quartzofeldspathic gneiss. Potassium feldspar in gneiss adjacent to veins typically is a distinctive salmon pink to brick red color. Red, hematite-stained potassium feldspar is a common feature of potassic alteration in felsic wallrocks near lode gold deposits; chlorite alteration is common where the protolith contains biotite or hornblende (Siems, 1991). Masses of nearly monomineralic salmon-colored potassium feldspar are associated with the quartz veins at the Kearsarge mine (Merlin Bingham, oral communication, 1993). Samples taken through the mineralized zone in drill core (average grade 4,000 ppb Au) from the Oro Cache vein illustrate the complex interleaving of heterogeneous protolith and variable styles of alteration. Textures vary from very weakly foliated fine-grained granitic gneiss to moderately foliated, coarse-grained, quartz-rich gneiss to pegmatite. The mineralized zone was intercepted at a depth of 380 ft. At 293 ft, weakly foliated granitic gneiss is composed of albite, weakly perthitic potassium feldspar ( $Or_{96}$ ), chloritized hornblende, rare biotite, blocky hematite, and partly rounded to equant 0.2 mm long zircons; veins and sulfide minerals are absent. Well within the mineralized zone at 454 ft, plagioclase is obliterated and the rock is an intimate intergrowth of microcline, cloudy orthoclase that replaces albite, quartz, and sericite cut by potassium feldspar veins that carry sulfide minerals and grade into ankerite veins (Fig. 5A). Microcline typically is alteration-free, and contains 0.5 to 1 wt. % BaO, 0.1 to 0.3 wt. %  $Na_2O$ , and <0.1 wt. % FeO (total iron reported as FeO). The cloudy, red potassium feldspar is as orthoclase-rich as the microcline, but contains higher concentrations of FeO (Fig. 6). These feldspars exhibit the same complexities that confounded Cole (1983) in his attempt to date the feldspar at the U.S. Grant mine. Iron-poor adularia ( $Or_{99}$ ) forms thin selvages or protrudes into quartz veins in samples from the unnamed adit driven into a northeast-trending quartz vein along Brown's Gulch. Millimeter-scale quartz veins parallel the foliation defined by mica pseudomorphs (altered to carbonate and clay) in pervasively altered

pyritic gneiss (Fig. 7). Dating of the adularia (in progress) should provide a reliable age for at least one of the episodes of potassic alteration associated with northeast-trending vein systems in the district.

Green sericite from pervasively altered (sericite-carbonate) quartzofeldspathic gneiss sample (98JH08) from the 7000-ft-level mine dump of Kearsarge mine was used to date the vein system. The sericite is itself deformed (bent around recrystallized, boudinaged quartz grains) and affected by late carbonate alteration. Microprobe analyses indicate that the sample contains sericite (Table 4A); however, parts of some grains approach an altered biotite composition. Sample 98JH08 lacks chlorite, which is the typical alteration product of most biotite. Minor substitution of chromium and vanadium explains the pale green color of the sericite. Unaltered, iron-rich (22 wt. % FeO), Cr-poor brown biotite is ubiquitous in garnetiferous gneiss in the host rock at the unnamed adit in Hungry Hollow Gulch and away from veins in other parts of the district.

Pyrite is the dominant sulfide mineral observed in all of the vein samples, with minor amounts of chalcopyrite, tetrahedrite, sphalerite, and galena. Other studies have reported a variety of additional ore minerals, including argentite, pyrrargyrite, nagyagite ( $Pb_5Au(Sb,Bi)Te_2S_6$ ), stibnite, sylvanite, and gold. We did not observe free gold in any samples, although many of the whole-rock samples contain anomalous gold (Table 2). The sulfide minerals are disseminated in the altered host rock adjacent to quartz veins, aligned along quartz vein selvages, or included within the quartz veins. No veins of sulfide minerals have been observed. Pyrite forms euhedral cubes along quartz veins (Fig. 5A); within brecciated veins exhibiting cataclastic quartz textures, pyrite is brecciated. Sphalerite engulfs brecciated pyrite (Fig. 5D) in ore from the Kearsarge mine, and tetrahedrite fills in open space between brecciated pyrite and sphalerite. The base-metal sulfide minerals (chalcopyrite, sphalerite, galena) do not appear to be brecciated, and were probably deposited in open spaces following brittle fracture of an earlier quartz-pyrite stage of mineralization.

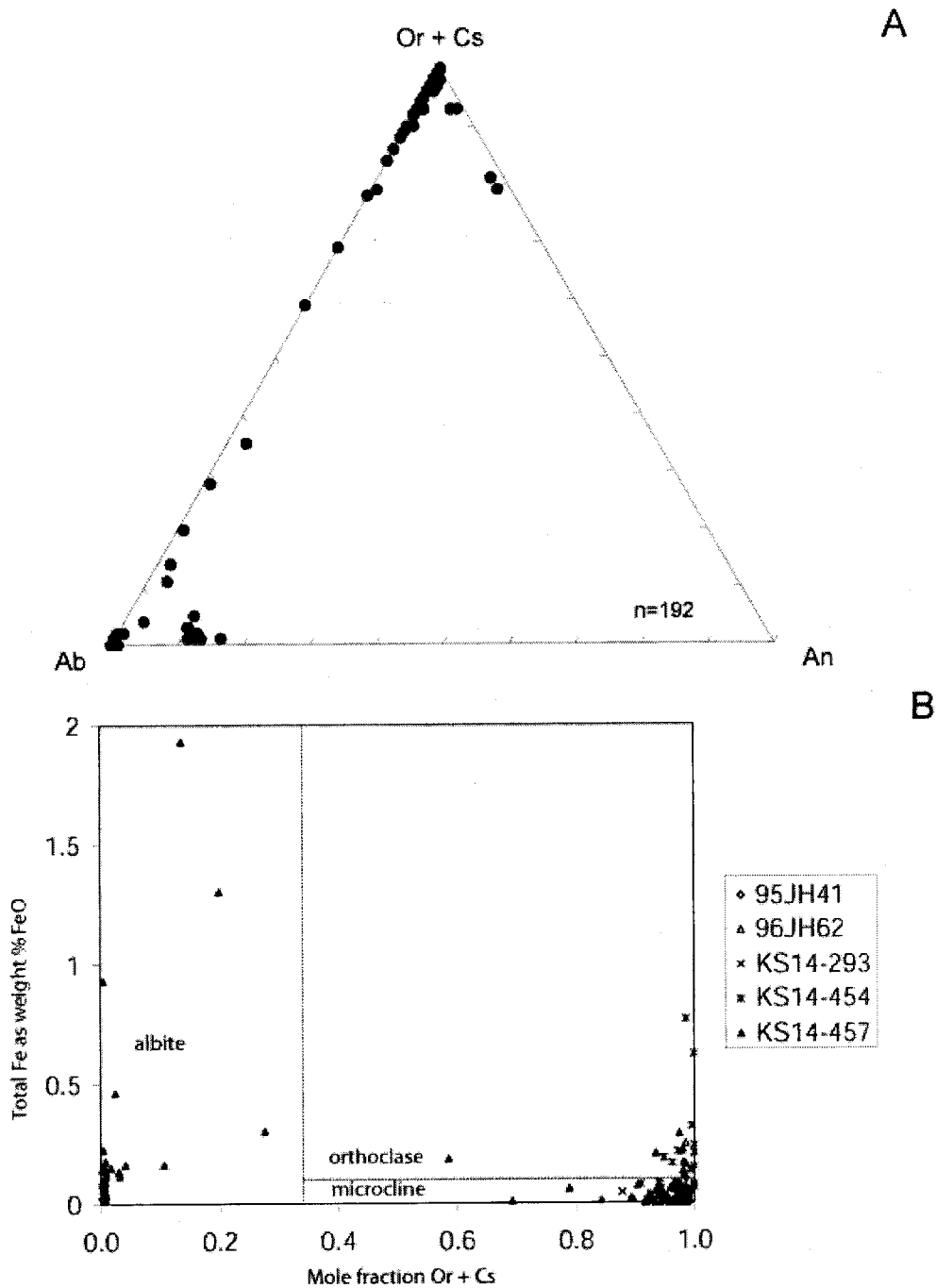


**Figure 6.** Feldspar compositions determined by electron microprobe. **A**, Ternary diagram showing the range of feldspar compositions for all six samples plotted in **B**. **B**, Plot of total iron (as FeO) in feldspars as a function of orthoclase (Or) plus celsian (Cs) content. The detection limit for FeO in feldspars is about 0.025 wt. %. The vertical dotted line separates albitic plagioclase from K-feldspar compositions; the horizontal dotted line at 0.1 wt. % FeO separates cloudy red orthoclase from microcline. “KS” samples are from drill core through mineralized quartzofeldspathic gneiss in the Oro Cache vein system at the depths indicated. Samples 95JH41 and 96JH62 are from Brown’s Gulch and the High Up mine, respectively.

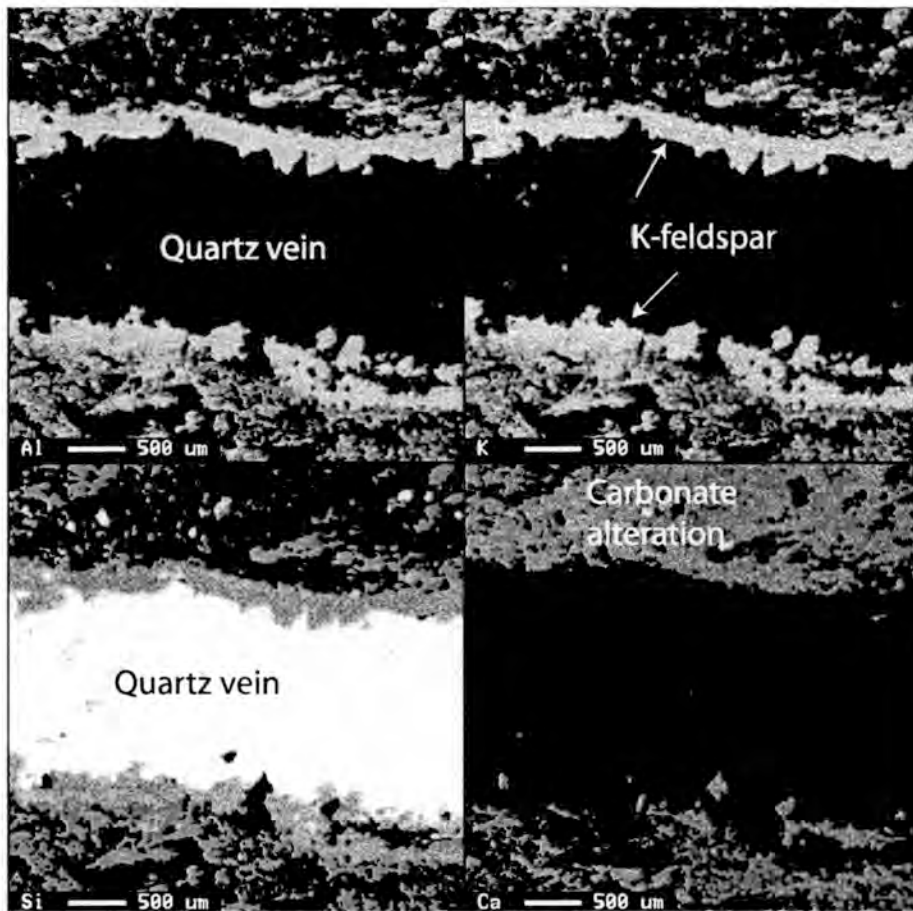


Figure 7

X-ray map showing K-feldspar rim on quartz vein in sample 95JH41 from an unnamed adit along Brown's Gulch. Point analyses of vein material are plotted in figure 6. White and lighter shades of gray represent higher concentrations of the element of interest. Note the pervasive nature of the carbonate alteration in the host rock, as indicated by the high Ca concentrations exterior to the K-feldspar vein selvage.

Representative sulfide mineral compositions are reported in Table 4. The tetrahedite-group mineral noted in Kearsarge ores in previous studies is an iron-poor sulfosalt mineral of intermediate composition between tetrahedite  $[(\text{Cu},\text{Fe},\text{Ag},\text{Zn})_{12}\text{Sb}_4\text{S}_{13}]$  and tennantite  $[(\text{Cu},\text{Fe},\text{Ag},\text{Zn})_{12}\text{As}_4\text{S}_{13}]$ , with an average composition of  $[(\text{Cu}_{9.4}\text{Fe}_{0.03}\text{Ag}_{0.3}\text{Zn}_{2.3})_{12}(\text{Sb}_{2.3}\text{As}_{1.6})_{3.9}\text{S}_{13}]$ . Tetrahedite is in contact with iron-poor sphalerite. Sphalerite contains minor amounts of cadmium. Pyrite is essentially stoichiometric  $\text{FeS}_2$ . Pyrite from the Pacific mine area averages 0.2 weight percent arsenic; other pyrites do not appear to be arsenic-enriched. During some analytical sessions, gold

was included in the analysis package. Under the operating conditions used, the detection limit for gold in sulfides is about 100 ppm (0.001 wt. %). Scanning the polished sections in backscattered-electron scanning electron microscope mode and x-ray mapping of sulfides failed to identify discrete grains of gold. Ion probe or laser-ablation mass spectrometry techniques would be ideal for examining the mineralogic residence of gold and trace metals in the sulfides.

#### $^{40}\text{Ar}/^{39}\text{Ar}$ dating

Suitable materials for radiometric dating of the Virginia City lode veins are difficult to find.

**Table 4.** Mineral chemistry\*.

## A. Electron microprobe analyses of micas from the Kearsarge vein system.

	Sericite		Altered biotite	
	Average n=9	S.D.	Average n=6	S.D.
SiO <sub>2</sub>	52	1	39	3
Al <sub>2</sub> O <sub>3</sub>	28	1	20	2
TiO <sub>2</sub>	0.07	0.08	0.68	0.9
Cr <sub>2</sub> O <sub>3</sub>	0.13	0.18	0.19	0.2
V <sub>2</sub> O <sub>3</sub>	0.24	0.1	0.32	0.2
FeO	2.9	0.5	10.3	1.3
MgO	2.6	0.2	7.0	1.8
MnO	0.02	0.02	0.08	0.05
CaO	0.01	0.01	0.04	0.04
Na <sub>2</sub> O	0.13	0.10	0.08	0.08
K <sub>2</sub> O	10.0	0.3	7.7	0.5
BaO	0.10	0.1	0.01	0.02
F	0.24	0.2	0.35	0.12
Cl	0.02	0.02	0.005	0.01
Total	96		86	

## B. Electron microprobe analyses of sulfide minerals.

Mine	Kearsarge	Kearsarge	Kearsarge	Brown's Gulch	Pacific	Millard tunnel
Sample	96JH7	96JH7	96JH8	95JH41	95JH48	95JH55
Mineral	tetrahedrite n=8	sphalerite n=14	pyrite n=7	pyrite n=20	pyrite n=12	pyrite n=9
Fe	0.135	0.170	46.756	46.877	46.859	46.659
Co	0.002	0.004	0.058	0.083	0.084	0.099
Zn	9.380	65.100	0.024	0.073	0.013	0.006
Cu	37.149	0.149	0.006	0.021	0.023	0.018
Pb	0.000	0.000	0.000	n.d.*	n.d.	n.d.
Se	0.025	0.011	0.002	0.006	0.007	0.009
As	7.421	0.007	0.039	0.093	0.233	0.100
Cd	0.108	1.242	0.000	0.011	0.008	0.007
Sb	17.121	0.036	0.001	0.006	0.002	0.010
Ag	2.305	0.000	0.007	0.009	0.007	0.010
Te	0.000	0.000	0.000	0.001	0.004	0.003
Mn	0.003	0.001	0.001	0.031	0.043	0.025
Au	0.007	0.002	0.008	n.d.	n.d.	n.d.
S	25.920	32.614	51.436	52.291	52.081	52.263
Total	99.575	99.335	98.338	99.502	99.363	99.209

\*n, number of analyses; S.D., standard deviation; n.d., not determined

Because of the difficulties of obtaining clean separates of intimately intergrown primary and secondary potassium feldspars, we attempted to date the distinctive green sericite at the Kearsarge mine. A mica sample (98JH08) was incrementally heated in twelve steps from 650°C to 1250°C. The data are presented in Table 5 and Figure 8. The age climbs from 115.9 Ma in the 650°C step to 159.8 Ma in the 1250°C step. The age spectrum developed two age plateaus,  $120.17 \pm 0.65$  Ma in the 650°C and 850°C steps, and  $120.68 \pm 0.65$  Ma in the 850°C -950°C steps. The age plateaus were determined using the definition of Fleck et al. (1977), as modified by Haugerud and Kunk (1988). The climb in

age in the higher temperature steps of the age spectrum suggests that the sample may have incorporated excess argon. Inverse isotope correlation analysis of the age spectrum data using the method of York (1969) indicates an apparent age of  $115.5 \pm 3.8$  Ma, with MSWD = 0.138, and initial  $^{40}\text{Ar}/^{36}\text{Ar} = 513 \pm 103$ . The calculated initial  $^{40}\text{Ar}/^{36}\text{Ar}$  is well above the current atmospheric value of 295.5, again suggesting the presence of excess argon. Because the inverse isotope correlation age is not different from the plateau ages at the two-sigma level, and because of the probability that the sample contains excess argon, we prefer the older of the two plateau ages,  $120.2 \pm 0.7$  Ma, as

**Table 5.** Age spectrum data for sericite sample 98JH08 (Kearsarge mine).

Temp (°C)	$^{39}\text{Ar}$ (% Total)	$^{40}\text{Ar}^*$ (%)	$^{39}\text{Ar}$ ( $\times 10^{-12}$ mol)	$^{40}\text{Ar}^*/^{39}\text{Ar}$	K/Ca	K/Cl	Apparent Age (Ma) and error ( $\pm 1\text{s}$ )	
650	12.9	37.9	0.07727	6.651	47	32	115.86	2.81
850	44.3	94.7	0.26661	6.915	146	900	120.31	0.52
900	8.8	90.4	0.05281	7.196	85	552	125.02	2.6
925	4.9	87	0.02927	7.44	63	315	129.11	4.49
950	4.2	82.6	0.02507	7.571	43	269	131.31	5.67
975	4.1	84.2	0.02488	8.181	76	251	141.48	6.48
1000	4.3	80.6	0.02600	8.312	94	239	143.66	5.71
1050	5.3	75.8	0.03216	7.784	87	178	134.88	4.74
1100	2.6	85.3	0.01570	7.001	53	125	121.76	8.6
1150	2.1	88.2	0.01285	8.135	46	3	140.72	10.24
1200	2.9	96	0.01759	8.08	25	66	139.8	8.29
1250	3.5	90.4	0.02113	9.286	26	169	159.78	6.82
Total Gas	100	83.6	0.60132	7.264	99	519	126.7	

57.19% of gas on plateau in 650 through 850 steps. Plateau Age =  $120.17 \pm 0.65$

62.15% of gas on plateau in 850 through 950 steps. Plateau Age =  $120.68 \pm 0.65$

Ages calculated assuming an initial  $^{40}\text{Ar}/^{36}\text{Ar} = 295.5 \pm 0$

All precision estimates are at the one sigma level.

Ages of individual steps do not include error in the irradiation parameter J.

No error is calculated for the total gas age.



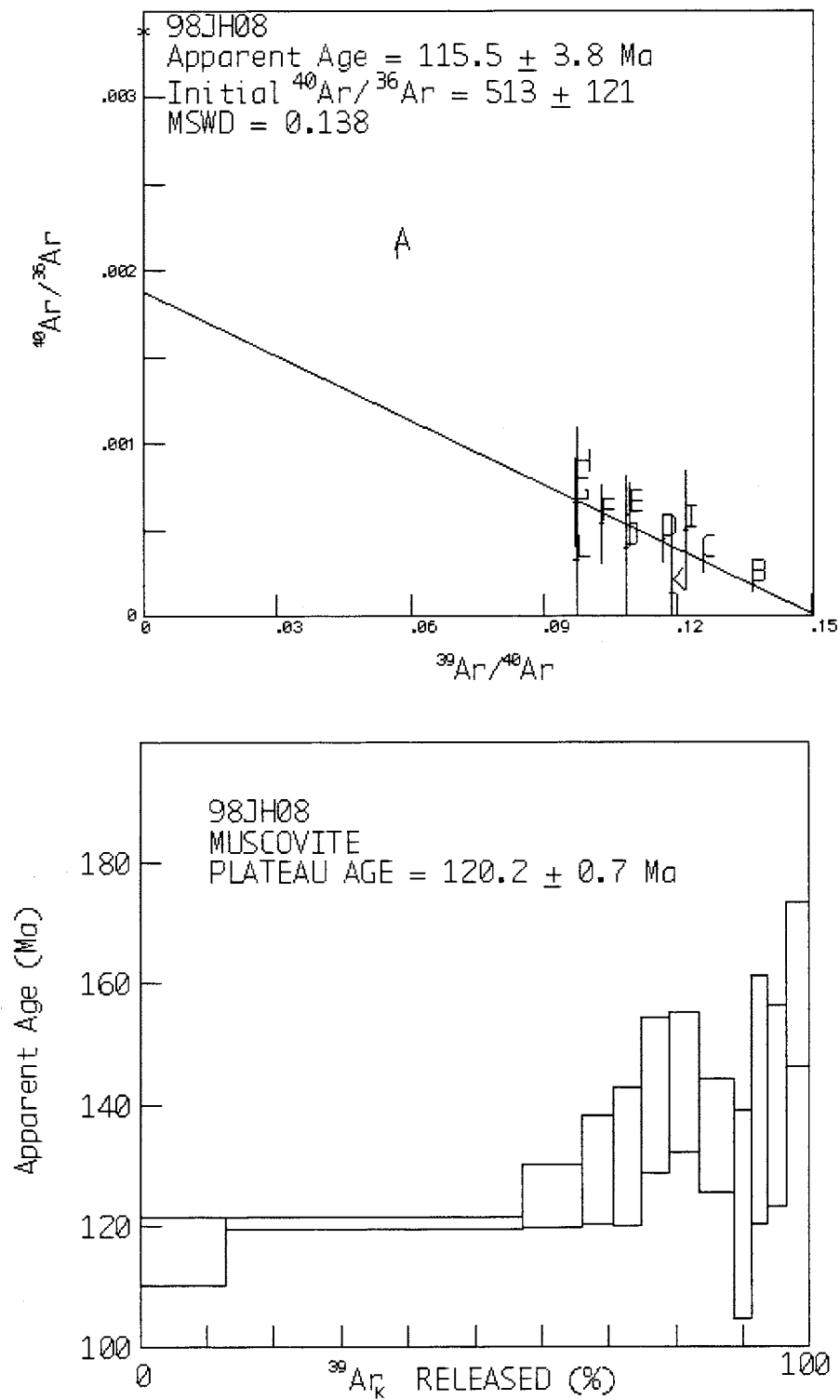


Figure 8. Age spectrum and correlation diagram for sericite sample 98JH08 from the Kearsarge mine.

the age of this sericite. The sericite is thought to have crystallized above its closure temperature for argon diffusion (~350°C), based on the apparent lower temperatures of mineralization in the district implied by Lockwood's (1990) fluid inclusion data for the Pacific mine. If the sericite crystallized at temperatures above its closure for argon diffusion, this age represents a minimum age for the time of its emplacement.

## DISCUSSION

The 120 Ma age on green sericite at the Kearsarge mine is difficult to interpret in light of the regional geology, because it does not coincide with any known geologic events in the area or region. The apparent age post-dates the 1.6 to 1.9 Ga Proterozoic regional metamorphic events and the age of pegmatites in the district, and predates the onset of Laramide tectonism and emplacement of Late Cretaceous batholiths. The age indicates that alteration associated with the northeast-trending Kearsarge vein system predates the Late Cretaceous Tobacco Root batholith, but does not rule out a much older age. Paleozoic rocks that unconformably overlie Archean gneisses at the head of Alder Gulch are not mineralized or altered to a significant extent.

Hammarstrom and Van Gosen (1995) evaluated geochemical signatures of different vein systems in the region and showed that gneiss-hosted veins in the Virginia City and Revenue districts are gold- and zinc-rich relative to quartz veins associated with iron formation in the Cherry Creek district. Relative to the Revenue and Blacktail districts, the Virginia City district veins have relatively more antimony and less tellurium. All of the vein systems sampled in the region are apparently enriched in arsenic relative to antimony or tellurium.

Geochemical data provide clues to deposit type, and also indicate the presence or absence of metals that can be detrimental to the environment, such as arsenic, cadmium, chromium, mercury, selenium, and lead. Consideration of the presence or absence of such elements, along with knowledge of the mineralogy and nature of the host rock for a particular deposit, can be used to qualitatively

assess the potential for negative environmental impacts on aquatic ecosystems, should further development occur. Low-sulfide gold quartz veins are among the less likely types of mineral deposits to develop significant acid drainage because near-surface deposits are typically sulfide-poor. Most of the historic lode gold workings in the Virginia City district exploited near-surface, oxidized parts of quartz vein systems and did not develop deeper, more sulfide-rich levels because gold grades dwindled to subeconomic values, given the ore-processing techniques of that era. In addition, carbonate minerals (dolomite or siderite) are present in many of the vein alteration assemblages and these minerals, though less reactive than calcite, may help neutralize any acidity generated by pyrite oxidation. This does not imply that tailings or drainages in contact with historic tailings are necessarily benign. A summary of abandoned hardrock mine priority sites by the Montana Department of State Lands identified a number of inactive or abandoned mine sites on both public and private lands in Beaverhead and Madison Counties that have tailings or waste rocks on-site that contain elevated metal concentrations (Pioneer Technical Services, 1995). At some sites, surface water or sediment discharges exceeded chronic aquatic life criteria for some elements. The priority sites are generally in mining districts that experienced extensive historic mining activity (Norris, Pony, Virginia City) and no seasonal monitoring of water quality over time was included in the study. The data reported for the mines in the Virginia City district indicate near-neutral pH conditions, and few instances where surface water concentrations of lead or mercury exceed standards (minimum contaminant levels for drinking water (MCL) or chronic aquatic life standards). Elevated mercury in surface water probably represents an anthropogenic source because historically, mercury was used to amalgamate gold.

Field measurements of surface water and adit drainage during our reconnaissance of the district corroborate the previous water quality information and the leachate data. The stream in Butcher Gulch, a former placer area northeast of the Kearsarge mine area, had a pH of 8 and low

total dissolved solids (300  $\mu\text{S}/\text{cm}$ ) when sampled in July, 1996. Adit water at the High Up mine site had a pH of 7.4, and specific conductance of 213  $\mu\text{S}/\text{cm}$ . Pristine mountain streams have specific conductance values in the range from about 10 to 100  $\mu\text{S}/\text{cm}$ ; drinking water may have specific conductance values of 500  $\mu\text{S}/\text{cm}$  or less (Ficklin and Mosier, 1999).

Compared to the types of mineral deposits present in other parts of Montana, most of the lode gold deposits in the Virginia City district are unlikely to pose significant threats to aquatic ecosystems in the form of acidic water generation or release of toxic metals if near-surface, oxidized ores are processed by heap leach methods. Most of the environmental concerns associated with such operations are likely to be related to land disturbances, cyanide use, and historic use of mercury in mineral processing. For low-sulfide quartz vein deposits, both mined and unmined, the low abundance of sulfide minerals and the presence of widespread acid-neutralizing carbonate alteration generally prevent development of significant acid drainage in associated surface waters (Ashley, 2002; Goldfarb et al., 1995). More significant amounts of sulfide minerals may be present at deeper levels in the veins, and underground development could pose risks for acidic drainage to develop. However, the precious metal content of the sulfide-rich zones may be too low grade and the discontinuous nature of many of the vein systems may not provide sufficient ore tonnage to warrant economic underground exploitation.

## MINERAL DEPOSIT MODELS

One of the difficulties in classifying the vein deposits in southwest Montana is that they are hosted by Archean gneisses in structurally complex terranes and many deposits lack an apparent association with an igneous intrusive center. The mineral assemblages, geochemical signatures, associated gold placer deposits, and pervasive carbonate alteration of the Virginia City deposits are all characteristics typical of low-sulfide gold vein deposits (Klein and Day, 1994). Veins are structurally controlled and are related to regional metamorphism and tectonics.

Many of the mineralized veins follow long-lived major structures that have been active intermittently since Archean time. Lockwood et al.'s (1991) fluid inclusion data from quartz at the Pacific mine is consistent with other low-sulfide lode gold deposits (low salinity fluid inclusions,  $\delta^{18}\text{O}$  of inclusion water in the range +10 to -60 per mil). Differences in wallrock alteration style (chlorite in more mafic rocks, for example) are characteristic of metasomatic reactions between hydrothermal fluids and diverse wall rocks in other epigenetic gold-bearing quartz veins in metamorphic terranes (Bohlke, 1989).

Grade and tonnage statistics for the Virginia City district are incomplete. However, Lorain's (1937) data show that the Easton-Pacific mine, the largest producer in the district, produced 70,049 tons (63,548 metric tons) of hypogene and oxidized ore between 1902 and 1935. Average gold grade was 0.32 ounces per ton (10 g/metric ton). Other mines in the district (U.S. Grant, Winnetka, Marietta) produced much lower tonnages (<3,000 short tons) with higher average gold grades (up to 56 g/t Au). These grade and tonnage data compare favorably with grade and tonnage distributions for well-characterized deposits used to construct grade and tonnage models. Tonnages for Archean low-sulfide Au-quartz vein deposits range from 0.008 to 100 million metric tons with a median size of 1.1 million metric tons; gold grades range from about 4 to 17 g/t with a median gold grade of 8.5 g/t (Klein and Day, 1994).

Genetic models for low-sulfide (Motherlode type) gold quartz veins indicate that arsenic typically is the best pathfinder element. In low-sulfide gold quartz veins, silver, arsenic, gold, and iron are consistently anomalous; tungsten and antimony are less consistently anomalous, and some deposits are anomalous for bismuth, copper, mercury, lead, zinc, tellurium, and (or) molybdenum (Berger, 1986; Goldfarb et al., 1995). Soils and sediments near unmined deposits may contain elevated arsenic (50 to 1,000 ppm) or antimony (>5 ppm) (Goldfarb et al., 1995). Such vein systems are zoned vertically and shallower deposits may contain anomalous mercury whereas arsenic, tungsten,

and iron are more typical of deeper, hotter parts of vein systems (greenschist- to amphibolite-facies conditions).

Veins in the westernmost part of the district have higher Ag:Au ratios and higher base-metal contents than the deposits along Brown's Gulch and Alder Gulch. Based on our data set, NE-trending veins in the northern part of Alder Gulch appear to be enriched in silver and base metals relative to NE-trending veins sampled to the south (Fig. 4). The Virginia City vein systems have no apparent connection to the Tobacco Root batholith or to any identified intrusive center. Hydrothermal events related to Proterozoic magmatism represented by the granite dikes, the intrusion (?) at the Easton-Pacific mine, and associated pegmatites are not necessarily genetically related to the lode gold deposits. Granitic magmas may have used the same regional-scale shear zones that host the quartz veins. Gold may have been episodically deposited and concentrated along long-lived reactivated structures over significant periods of geologic time. Encapsulation of brecciated pyrite within unbrecciated base-metal sulfide minerals suggests that the character of the hydrothermal fluids changed over time.

The fact that copper, lead, and zinc were produced from some of the Virginia City vein systems argues against a low-sulfide gold quartz vein model. Most of the mines produced only gold and silver. The NW-trending Easton-Pacific vein systems and NE-trending veins in the western part of the district may eventually be shown to better fit a gold-rich polymetallic vein model, or an overprint of base-metal rich mineralization upon an earlier low-sulfide gold-quartz vein system. Although chalcopyrite, galena, and lead are identified in many samples, they fill open space in previously brecciated samples (Lockwood, 1990; this study). Ashley (2002) noted that in some relatively base-metal rich and high-silver low-sulfide gold-quartz vein deposits, silver is present in tetrahedrite. Important ore-related minerals for all low-sulfide gold-quartz vein deposits, in decreasing order of abundance, include pyrite, galena, arsenopyrite, chalcopyrite, sphalerite, pyrrhotite, stibnite, tetrahedrite, and scheelite (Bliss and

Jones, 1988). Thus, the observed mineral assemblages in the district are compatible with this model. Until a detailed ore genesis study is conducted and additional ages are acquired, models for the lode deposits in the Virginia City mining district will continue to be debated. A district-scale structural analysis in light of evolving models of southwest Montana tectonics and characterization of fluid inclusions in different types of vein systems, as well as additional dating and documentation of alteration assemblages, are needed to evaluate the nature of the lode vein systems. The prominent NW- and NE vein orientations in the district parallel long-active Precambrian basement structures that are now being recognized as controls on emplacement of magmas and localization of mineral deposits in western Montana (Sims et al., 2002). Crustal-scale shear zones are an important control on the locus of orogenic gold deposits (Groves et al., 1998; Eisselohr et al., 1989), a term that includes deposits that have been described by a variety of names in the past (mesothermal gold, Mother lode type, Homestake-type low-sulfide gold, quartz-carbonate lode, turbidite-hosted gold, synorogenic gold, structurally-hosted vein systems in metamorphic terranes). Available data indicate that many of the Virginia City lode gold deposits, such as the Kearsarge-Oro Cache vein systems, represent a gneiss-hosted variant of existing models of structurally controlled low-sulfide gold quartz veins. These types of deposits are associated with significant placer gold deposits in many other parts of the world.

## ACKNOWLEDGEMENTS

We would like to thank Bill Neal and Merlin Bigham, formerly with Hanover Gold Corporation, for discussions of the deposits in the Kearsarge area and for providing samples. Joe Bardswich offered insights on the mines in the northern part of the district. Paul Eimon graciously shared his ideas and background information on the southern part of district. Guyon Saunders allowed us access to the former King of Kings claim area in upper Alder Gulch and allowed us to examine core from that part of the district. USGS colleagues Jim Elliott and Ed DeWitt participated in field studies and shared

their observations. Larry Drew and Harvey Belkin provided helpful reviews of this paper. Discussions with Larry Drew provided numerous insights on the nature of low-sulfide gold mineralization.

## REFERENCES

- Alexander, E.C., Jr., Mickelson, G.M., and Lanphere, M.A., 1978, Mmhb-1—A new  $^{40}\text{Ar}/^{39}\text{Ar}$  dating standard, *in* Zartman, R.E., ed., Short papers of the Fourth International Conference, Geochronology, Cosmochronology, Isotope geology, 1978: U.S. Geological Survey Open-File Report 78-701, p. 6-8.
- Arbogast, B.F., ed., 1996, Analytical methods manual for the Mineral Resource Surveys Program, U.S. Geological Survey: U.S. Geological Survey Open-File Report 96-525, 248 p.
- Ashley, R.P., 2002, Geoenvironmental model for low-sulfide gold-quartz vein deposits, *in* Seal, R.R., II and Foley, N.K., 2002, Progress on geoenvironmental models for selected mineral deposit types: U.S. Geological Survey Open-File Report 02-195, p. 176-195.
- Barnard, Fred, 1993, District-scale zoning patterns, Virginia City, Montana USA: 96th Western Mining Conference of the Colorado Mining Association (Denver), Reprint 93-29, 18 p.
- Berger, B.R., 1986, Descriptive model of low-sulfide Au-quartz veins, *in* Cox, D.P. and Singer, D.A., eds. Mineral deposit models: U.S. Geological Survey Bulletin 1693, p. 239-243.
- Bliss, J.D., and Jones, G.M., 1988, Mineralogic and grade-tonnage information on low-sulfide gold-quartz veins: U.S. Geological Survey Open-File Report 88-229, 99 p.
- Bohlke, J.K., 1989, Comparison of metasomatic reactions between a common  $\text{CO}_2$ -rich vein fluid and diverse wall rocks—Intensive variables, mass transfers, and Au mineralization at Alleghany, California: *Economic Geology*, v. 84, no. 2, p. 291-327.
- Boyle, R.W., 1991, Auriferous Archean greenstone-sedimentary belts: *Economic Geology*, Monograph 8, p. 164-191.
- Cole, M.M., 1983, Nature, age, and genesis of quartz-sulfide-precious-metal vein systems in the Virginia City mining district, Madison County, Montana: Bozeman, Montana State University, M.S. thesis, 63 p.
- Dalrymple, G.B., Alexander, E.C., Lanphere, M.A., and Kraker, G.P., 1981, Irradiation of samples for  $^{40}\text{Ar}/^{39}\text{Ar}$  dating using the Geological Survey TRIGA reactor: U.S. Geological Survey Professional Paper 1176, 55 p.
- Despotovic, Pero, 2000, Geology and geochemistry of Au-Ag-mineralizations in the Virginia City mining district (VCMD), Montana, U.S.A.: Technical University of Berlin, M.S. thesis, 100 p. <http://www.physik.tu-berlin.de/~bato/Montana.pdf>
- Eimon, P.I., 1997, The economic geology of Montana's Virginia City mining district: *Society of Economic Geologists Newsletter*, no. 28, January, 1997, 6 p.
- Eisenlohr, B.N., Groves, D., and Partington, G.A., 1989, Crustal-scale shear zones and their significance to Archean gold mineralization in Western Australia: *Mineralium Deposita*, v. 24, p. 1-8.
- Ficklin, W.H., and Mosier, E.L., 1999, Field methods for sampling and analysis of environmental samples for unstable and selected stable constituents, *in* Plumlee, G.S. and Logsdon, M.J. eds., The environmental geochemistry of mineral deposits, Part A—Processes, techniques, and health issues: *Society of Economic Geologists, Inc., Reviews in Economic Geology*, v. 6A, p. 249-264.
- Fleck, R.J., Sutter, J.F., and Elliott, D.H., 1977, Interpretation of discordant  $^{40}\text{Ar}/^{39}\text{Ar}$  age-spectra of Mesozoic tholeiites from Antarctica: *Geochimica et Cosmochimica Acta*, v. 41, no. 1, p. 15-32.
- Franklin, R.J., 1994, Geology and mineralization of part of the Virginia City mining district, Madison County, Montana: SME/AIME Symposium Abstract, 1 p.
- Godfrey, P.E., 1995, A cordilleran vein model for mineralization in the Virginia City mining district, Montana: *Proceedings, Nebraska Academy of Sciences*, p. 54.
- Goldfarb, R.J., Berger, B.R., Klein, T.L., Pickthorn, W.J., and Klein, D.P., 1995, Low-sulfide Au quartz vein deposits, *in* du Bray, E.A., ed., Preliminary compilation of descriptive geoenvironmental mineral deposit models: U.S. Geological Survey Open-File Report 95-831, p. 261-267.
- Groves, D.I., Goldfarb, R.J., Gebre-Mariam, M., Hagemann, S.G., and Robert, F., 1998, Orogenic gold deposit—A proposed classification in the context of their crustal distribution and relationship to other gold deposit types: *Ore Geology Reviews*, v. 13, p. 7-27.
- Hadley, J.B., 1969, Geologic map of the Varney quadrangle, Madison County, Montana: U.S. Geological Survey Geologic Quadrangle Map GQ-814, scale 1:62,500.

- Hageman, P.L., and Briggs, P.H., 2000, A simple field leach test for rapid screening and qualitative characterization of mine waste dump material on abandoned mine lands: ICARD 2000, Proceedings from the Fifth International Conference on Acid Rock Drainage, v. II, p. 1463-1475.
- Hammarstrom, J.M. and Van Gosen, B.S., 1998, Selected geochemical data for the Dillon BLM Resource Area (including the Virginia City mining district), Madison and Beaverhead Counties, southwest Montana—Mineral-resource and mineral-environmental considerations: U.S. Geological Survey Open-File Report 98-224-C, 106 p.
- Hammarstrom, J.M., Eppinger, R.G., Van Gosen, B.S., Briggs, P.H., and Meier, A.L., 2002, Case study of the environmental signature of a recently abandoned, carbonate-hosted replacement deposit: The Clayton Mine, Idaho: U.S. Geological Survey Open-File Report 02-10, 44 p. <http://pubs.usgs.gov/openfile/of02-010/>
- Hanna, W.F., Kaufmann, H.E., Hassemer, J.H., Ruppel, B.D., Pearson, R.C., and Ruppel, E.T., 1993, Maps showing gravity and aeromagnetic anomalies in the Dillon 1° x 2° quadrangle, Idaho and Montana: U.S. Geological Survey Miscellaneous Investigations Series Map I-1803-1, scale 1:250,000, includes 27 p. pamphlet.
- Hanover Gold Company, Inc., 1997, 1997 Annual Report, 12 p.
- Haugerud, R. A., and Kunk, M.J., 1988, ArAr\*, a computer program for reduction of <sup>40</sup>Ar-<sup>39</sup>Ar data: U.S. Geological Survey Open-File Report 88-261, 68 p.
- Kellogg, K.S. and Williams, V.S., 2000, Geologic map of the Ennis 30' x 60' quadrangle, Gallatin and Madison Counties, Montana, and Park County, Wyoming: U.S. Geological Survey Geologic Investigations Series Map I-2690, scale 1:100,000.
- Klein, T.L., and Day, W.C., 1994, Descriptive and grade-tonnage models of Archean low-sulfide Au-quartz veins and a revised grade-tonnage model of Homestake Au: U.S. Geological Survey Open-File Report 94-250, 18 p. <http://greenwood/cr/usgs.gov/pub/open-file-reports/ofr-94-0250/>
- Kunk, M.J., Winick, J.A., and Stanley, J.O., 2001, <sup>40</sup>Ar/<sup>39</sup>Ar age-spectrum and laser-fusion data for Cenozoic volcanic rocks in west-central Colorado: U.S. Geological Survey Open-File Report 01-472, 94 p.
- Lockwood, M.S., 1990, Controls on precious-metal mineralization, Easton-Pacific Vein, Virginia City mining district, Madison County, Montana: Socorro, New Mexico Institute of Mining and Technology, M.S. thesis, 136 p.
- Lockwood, M.S., Campbell, A.R., and Chavez, W.X., Jr., 1991, Evolution of mineralizing fluids, Virginia City mining district, Montana: Geological Society of America Abstracts with Programs, v. 23, no. 4, p. 43.
- Loen, J.S., 1992, Mass balance constraints on gold placers—Possible solutions to “source area problems”: Economic Geology, v. 87, p. 1624-1634.
- \_\_\_\_\_, 1997, Character and occurrence of gold nuggets, western Montana: Northwest Geology, v. 27, p. 21-30.
- Lorain, S.H., 1937, Gold lode mining in the Tobacco Root Mountains, Madison County, Montana: U.S. Bureau of Mines Information Circular 6972, 74 p.
- Marvin, R.F., and Dobson, S.W., 1979, Radiometric ages - Compilation B, U.S. Geological Survey: Isochron/West, no. 26, p. 3-32.
- McFaul, E.J., Mason, G.T., Jr., Ferguson, W.B., and Lipin, B.R., 2000, U.S. Geological Survey Mineral Databases—MRDS and MAS/MILS: U.S. Geological Survey Digital Data Series DDS-52, 2 disks.
- McLeod, J.W., 1986, Report on the U.S. Grant gold mine, Virginia City area, Madison County, Montana: Unpublished report prepared on behalf of U.S. Grant Gold Mining Co., Ltd.
- O'Neill, J.M., Klepper, M.R., Smedes, H.W., Hanneman, D.L., Frazer, G.D., and Mehnert, H.H., 1996, Geologic map and cross sections of the central and southern Highland Mountains, southwestern Montana: U.S. Geological Survey Miscellaneous Investigations Series Map I-2525, scale 1:50,000.
- Pinckney, D.M., Hanna, W.F., and Kaufmann, H.E., 1980, Resource potential of the Bear Trap Canyon Instant Study Area, Madison County, Montana: U.S. Geological Survey Open-File Report 80-835, 37 p.
- Pioneer Technical Services, Inc., 1995, Abandoned hardrock mine priority sites, 1995, Summary Report, Prepared for Montana Department of State Lands, Abandoned Mine Reclamation Bureau, Helena, Mont., variously paginated.
- Rickwood, P.C., 1983, Crustal abundance, distribution, and crystal chemistry of the elements, in Govett, G.J.S., Handbook of exploration geochemistry, vol. 3, Rock geochemistry in mineral exploration: Amsterdam, Elsevier Scientific Publishing Company, p. 347-387.

- Roddick, J.C., 1983, High precision intercalibration of  $^{40}\text{Ar}$ - $^{39}\text{Ar}$  standards: *Geochimica et Cosmochimica Acta*, v. 47, no. 5, p. 887-898.
- Ruppel, E.T., 1993, Cenozoic tectonic evolution of southwest Montana and east-central Idaho: Montana Bureau of Mines and Geology Memoir 65, 62 p.
- Ruppel, E.T., and Liu, Y., (in press), The gold mines of the Virginia City mining district, Madison County, Montana: Montana Bureau of Mines and Geology.
- Ruppel, E.T., O'Neill, J.M., and Lopez, D.A., 1993, Geologic map of the Dillon 1° x 2° quadrangle, Idaho and Montana: U.S. Geological Survey Miscellaneous Investigations Series Map I-1803-H, scale 1:250,000.
- Shawe, D.R., and Wier, K.L., 1989, Gold deposits in the Virginia City-Alder Gulch District, Montana: U.S. Geological Survey Bulletin 1857-G, p. G12-G19.
- Sheets, M.R., 1980, A geological investigation and evaluation of R and D Minerals, Inc., Virginia City, Madison County, Montana: Unpublished report prepared for the Kemmerer Corporation, 83 p.
- Siems, P.L., 1991, Hydrothermal Alteration for Mineral Exploration Workshop [Lecture manual]: Moscow, University of Idaho.
- Sims, P.K., O'Neill, J.M., and Bankey, V., 2002, Precambrian basement geologic map of Montana—An interpretation of aeromagnetic anomaly map: Geological Society of America Abstracts with Programs v. 34, no. 4, p. A-49.
- Steiger, R.H., and Jäger, Emilie., 1977, Subcommittee on geochronology—Convention on the use of decay constants in geo- and cosmochronology: *Earth and Planetary Science Letters*, v. 36, p. 359-363.
- Tansley, Wilfred, Schafer, P.A., and Hart, L.H., 1933, A geological reconnaissance of the Tobacco Root Mountains, Madison County, Montana: Montana Bureau of Mines and Geology Memoir 9, 57 p.
- Trauerman, C.J., and Waldron, C.R., Supervisors, 1940, Directory of Montana mining properties, 1949: Montana Bureau of Mines and Geology Memoir 20, 135 p.
- U.S. Environmental Protection Agency, 1994, Test methods for evaluating solid waste, physical/chemical methods (SW-846), 3<sup>rd</sup> edition, update 2B: Environmental Protection Agency, National Center for Environmental Publications, Cincinnati, OH 45268, telephone 800-553-6847, order number EPASW-846.3.2B. URL: <http://www.epa.gov/epaoswer/hazwaste/test/sw846.htm>
- Vitaliano, C.J., and Cordua, W.S., 1979, Geologic map of southern Tobacco Root Mountains, Madison County, Montana: Geological Society of America Map and Chart Series Map MC-31, scale 1:62,500.
- Wier, K.L., 1982, Maps showing geology and outcrops of part of the Virginia City and Alder Gulch quadrangles, Madison County, Montana: U.S. Geological Survey Miscellaneous Field Studies Map MF-1490, 2 sheets, scale 1:12,000.
- Winchell, A.N., 1914, Mining districts in the Dillon Quadrangle, Montana, and adjacent areas: U.S. Geological Survey Bulletin 574, 191 p.
- York, Derek, 1969, Least squares fitting of a straight line with correlated errors: *Earth and Planetary Science Letters*, v. 5, p. 320-324.

# Using Fluid Inclusions to Help Unravel the Origin of Hydrothermal Talc Deposits in Southwest Montana

Christopher H. Gammons } Department of Geological Engineering, Montana Tech of  
Duane O. Matt } The University of Montana, Butte, MT 59701

---

## ABSTRACT

Fluid inclusions were examined from two hydrothermal talc deposits located in the Gravelly Range, Southwest Montana. The fluids responsible for talc formation were saline brines (roughly 7x saltier than modern seawater), and were highly enriched in  $\text{CaCl}_2$ . Vapor bubble homogenization temperatures averaged 140°C at the Cadillac Deposit, and 88°C at the Yellowstone Mine. These temperatures are believed to be too low for talc formation, and need to be pressure-corrected. By applying Na-K-(Ca) geothermometry, the true trapping temperatures of fluid inclusions from the Cadillac Deposit are estimated to range from 190° to 250°C. The difference between the homogenization and trapping temperatures can be used to estimate a pressure of trapping of roughly 1 to 4 kbar. Assuming a lithostatic gradient, these pressures correspond to depths of 3.5 to 14 km.

Based on the fluid inclusion results, we argue that the hydrothermal talc deposits of the Gravelly Range did not form in a near-surface, hot-spring setting, nor were they the products of contact metamorphism. The deposits more likely owe their origin to regional fluid migration associated with Proterozoic rifting, synchronous with the opening of the Belt Basin. We suggest that high heat flow, enhanced by injection of thick sills into the Belt sedimentary pile, forced connate brines out of the bottom of the Basin and into the underlying or adjacent Precambrian basement, where they caused retrograde metamorphism and formation of economic talc and chlorite deposits.

## INTRODUCTION

Southwest Montana is the U.S. leading producer of high-purity talc. The deposits occur as hydrothermal replacements of dolomitic marble (Olson, 1976; Berg, 1979), and are similar in this respect to many large talc deposits elsewhere in the world (Moine et al., 1989; Piniakiewicz et al., 1994). Although dolomite is widespread in the Paleozoic section of Montana, the talc occurrences are restricted to Archean meta-sediments of the Wyoming Province, exposed in the core of mountain ranges of the southwest portion of the state. Active mining operations include the Yellowstone Mine (owned by Luzenac Int.) in the Gravelly Range southwest of Ennis MT, and the Treasure and Regal Mines (owned by Barretts Minerals) in the Ruby Range northeast of Dillon MT.

The Archean basement of southwest Montana consists mainly of metasedimentary and metavolcanic rocks intruded by granite gneiss. In the vicinity of the Yellowstone mine (Fig. 1), the metasediments are referred to as the Cherry Creek Group (Peale, 1896), and include a thick sequence of phyllite, quartzite and quartz schist, banded iron formation, amphibolite, mica±kyanite±staurolite schist, quartzofeldspathic gneiss, and dolomitic marble (Heinrich and Rabbitt, 1960). These rocks are highly deformed, and were subjected to amphibolite facies regional metamorphism at roughly 2.7 Ga (Giletti, 1966; James and Hedge, 1980). South of the Yellowstone Mine, thrust faulting repeats the stratigraphy, and has juxtaposed rocks of differing metamorphic grade (Vargo, 1990).

Throughout the northwestern Wyoming Province, a widespread greenschist-facies retrograde event occurred at roughly 1.6 Ga (Giletti, 1966; Anderson, 1987). Most previous workers have concluded that the Montana talc



deposits formed during the waning stages of this thermal event (Okuma, 1971; Garihan, 1973; Berg, 1979; Anderson, 1987). A recent  $^{40}\text{Ar}/^{39}\text{Ar}$  date of 1.36 Ga for muscovite intergrown with talc from the Ruby Range (Brady et al., 1998) supports this hypothesis. Concentrations of Mg-rich chlorite replacing quartzo-feldspathic gneiss in southwest Montana (e.g., the Antler Mine near Silver Star, MT) are believed to have formed during the same general time period as the talc deposits (Berg, 1979).

Despite over a century of scrutiny, many details remain unknown regarding the origin of the southwest Montana talc deposits. In the present study, we address this problem by examining fluid inclusions in quartz associated with talc from the Yellowstone and nearby Cadillac deposits. Both deposits are located in Johnny Gulch, in the Gravelly Mountains, southwest of Ennis, MT. These results represent the first fluid inclusion information obtained to date for the Montana talc deposits.

#### SAMPLE COLLECTION AND ANALYSIS

The success of this study hinged upon finding samples of hydrothermal quartz contemporaneous with talc formation. Based on repeated trips to mines and prospects in southwest Montana, we have recognized multiple generations of quartz in the vicinity of talc occurrences. In most cases, quartz is clearly younger than the main stage of talc formation. Late quartz typically occurs as narrow, anastomosing veinlets cutting massive talc (Fig. 2a), with bleached alteration halos (so-called "bone talc"). This form of quartz is extremely fine-grained (chalcedonic), and contains no fluid inclusions suitable for microthermometric analysis. More rare types of quartz include boudined milky quartz ("bull quartz") veins (Fig. 2b), or lineated rods of fine-grained, mosaic-textured quartz (common at the Regal Mine, Ruby Range). These types

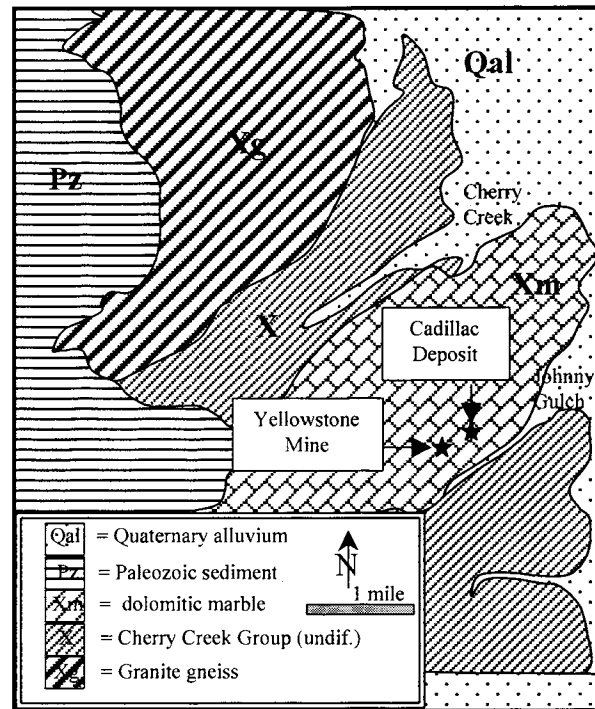


**Figure 1. Simplified geologic map of part of the Gravelly Range, showing the location of talc deposits.**

of strained quartz are clearly pre-deformational in origin, and therefore must pre-date talc formation.

Of much greater interest to this study were occurrences of coarse-grained quartz, occurring as small pods or stringers completely surrounded by talc. One such sample (Fig. 2c) was collected in 1992 by Dick Berg from an outcrop near the former Cadillac deposit (also known as the Burlington-Northern Mine). This deposit, now reclaimed, was located roughly 1 mile NE of the present day Yellowstone Mine. A second sample of podular quartz (Fig. 2d) was collected by mine geologist Mike Cerino (Luzenac) in 1999, from the active Yellowstone pit. In both cases, quartz of obvious hydrothermal origin occurs as very coarse grained, translucent to transparent aggregates intergrown with - and completely surrounded by - pale green talc. In contrast to quartz associated with bone talc, the podular quartz samples contain abundant, large, primary fluid inclusions concentrated along mineral growth zones, the latter visible in hand specimen.

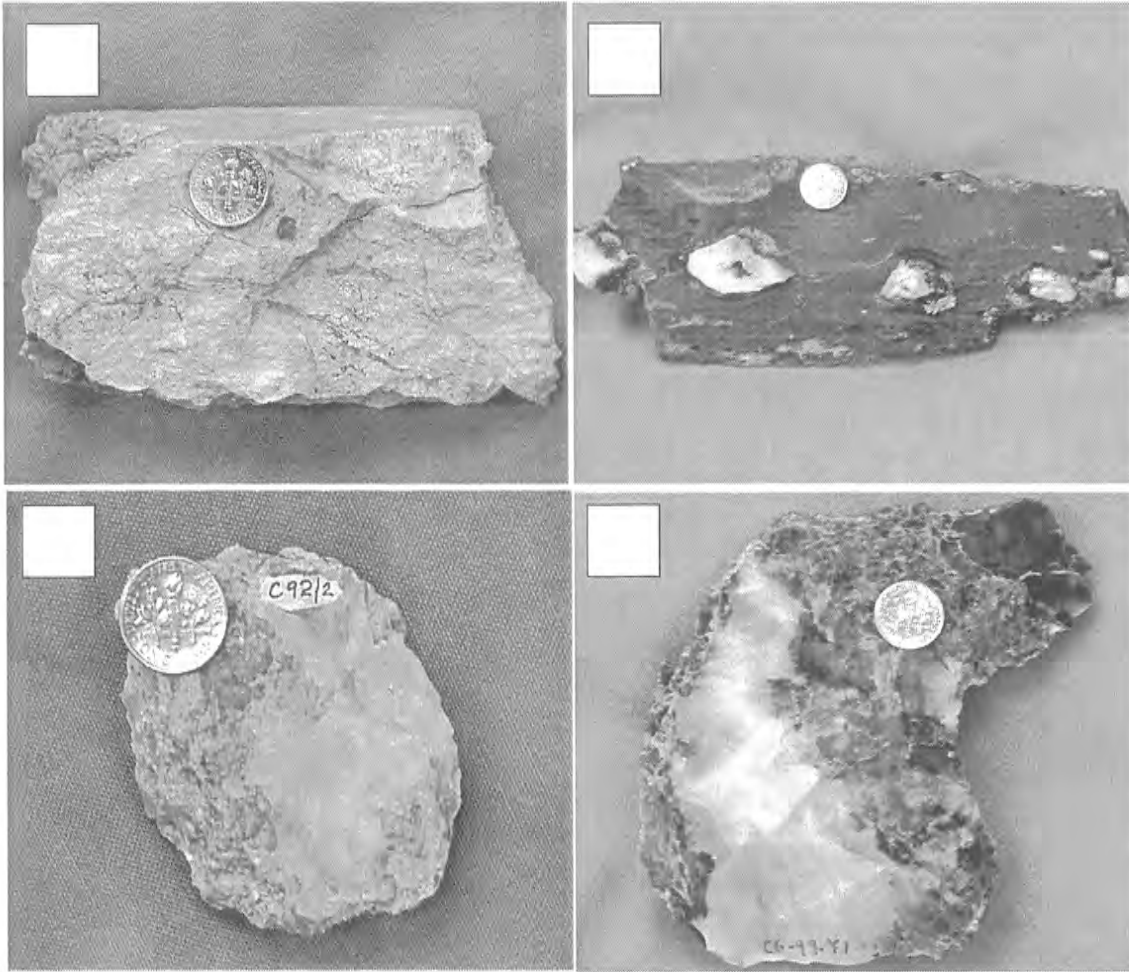
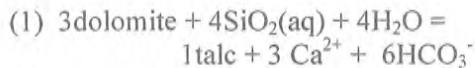


**Figure 2.** Photographs of hydrothermal quartz from the Gravelly Range: 2a) chalcedonic quartz veins cutting “bone talc”; 2b) a boudinaged milky quartz vein within sheared dolomite; 2c) coarse, podular quartz (light gray, on right side of hand sample) intergrown with talc from the Cadillac Deposit; 2d) coarse, podular quartz (white, with growth zones defined by primary fluid inclusions) intergrown with dark green talc from the Yellowstone mine. In all cases, a dime was used for scale.

We believe that this form of quartz precipitated from the same hydrothermal fluids that converted dolomite to talc, for example, by the following reaction:



Once the surrounding dolomite was converted to talc, residual dissolved silica precipitated in open space as quartz.

Five doubly-polished sections were prepared of podular quartz from the Yellowstone and

Cadillac deposits. These samples were analyzed via conventional fluid inclusion methods using a USGS heating/freezing stage calibrated with synthetic fluid inclusion standards. In addition, triplicate samples of quartz from the Cadillac deposit were carefully crushed and leached with de-ionized water, and the relative concentrations of NaCl-KCl-MgCl<sub>2</sub>-CaCl<sub>2</sub> were determined on each bulk leachate by ICP-AES (see Matt, 1999, for further details).

## RESULTS

Fluid inclusions in quartz examined from the Cadillac and Yellowstone deposits had similar overall characteristics. The vast majority of inclusions were simple, 2-phase, liquid-rich fluid inclusions with relatively small vapor bubbles. Very rarely, primary inclusions contained a small NaCl (halite) daughter mineral. Trails of vapor-rich fluid inclusions were sometimes found along fracture planes, but were not examined in this study due to their obvious secondary origin.

### Freezing Studies

Histograms summarizing freezing results from the Yellowstone and Cadillac deposits are given in Figure 3. The fluid inclusions are separated into two groups: those that showed final melting in the presence of ice, and those that showed final melting in the presence of hydrohalite (NaCl $\cdot$ 2H $_2$ O). The latter mineral is distinguished from ice by its brownish color and high relief. The presence of hydrohalite indicates NaCl concentrations > 23.3 wt% (assuming a pure NaCl-H $_2$ O system). The majority of fluid inclusions examined in this study formed hydrohalite during freezing runs. No evidence of liquid CO $_2$  or CO $_2$ -clathrate was found during freezing, which means that the concentration of dissolved CO $_2$  in the fluid inclusions was relatively low.

Melting temperatures ( $T_m$ ) were often less than the eutectic for pure NaCl solutions (-21°C), especially for inclusions from the Yellowstone Mine. This is explained by the presence of CaCl $_2$ , which can lower the eutectic melting temperature of salt water to values as low as -49.8°C (Crawford, 1981). High CaCl $_2$  concentrations were confirmed by the bulk leachate analyses of quartz from the Cadillac deposit (Table 1). The bulk salinity (in weight %) of the inclusion fluids was estimated from regression equation 2 in Oakes et al. (1990). This equation assumes that the inclusion fluids can be approximated by NaCl-CaCl $_2$  mixtures. The total salinity was determined from the final melting temperature of ice, and the mole ratio of Na/(Na+Ca) in the solution. The latter was determined by bulk chemical analysis (Table 1) to be 0.62. The results gave a tight clustering

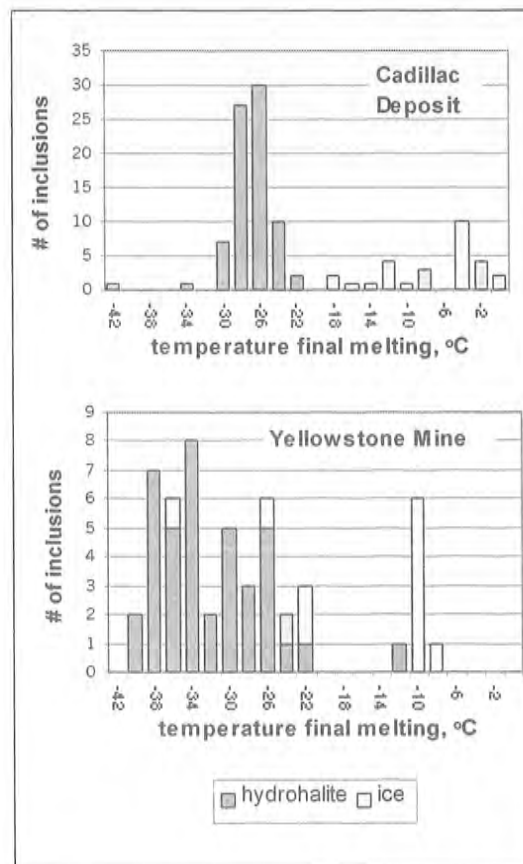


Figure 3. Histograms of final melting temperatures.

of salinity values near 25 wt %. From the cation ratios given in Table 1, and assuming that all cations are charge-balanced with chloride, the absolute concentration (mass basis) of each salt making up the 25 wt% salinity fluid becomes: 11% CaCl $_2$ , 10% NaCl, 3.0% MgCl $_2$ , and 1.0% KCl. Converting to molal units, the average composition of inclusion fluids from the Cadillac Deposit is computed to be 2.2m Na $^+$ , 1.4m Ca $^{2+}$ , 0.41m Mg $^{2+}$ , and 0.18m K $^+$ .

### Heating Studies

The only phase transformation noticed during heating runs was the disappearance of the vapor-bubble, corresponding to the temperature of homogenization ( $T_h$ ). Results are summarized in Figure 4, and are compared to  $T_m$  results. In general, fluid inclusions from the Cadillac Deposit homogenized at a higher

**Table 1. Cation ratios (ppm) of bulk leachates of hydrothermal quartz from the Cadillac Deposit.**

	Na/Ca	Na/Mg	Na/K	Ca/Mg
Rep-1	0.82	6.06	6.92	7.39
Rep-2	1.04	4.56	7.45	4.37
Rep-3	0.95	4.60	6.94	4.85
Mean	0.94	5.07	7.1	5.54
Std. dev.	± 0.09	± 0.7	± 0.25	± 1.62
RSD	9.60%	13.70%	3.40%	29.3%
Seawater <sup>a</sup>	26.1	8.35	27.0	0.32

<sup>a</sup> Average seawater composition from Stumm and Morgan (1981).

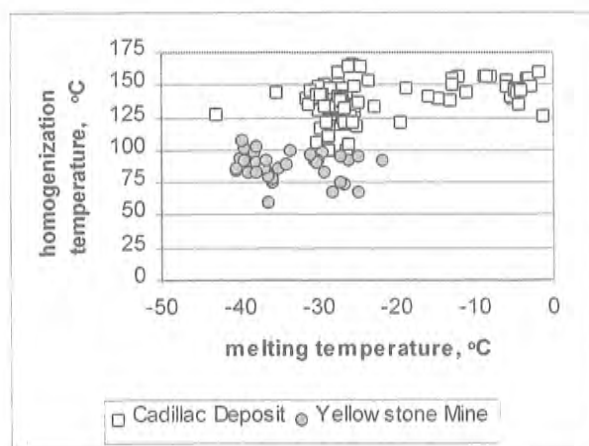


**Figure 4. Th vs. Tm for all fluid inclusions examined in this study.**

temperature (avg  $T_h = 140^\circ\text{C}$ ) than those from the Yellowstone Mine (avg  $T_h = 88^\circ\text{C}$ ).

### Na-K-Ca geothermometry

The temperatures obtained from the homogenization study are minimum estimates of the true trapping temperature, and need to be pressure corrected. To determine the magnitude of the pressure correction, it was necessary to develop an independent geothermometer. In the absence of isotopic or petrological temperature indicators, we focused on the use of empirical geothermometers based on cation ratios in the inclusion fluids. Three formulae were used:

$$(2) T^\circ\text{C} = 1217/(\log(\text{Na}/\text{K})+1.483) - 273.15$$

$$(3) T^\circ\text{C} = 855.6/(\log(\text{Na}/\text{K})+0.8573) - 273.15$$

$$(4) T^\circ\text{C} = 1647/(\log(\text{Na}/\text{K}) + 1/3[\log(\text{Ca}/\text{Na})+2.06]+2.47) - 273.15$$

Equations (2) and (3) are referred to as the “Fournier” and “Truesdell” formulae, respectively (Truesdell, 1984). In these equations, Na/K is in ppm units, and was assigned a value of 7.1, based on bulk leachate examples found in Table 1. For these formulae to be used as geothermometers there must have been equilibrium between the hydrothermal fluid and two feldspars (a plagioclase feldspar and an alkali feldspar). The absence of these feldspars in dolomitic marble might seem to make these equations invalid. However, the hydrothermal fluids in all likelihood passed through the surrounding quartzo-feldspathic gneiss - and equilibrated with the feldspars contained in these rocks - before the fluids reacted with the dolomitic marble to create talc. Equation (4) above is the Na-K-Ca geothermometer based on Fournier and Truesdell (1973). This equation is recommended for fluids that have equilibrated with two feldspars, as well as the minerals calcite and epidote. Both calcite and epidote are common retrograde minerals, and may be present in altered granitic rock or quartzo-feldspathic gneiss. The concentrations in equation (4) are in ppm units. The Na-K-Ca geothermometer was corrected for the presence of Mg ions. The correction factor is based on the mole fraction of  $\text{Mg}/(\text{Mg}+\text{Ca}+\text{K})$ , and was estimated from Figure 3.2 of Truesdell (1984).

The results from equations (1), (2), and (3) gave temperature estimates of  $249^\circ\text{C}$ ,  $227^\circ\text{C}$ , and  $190^\circ\text{C}$ , respectively. In the following discussion, the entire range of possible trapping temperatures from  $190^\circ\text{C}$  to  $249^\circ\text{C}$  is used.

### P-T conditions of talc formation

A phase diagram for the  $\text{H}_2\text{O}$ -NaCl system was used to help determine the pressure and

temperature conditions of “trapping” for the fluid inclusions in this study. The diagram in Figure 5 was redrawn from Roedder and Bodnar (1997), and applies to a 25 wt% NaCl solution. This is close to the average salinity of the talc-forming fluids at the Cadillac deposit. Different parts of Figure 5 need to be explained. First, the solid curve shows the boundary between liquid and vapor (L-V curve), and ends at the critical point above which only one fluid phase is present. All of the fluid inclusions examined in this study had both a vapor bubble and liquid at ambient temperature, and would therefore fall on this line. During a heating run, the inclusion follows a path of increasing temperature and pressure along the L-V curve until the point that the vapor bubble disappears. This is the homogenization temperature. At this point, more heating causes the fluid to leave the L-V curve and enter into the single phase, liquid-only field of the diagram. The P-T path that the fluid now takes is shown by the thin diagonal lines extending upwards from left to right. These lines are called “isochores”, and show the interrelationship between pressure and temperature for a fluid of constant volume and density. Because water is much less compressible than gas, these lines have a steep slope compared to the L-V curve. This explains why fluid inclusions will typically explode if you heat them way beyond their homogenization temperature. Each isochore is labeled depending on the temperature of homogenization. The isochores of interest in this study fall in the range of 100 to 160°C, which is the range in fluid inclusion homogenization temperatures obtained from quartz from the Cadillac talc deposit (Section 4.1).

Superimposed on Figure 5 is the range in estimated temperature (190 to 249°C) based on the Na/K and Na/K/Ca geothermometers. The intersection of these temperatures (vertical dashed lines) with the isochores of interest define a box which shows the full range in possible trapping pressure and temperature. The darker box was drawn for a narrower range in isochore homogenization temperature, centered around the average of all the fluid

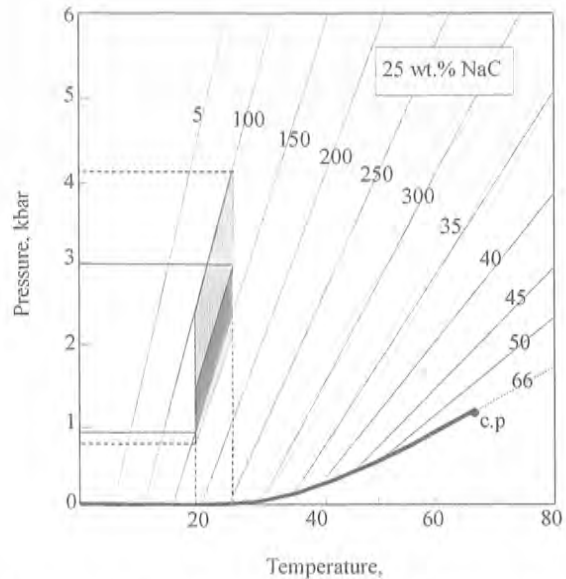


**Figure 5. Pressure-temperature diagram for the NaCl-H<sub>2</sub>O system (modified after Roedder and Bodnar, 1997). The thin diagonal lines represent isochores (lines of constant bulk density) for a 25 wt% NaCl solution that homogenizes along the liquid-vapor curve (bold curve). The lightly shaded region represents the intersection of the isochores obtained from the fluid inclusion homogenization temperatures in this thesis with the estimated temperatures from the Na/K and Na/K/Ca geothermometers (vertical dashed lines). The dark shaded region represents the most likely P-T range of trapping of the fluids studied, assuming an average homogenization temperature of 140±10°C.**

inclusion data (140 ±10°C). The steep slope of the isochores means that a small uncertainty in temperature translates to a very large uncertainty in pressure. The range in pressure for the larger box is 0.75 to 4.2 kbars. For the smaller box, the range is roughly 1 to 3 kbar. Using the average geobaric gradient (3.5 km/kbar), this translates to a depth of 3.5 to 10.5 km, or roughly 2 to 6 miles.

Fluid inclusions from the Yellowstone Mine had lower homogenization temperatures than

those from the Cadillac deposit. If it is assumed that the trapping temperatures were similar in both deposits, then the pressures of formation of the Yellowstone quartz+talc pod must have been significantly higher than those for the Cadillac deposit. This is somewhat difficult to explain given the close proximity of the two talc deposits. An alternate explanation is that the quartz+talc pod at the Yellowstone Mine crystallized at a lower temperature, but at similar pressures.

## DISCUSSION

All previous workers agree that the economic talc deposits in Southwestern Montana formed by hydrothermal or metasomatic replacement of dolomitic marble. Several authors (e.g., Berg, 1979; Anderson et al., 1990) have pointed out that very large quantities of water are needed to completely replace dolomite by talc. Referring to the general reaction for talc formation (reaction 1), Berg (1979) stated that the rarity of calcite in close association with talc implies that calcium was flushed from the area by hydrothermal water passing through the deposit. Anderson et al. (1990) expanded on this idea by calculating the mass of water needed to bring silica in and flush calcite out during the formation of the talc deposits in the Ruby Range. They concluded that volumetric water-rock ratios were probably  $> 600$ . Exactly where this large amount of water came from is more of a mystery. Berg (1979) raised the possibility that the talc-forming fluids could be meteoric water that dissolved silica from the overlying rocks during its downward and perhaps lateral movement. Anderson et al. (1990) speculated that the ore-forming fluids could have been derived from Mg-rich seawater in the overlying Belt basin, and probably formed at  $P < 2$  kbar and  $T < 400^{\circ}\text{C}$ . In a more recent paper by Brady et al. (1998), stable isotopes and  $^{40}\text{Ar}/^{39}\text{Ar}$  age dating were used to place further constraints on the timing and conditions of formation of talc in the Ruby Range. Brady et al. (1998) concluded that the talc formed from  $200^{\circ}\text{--}300^{\circ}\text{C}$  metasomatic fluids derived from seawater, at a depth of 5-10 km. These calculations overlap with the P-T estimates of this study for talc in the Gravelly

Range. However, the results of Brady et al. were based on several assumptions. For example, to calculate the temperature range of talc formation from stable isotopes of calcite and dolomite, it was necessary to assume that the ore-forming fluids were seawater, and had a  $\delta^{18}\text{O}$  composition of 0‰, the same as modern day oceans.

The results of this study provide new constraints on the range of pressure, temperature and composition of the talc-forming fluids in the Gravelly Range. The fact that the fluids were extremely saline (~ 7 times modern seawater) suggests they could not be derived from meteoric groundwater recharge alone. It also suggests that the fluids were not "typical" ocean water, although they could have come from a restricted marine basin with an unusually high salinity, such as the modern day Dead Sea. However, the very high Ca/Na ratio of the fluids in this study are not typical of evaporated seawater.

Another possible source of ore-forming fluids is connate water, or water trapped in the bottom of sedimentary basins. Direct sampling of connate water from basins around the world shows that they are typically extremely salty, and have cation ratios different from those of normal seawater due to water-rock interaction and shale membrane effects (Hanor, 1979). Connate waters have been proposed as the most likely ore-forming fluids for certain types of mineral deposits which occur in sedimentary basins, such as "Mississippi-Valley Type (MVT)" lead-zinc deposits, "Red-bed" copper deposits, "Sedimentary-Exhalative" (SEDEX) Pb-Zn-Cu deposits, as well as "Unconformity-type" uranium deposits (Ruzicka, 1995). Both Red-bed copper and SEDEX type deposits occur in the Belt Basin in NW Montana and southern British Columbia (Ethier et al., 1976). Sporadic and sub-economic copper mineralization is associated with talc deposits of the Gravelly Range and southern Tobacco Root Mountains (Berg, 1979). Although unconformity uranium deposits have not been discovered in the Belt Basin, world-class

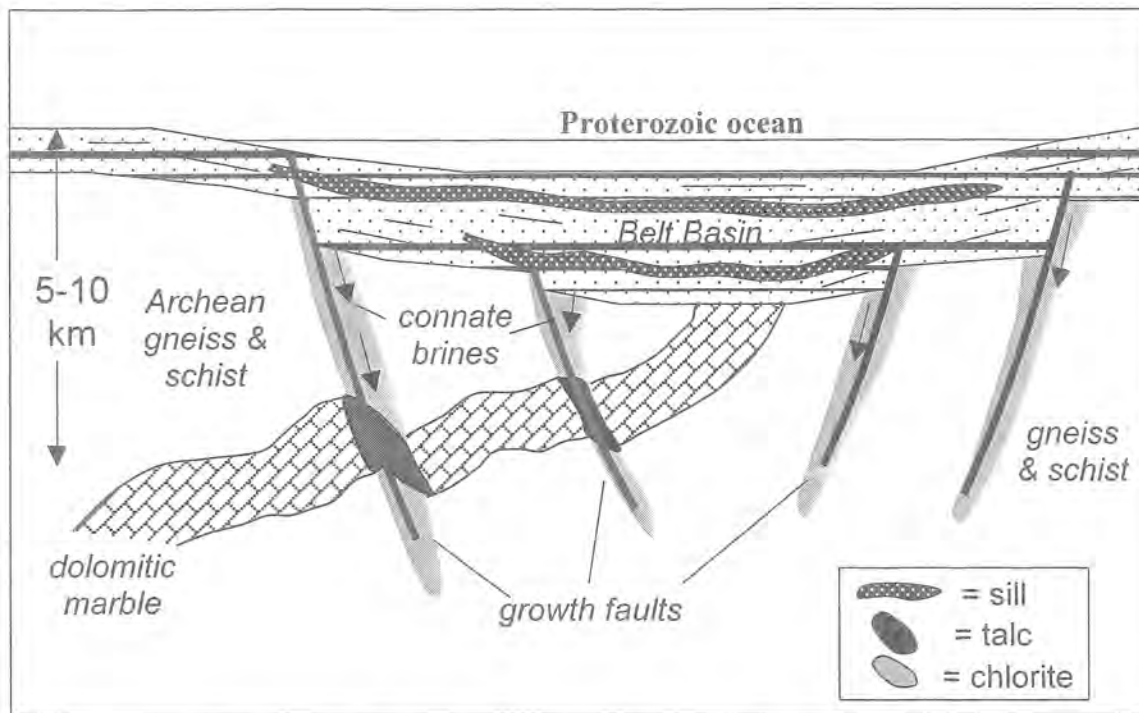


**Figure 6.** Schematic cartoon showing the inferred origin of hydrothermal talc and chlorite deposits of SW Montana. Connate brines from the Proterozoic Belt Basin are forced into the Archean basement by high heat flow and injection of mafic sills. These brines cause widespread retrograde metamorphism and formation of economic talc and chlorite deposits.

deposits exist in the similarly-aged Athabaska Basin of northern Saskatchewan. These deposits formed when basinal brines rich in dissolved uranium interacted with metamorphic basement rocks, and left widespread chlorite and local talc alteration (Ruzicka, 1995). Fluid inclusion studies of the Athabaska uranium deposits show the ore fluids were  $\text{CaCl}_2$ -rich brines with inferred temperatures and pressures similar to those proposed in this paper for the SW Montana talc deposits (Ruzicka, 1995).

Our model for the formation of talc deposits in the Gravelly Range is summarized in the drawing of Figure 6. In this model, the ore-forming fluids come either from connate brines in the bottom of the Belt Basin, or from Proterozoic seawater. The descending fluids cause retrograde alteration of the Archean basement rocks, replacing quartzo-feldspathic gneiss by chlorite, and dolomitic marble by talc. Based on the results of this study, this process probably formed in the temperature range of 190 to 250°C, and at considerable depth (> 3 km, and possibly as deep as 10 km or more). It is easier to imagine the fluids penetrating to these great depths if they

started out near the bottom of the Belt sedimentary basin - which is known to be many km in total thickness - than if they had to come all the way from the overlying ocean. It is possible that connate brines may have been “squeezed” out of the bottom of the basin due to igneous activity. Rifting in the region caused the intrusion of numerous large mafic sills and dikes throughout the Belt Supergroup. The heat from these dikes and sills may have warmed the connate brines to a temperature of 200°C or greater (tying in with the results from this study). The combination of the increased pressure from the huge pile of overlying Belt sediments and the thermal expansion from the heating of the connate brines could have been enough to set up large scale gradients in hydrostatic pressure, driving the brines into the underlying or adjacent basement rocks. This driving force would most likely have occurred along faults or fractures active during formation of the Belt basin (e.g., growth faults), resulting in focused fluid flow along these structures.

#### ACKNOWLEDGEMENTS

The authors are deeply indebted to Dick Berg (Montana Bureau of Mines and Geology), for introducing us to the Montana talc deposits, and furnishing a superb sample of hydrothermal quartz from the Cadillac deposit. This project would not have gotten off the ground without Dick's help and advice. Likewise, we thank Mike Cerino (Luzenac) for several mine tours and field trips, for collecting a couple nice quartz samples from the Yellowstone pit, and for many lively discussions about talc. This research was partially funded by an NSF-MONTS grant to CHG.

## REFERENCES

- Anderson, D. L., 1987, Timing and mechanism of formation of selected talc deposits in the Ruby Range, Southwestern Montana [M.S. thesis]: Montana State University, 86p.
- Anderson, D. L., Mogk D. W., and Childs J. F., 1990, Petrogenesis and timing of talc formation in the Ruby Range, Southwestern Montana: *Economic Geology*, v. 85, p. 585-600.
- Berg, R. B., 1979, Talc and chlorite deposits in Montana: Montana Bureau of Mines and Geology Memoir 45, 63p.
- Brady, J. B., Cheney J. T., Rhodes A. L., Vasquez A., Green C., Duvall M., Kogut A., Kaufman L., and Kovaric D., 1998, Isotope geochemistry of Proterozoic talc occurrences in Archean marbles of the Ruby Mountains, southwest Montana, U.S.A.: *Geological Materials Research*, v. 1(2), p. 1-40.
- Crawford, M. L., 1981, Phase equilibria in aqueous fluid inclusions: *Mineralogical Society of Canada Short Course*, v. 6, p. 75-100.
- Ethier, V. G., Campbell, F. A., Both R. A., and Krouse H. R., 1976, Geological setting of the Sullivan orebody and estimates of temperatures and pressure of metamorphism: *Economic Geology*, v. 71, p. 1570-1588.
- Fournier, R. O. and Truesdell, A. H., 1973, An empirical Na-K-Ca geothermometer for natural waters: *Geochimica et Cosmochimica Acta*, v. 37, p. 1255-1275.
- Garihan, J. M., 1973, Geology and talc deposits of the central Ruby Range, Madison county, Montana [Ph.D. dissert.]: Penn State University, 206p.
- Giletti, B. J., 1966, Isotopic ages from southwestern Montana: *Journal of Geophysical Research*, v. 71, p. 4029-4036.
- Hanor, J. S., 1979, The sedimentary genesis of hydrothermal fluids: *in* Barnes H. L. ed., *Geochemistry of Hydrothermal Ore Deposits*, 2<sup>nd</sup> ed., John Wiley & Sons, New York, p. 137-172.
- Harrison, J. E., 1972, Precambrian Belt basin of northwestern United States: Its geometry, sedimentation, and copper occurrences: *Geological Society of America Bulletin*, v. 83, 1215-1240.
- Heinrich E. W. and Rabbitt J. C., 1960, Pre-Beltian geology of the Cherry Creek and Ruby Mountain areas, southwestern Montana: *Montana Bureau of Mines and Geology Memoir* 38, 40p.
- James, H. L. and Hedge C. E., 1980, Age of basement rocks of southwest Montana: *Geological Society of America Bulletin*, v. 91, p. 11-15.
- Matt D. O., 1999, Fluid inclusion study of the origin of the Cadillac talc deposit, Johnny Gulch, Montana [M.S. thesis]: Montana Tech of The University of Montana, 56p.
- Moine, B. Fortune J. P., Moreau, P., and Viguiet, F., 1989, Comparative mineralogy, geochemistry, and conditions of formation of two metasomatic talc and chlorite deposits: Trimouns (Pyrenees, France) and Rabenwald (Eastern Alps, Austria): *Economic Geology*, v. 84, p. 1398-1416.
- Oakes C. S., Bodnar R. J., and Simonson J. M., 1990, The system NaCl-CaCl<sub>2</sub>-H<sub>2</sub>O: I. The ice liquidus at 1 atm total pressure: *Geochimica et Cosmochimica Acta*, v. 54, p. 603-610.
- Okuma, A. F., 1971, Structure of the Southwest Ruby Range near Dillon, Montana [Ph.D. dissert.]: Penn State University, 118p.
- Olson, R. H., 1976, The geology of Montana talc deposits: *Montana Bureau of Mines and Geology Special Publication* 74, p. 99-143.
- Peale, A. C., 1896, *Geologic atlas of the United States: Three Forks Folio*, Montana.
- Piniakiewicz R. J., McCarthy E. F., and Genco N. A., 1994, *Industrial Minerals and Rocks*, 6<sup>th</sup> ed: Society for Mining, Metallurgy, and Exploration.
- Roedder, E., 1984, Fluid Inclusions: *Mineralogical Society of America, Reviews in Mineralogy*, v. 12, 644p.
- Roedder, E. and Bodnar, R. J., 1997, Fluid inclusion studies of hydrothermal ore deposits: *in* Barnes, H. L. ed., *Geochemistry of Hydrothermal Ore Deposits*, 3<sup>rd</sup> ed., John Wiley & Sons, New York, p. 657-698.
- Ruzicka, V., 1995, Unconformity-associated uranium: *in* Eckstrand, O. R., Sinclair, W. D., and Thorpe, R. I. eds., *Geology of Canada*, v. 8, p. 197-210.



- Schmidt, C. J. and Garihan J. M., 1986, Middle Proterozoic and Laramide tectonic activity along the southern margin of the Belt Basin: Montana Bureau of Mines and Geology Special Publication 94, p. 217-235.
- Stumm, W. and Morgan J. J., 1981, Aquatic Chemistry, 2<sup>nd</sup> edition, John Wiley & Sons, New York, 780p.
- Truesdell, A. H., 1984, Chemical geothermometers for geothermal exploration: Society of Economic Geologists, Reviews in Economic Geology, v. 1, p. 31-44.
- Vargo, A. G., 1990, Structure and petrography of the pre-Beltian rocks of the north-central Gravelly Range, Montana [M.S. thesis]: Colorado State University, 157p.
- Wooden J. L., Vitaliano, C. J., Koehler, S. W., and Ragland, P. C., 1978, The late Precambrian mafic dikes of the southern Tobacco Root Mountains, Montana: geochemistry, Rb-Sr geochronology and relationship to Belt tectonics. Canadian Journal of Earth Sciences, v. 15, p. 467-479

# Response of Douglas Firs Along the Fault Scarp of the 1959 Hebgen Lake Earthquake, Southwestern Montana

Paul E. Carrara - U.S. Geological Survey, Mail Stop 913, Denver Federal Center,  
Denver, CO 80225, [pcarrara@usgs.gov](mailto:pcarrara@usgs.gov)

## ABSTRACT

In order to determine the effect of the 1959 Hebgen Lake earthquake on the annual growth rings of trees, 15 Douglas-firs along the fault scarp were sampled in the Cabin Creek area. Many of these trees were tilted and their root systems were damaged during the earthquake. For control purposes three Douglas-firs, which appeared to be unaffected by the faulting, were sampled about 50 m south of the scarp. Samples consisted of both cores and cross sections. In contrast to the control trees, almost all trees sampled along the fault scarp recorded some disturbance in their tree-ring record as a result of the earthquake. Because the earthquake occurred in mid-August, when the growing season was near its end, 1959 annual rings appear normal, and initial tree response is recorded in the 1960 annual rings. The most common response to earthquake damage was a marked reduction in annual ring width, lasting from as little as two years to more than 20 years. Less commonly, the response of trees to the earthquake included discontinuous or missing annual rings, formation of reaction wood, and an abrupt increase in annual ring width.

The use of tree-ring analysis can be a valuable tool to date earthquakes, or other geologic events, in regions lacking long historical records. In this study, because of the relatively young ages of the trees sampled, information concerning possible earthquake events prior to the 1959 Hebgen Lake earthquake could only be extended back to about 1850. The only earthquake recorded in the tree-ring record at the Cabin Creek site is that of the 1959 earthquake.

## INTRODUCTION

Trees near fault scarps may suffer damage, such as tilting, root breakage or topping, from ground shaking or ground breakage during an

earthquake. Because many tree species can live for several centuries or more (Brown, 1996) tree-ring analysis of trees along fault scarps could be a valuable tool to date earthquakes in regions lacking long historical records. Whereas radiocarbon ages within the last few centuries have relatively large error limits, disturbance in the tree-ring record beginning in a specific year indicates that the tree was damaged sometime between the previous autumn and the following summer growing season. This study reports the results of a tree-ring analysis of 15 Douglas-firs (*Pseudotsuga menziesii*) along the scarp produced by the 1959 Hebgen Lake earthquake and describes the response of these trees to that earthquake.

The Hebgen Lake earthquake, centered in the Hebgen Lake area of southwestern Montana (Fig. 1), occurred during the night of August 17, 1959. This magnitude 7.5 earthquake (Doser, 1985) is the strongest ever recorded in Montana and was felt throughout an area of 1,500,000 km<sup>2</sup> (Witkind and Stickney, 1987). In the Hebgen Lake area the earthquake caused considerable damage. It released a large rockslide that overran a campground and killed 26 people, burying them under an estimated 21 million m<sup>3</sup> of debris (Witkind and Stickney, 1987). This rockslide dammed the Madison River and formed Earthquake Lake. The scarp formed by this earthquake parallels the northern shore of Hebgen Lake for about 12 km from near Red Canyon to west of Cabin Creek. The scarp follows the trace of the Hebgen normal fault that dips southwestward (Witkind, 1964). For most of its length the scarp is about 3 m high, although in a few places near the center the scarp is about 6 m high (Witkind and Stickney, 1987).

Cabin Creek flows west-southwest for about 5 km to join the Madison River in Madison Canyon, at an altitude of 1975 m, about 1 km

west of the lower end of Hebgen Lake (Fig. 1). Here the fault scarp, about 3 m high, offsets the alluvial fan of Cabin Creek. Initial slope angles on this scarp ranged from 70° to 90°, by 1978 the scarp crest had retreated at least 1 m (Wallace, 1980). Under tree roots the alluvium was vertical or overhung. However, below the root system the slope had declined to an angle of about 40°, while at the toe of the slope, angles ranged between 20° and 30° due to the accumulation of material (Wallace, 1980).

The Cabin Creek alluvial fan is forested mainly by Douglas-firs and some Engelmann spruces (*Picea engelmanni*). Many of the trees near the fault scarp are tilted and some are topped. The area is now an U.S. Forest Service exhibit and several large stumps along the fault scarp indicate that some of the more severely damaged or dead trees were removed.

## PREVIOUS WORK

Other investigators have reported the results of tree-ring studies along faults at various sites in western North America, mainly in Alaska and California. In Glacier Bay National Monument, Alaska, Page (1970) sampled 25 trees along the scarp of the 1958 Fairweather earthquake. This earthquake produced at least 6.5 m of right-lateral and 2 m of vertical displacement (Page 1970). Trees sampled included Sitka spruce (*Picea sitchensis*) and western hemlock (*Tsuga heterophylla*) and most ranged in age from 65 to 90 years. Despite the fact that most of the trees sampled were located within a few meters of the fault scarp, only six showed signs of disturbance in their tree-ring record (Page, 1970). At Icy Cape, Alaska, Jacoby and Ulan (1983) used tree-ring analyses of Sitka spruce on a low terrace to demonstrate that the terrace was uplifted several meters by two great earthquakes in 1899. In the Cape Suckling area of Alaska, Sheppard and Jacoby (1989) demonstrated that the 1964 Alaska earthquake was recorded in the annual rings of Sitka spruce, about 240 km from the earthquake's epicenter.

In northern California, LaMarche and Wallace (1972) and Wallace and LaMarche (1979) took core samples from nine trees, at five sites, along

the trace of the 1906 earthquake on the San Andreas fault. Trees sampled included Coast Redwoods (*Sequoia sempervirens*) and Douglas-fir. Despite the fact that the earthquake visibly damaged most of the sampled trees many did not record any disturbance in their tree-ring record. At Stevens Pass, in northeastern California, nine trees recorded anomalously narrow annual rings beginning in 1979, corresponding to a 1978 earthquake in this area (Sheppard and White, 1995). This earthquake is unique in that it caused a tree-ring response even though it only had a magnitude of 4.6.

In southern California near the town of Wrightwood, Meisling and Sieh (1980) cored eight conifers, at two sites, along the 1857 break of the Fort Tejon earthquake on the San Andreas fault. Trees sampled included Jeffrey pine (*Pinus jeffreyi*), white fir (*Abies concolor*), and ponderosa pine (*Pinus ponderosa*). Of the trees sampled, six were visibly damaged. The tree-ring records in five of these trees showed damage or growth anomalies attributable to the 1857 earthquake. Also near Wrightwood, trees along the trace of the San Andreas fault displayed evidence of the 1812 San Juan Capistrano earthquake (Jacoby et al., 1988; Sheppard and Jacoby, 1989). In the above-mentioned studies the most common response in the tree-ring record to earthquake damage was an abrupt reduction in annual ring width.

## METHODS

In this study, 15 Douglas-firs were sampled within eight meters of the fault scarp in the Cabin Creek area (Table 1). Twelve Douglas-firs on the alluvial fan of Cabin Creek (Fig. 2) were sampled in July 1984 with a 5-mm-diameter increment borer (an increment borer is a hand tool with a hollow drill bit, that is screwed into a tree and allows the removal of a thin cylinder of wood with minimal damage to the tree). These trees ranged between 17 and 65 cm in diameter, and 6.5 to 30 m in height. Trunks of eight of the twelve trees were tilted, angles of tilt ranged from 12° to 22°. On tilted trees a complete core was taken through the tree from the upper side to the lower side. On those trees showing no obvious tilt, cores were

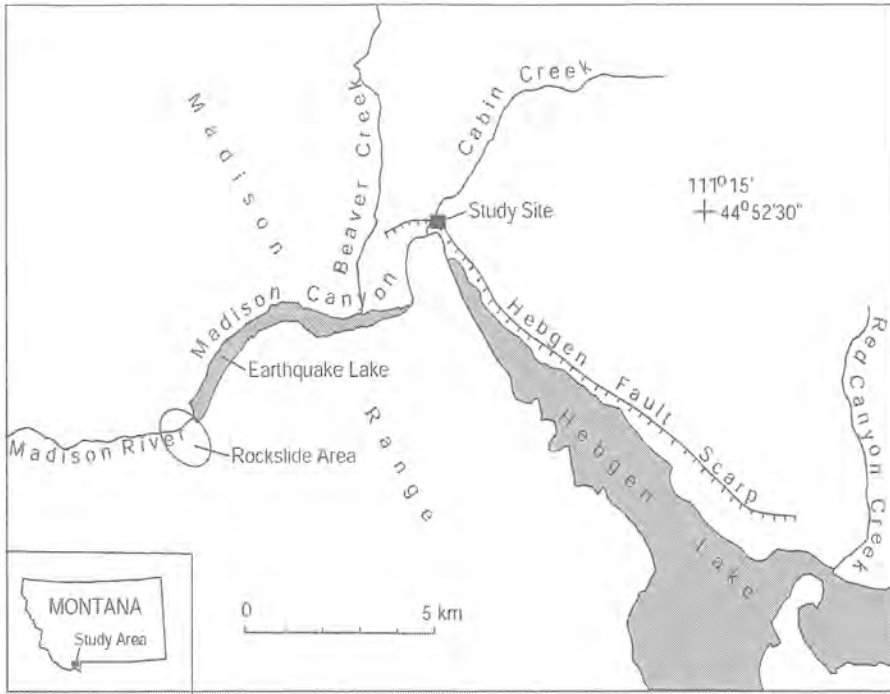


Figure 1- Location map of the Hebgen Lake area.

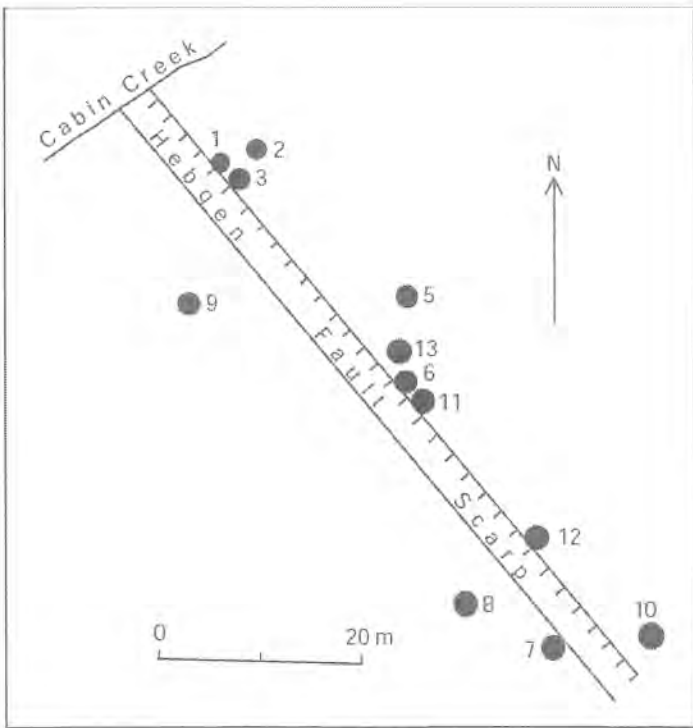


Figure 2- Sketch map of Cabin Creek fan area showing location of trees (#1 to #13) sampled in this study. Trees #14, 15, and 16 about 50 to 100 m to southeast.

**Table 1.** Response of Douglas-firs along the 1959 Hebgen fault scarp near Cabin Creek.

Field no.	Innermost ring	Useful record	Distance from scarp (m)	Above (+) below (-) scarp	Tilt (degrees)	Response of tree to earthquake (opposite radii separated by /)
15	1940 (P)	1941-83	1	-	20	60-62 VN, 63 N, 64-83 GF/ 60-62 VN, 63 N, 64-71 RW
8	1933	1935-83	5	-	none	60-61 N, 62 SN/ 60 N, 61 VN, 62 SN
12	1932	1933-83	<1	+	none	60 N/ 60-61 N
16	1926 (P)	1929-93	<1	-	12	60-62 N/ 60-72 RW
14	1923 (P)	1929-83	<1	-	15	60-83 VN/60-83 N, 60-72 RW)
7	1913 (P)	1914-83	1	-	14	60-68 VN, 69-79 N, 80-83 SN/ 60-63 VN, 64-67 N, 68 SN, 69-72 RW
10	1909	1909-83	3	+	none	no response
11	1904	1905-83	<1	+	13	60 SN/ 60-61 SN
1	1874	1875-1983	<1	+	13	60-61 SN/ 60-61 N, 62 SN, 63-72 RW
6	1869	1870-1983	<1	+	none	60 N/ 60-61 SN
13	1867	1867-1983	4	+	12	60 SN/ 60-61SN
5	1856	1857-1983	8	+	20	60-61 SN/ 60-61 SN
2	1845	1846-1983	4	+	22	60-69 N, 70-71 SN/ 60-61 N, 62-65 SN, 68-78 RW
9	1843	1844-1983	7	-	12	no response
3	1840	1841-1983	1	+	17	60-61 M, 62-65 SN/ 60-61 M, 62-63 N, 64-83 SN, 68-70 RW

VN- very narrow (width of annual ring <25% of width of 1959 ring)  
 N- narrow (width of annual ring 26-50% of width of 1959 ring)  
 SN- slightly narrow (width of annual ring 51-75% of width of 1959 ring)  
 GF- growth flush, M- missing, P-pith, RW- reaction wood, X- cross section

obtained along a diameter at a right angle to the fault scarp. Cross sections were taken from two small Douglas-firs (#14 and 15, Table 1) along the fault scarp about 100 m southeast of the Cabin Creek alluvial fan. In August 1993 an additional cross section was collected (tree #16) about 50 m southeast of the alluvial fan. These cross sections were collected from trees that ranged between 10 and 15 cm in diameter, 2 to 3 m in height, and were tilted 12° to 20° (Table 1). For control purposes three Douglas-firs, about 50 m south of the scarp, which appeared to be unaffected by the faulting were sampled.

The cores were prepared using standard procedures as discussed in Stokes and Smiley (1968). The cores were initially stored for several weeks in grooved redwood drying boxes that allowed the cores to dry with minimal twisting and curling. The cores were then glued into a semicylindrical groove in a small board and sanded several times with progressively finer grits to a fine finish (600 grit). Finally, the cores were rubbed with fine steel wool to a high polish. The cross sections taken from the three small Douglas-firs were allowed to dry for several weeks, then sanded to a flat surface with

a belt sander to 120 grit. Finer sanding was accomplished with a rotary sander to 320 grit and then by hand with progressively finer grits to 600 grit. The cross sections were then polished with fine steel wool.

Annual growth rings in the cores and cross sections were inspected under a binocular microscope (6X, 12X, and 25X) for signs of disturbance. One year was assigned to each ring counted. In temperate regions a tree will add (grow) one ring every year. Each annual ring consists of two parts, earlywood and latewood. Earlywood is produced in the early part of the growing season and is characterized by large, porous, thin-walled cells. Latewood is produced in the later part of the growing season and is characterized by small, thick-walled cells that commonly are darker than earlywood cells (Panshin and de Zeeuw, 1970). It is the sharp contrast between the last-formed latewood cells of one year and the first-formed earlywood cells of the following season that distinguishes the boundary of the annual ring.

False annual rings were noted in several cores and may have resulted from cold periods during growing seasons. False annual rings can be distinguished from annual rings in that the cells composing the latewood in the false annual rings grade to the inside and outside into more porous tissue. In true annual rings the transition from the latewood of one year to the earlywood of the next year is abrupt (Panshin and de Zeeuw, 1970).

### TYPES OF DISTURBANCE IN THE TREE-RING RECORD

Several types of disturbance in the tree-ring record, as a result of the 1959 Hebgen Lake earthquake, were present among the trees sampled in this study. As in the previous studies mentioned, the most common response of the trees to earthquake damage was (1) an abrupt reduction in annual ring width, either for several years or an extended period (Fig. 3). Less commonly, the response of trees to disturbance included (2) discontinuous or missing annual rings, (3) the formation of reaction wood, and (4) an abrupt increase in annual ring width.

Because the main shock of the Hebgen Lake earthquake, when many of the Douglas-firs along the scarp suffered damage, occurred on August 17, 1959, near the end of the growing season, 1959 annual rings are normal, and disturbance is first detected in the 1960 annual rings.

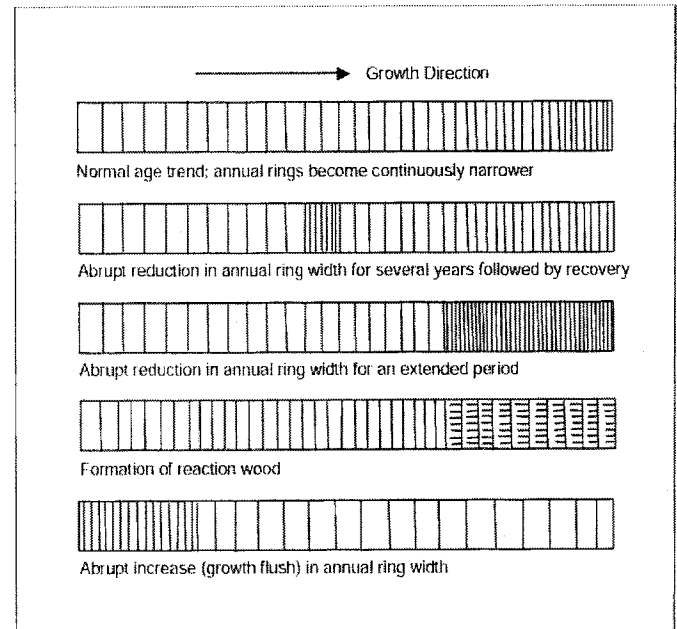


**Figure 3-** Types of disturbance displayed in the tree-ring records of Douglas-firs damaged by the 1959 Hebgen Lake earthquake in this study (after Kienast and Schweingruber, 1986).

### Reduction in annual ring width

A reduction in annual ring width (Figs. 4a, 5a, and 6) for several years or more can be the result of injury, such as root damage, loss of a major limb, or topping. In this study, the tree-ring records of most (13 of the 15 trees) of the Douglas-firs sampled along the Hebgen Lake scarp exhibited a reduction in annual ring width (commonly less than 50% the thickness of the 1959 annual ring) beginning in 1960 (Table 1) that is not displayed by control trees sampled about 50 m south of the study site (Fig. 5b). In most cases (9 trees), the response consisted of the formation of narrow annual rings beginning in 1960 and continuing for 1, 2, or 3 years. However, several trees produced narrow annual rings for a number of years after the earthquake.

For instance, tree #14 (Figs. 4a and 6) produced narrow annual rings along its entire circumference from 1960 to 1983, the last complete year of growth for this tree prior to sampling. However, the response of the trees was not necessarily uniform along opposing radii. Tree #7 produced narrow annual rings from 1960 to 1983 along one radius and narrow annual rings from 1960 to 1968 along the opposing radius (Table 1). It was noted that in many cases the reduction in annual ring width continued after 1960, such that in many trees 1961 was the narrowest annual ring before the tree began to recover and annual rings became thicker.

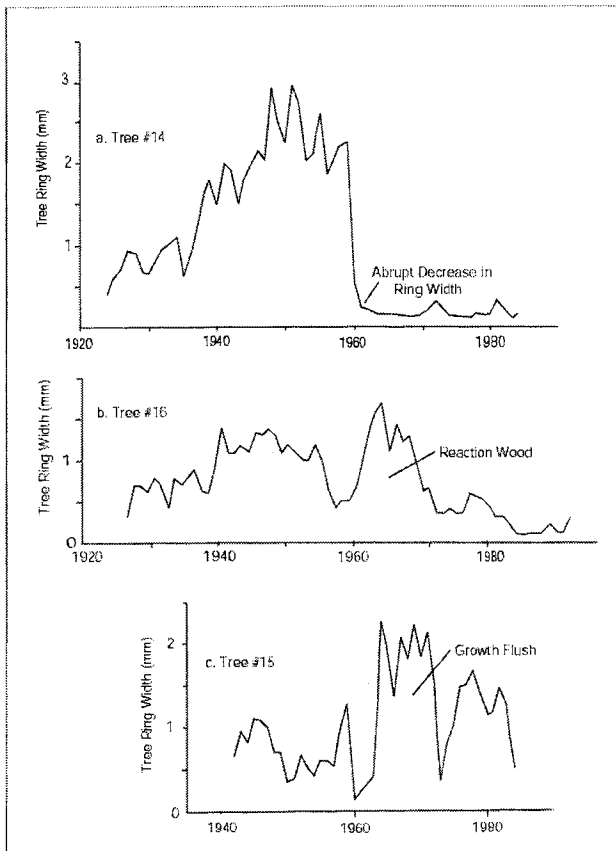


**Figure 4-** Graphs of annual ring widths indicating various types of disturbance in the tree-ring record of trees sampled in this study. 4a, graph of tree #14 showing abrupt reduction in tree-ring width; 4b, graph of tree #16 showing formation of reaction wood; 4c, graph of tree #15 showing growth flush.

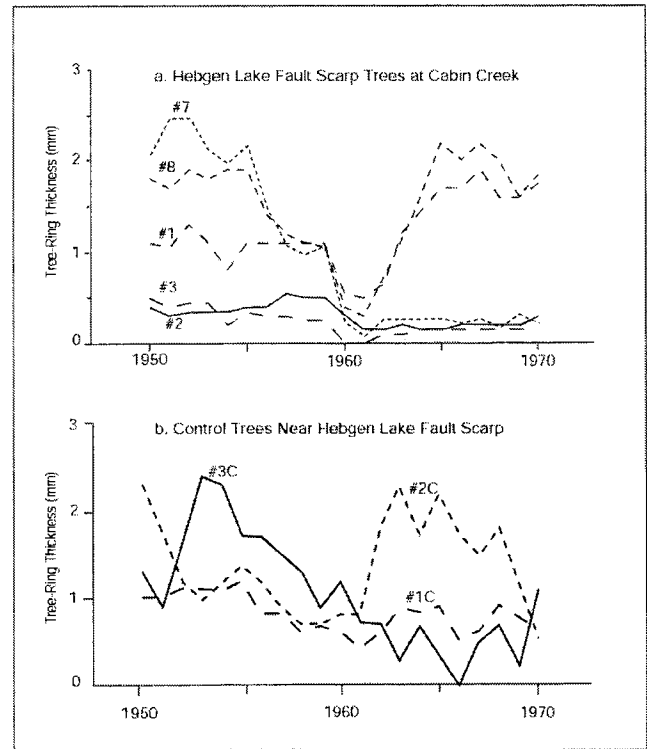


**Figure 5-** Graphs of annual ring widths of trees near the Hebgen fault scarp in the Cabin Creek area. 5a, Graphs of trees #1, 2, 3, 7, and 8 (Table 1) showing an abrupt reduction in tree-ring widths beginning in 1960. 5b, Graphs of annual ring widths for three control trees sampled about 50 m south of the Hebgen fault scarp in the Cabin Creek area.

### Discontinuous and missing annual rings

Discontinuous and missing annual rings result when the cambium remains dormant along part (discontinuous) or all (missing) of the tree's circumference during the growing season. They can be common in older, environmentally stressed (drought), or severely damaged trees (Panshin and de Zeeuw, 1970). In this study, discontinuous annual rings were noted in several trees, usually on the upper side of a tilted tree.

Missing annual rings can be detected by cross-dating, (the recognition of commonly shared distinctive annual rings of known age (Douglas, 1941) with nearby trees). In this study, missing

annual rings were noted in one tree. The oldest tree sampled in this study, tree #3, is missing annual rings for the years of 1960 and 1961. This tree then formed narrow annual rings from 1962 until 1965 along one radius, and from 1962 until 1983, its last complete year of growth prior to sampling, along the other radius (Table 1).

### Reaction wood formation

Reaction wood is formed on the underside of a tilted conifer. Tilting of a conifer will result in eccentric growth, the formation of wide annual rings of reaction wood (Figs. 4b and 7) on the underside of the tilted tree and narrow annual rings (or discontinuous annual rings) on the upper side of the tree (Panshin and de Zeeuw, 1970). Reaction wood in conifers is similar in appearance to latewood but generally darker and denser. It is usually characterized by reddish-yellow color and small, thick-walled cells. Tracheids in reaction wood are shorter and have more rounded cross sections than normal tracheids that are longer and have angular cross sections (Panshin and de Zeeuw, 1970). The initial year of reaction wood formation provides a minimum estimate of the date of tilting. In this study, reaction wood formation was observed in seven trees that were tilted as a result of the earthquake. In trees #14 and 16, reaction wood was formed on the underside of the tilted trees from 1960 to 1972 (Table 1). In other trees, reaction wood formation was delayed for several years after the 1959 Hebgen Lake earthquake. These trees (#1, 2, 3, 7, and 15) were severely damaged and formed narrow annual rings on both the upper and underside of the tree as an initial response to the damage. After a recovery period of 3 to as many as 9 years, formation of reaction wood was initiated. For instance, tree #1 produced narrow annual rings from 1960 to 1962, then formed reaction wood from 1963 to 1972, whereas tree #7 formed narrow annual rings from 1960 to 1968 before reaction wood formation began in 1969.

Although reaction wood is readily recognized in cross sections, it is difficult to identify in cores. As many of the samples in this study consisted of cores, the occurrence of reaction wood in this study is probably underrepresented.

### Increase in annual ring width

An abrupt increase in annual ring width (growth flush) (Figs. 4c and 8) may occur due to changes in environmental conditions that are beneficial to growth. A large earthquake may cause changes in soil moisture, ground water, or the amount of sunlight available to a given tree. In this study, an increase in annual ring width was noted in one tree (#15), probably due to an increase in sunlight because nearby taller shading trees were felled by the earthquake. However, this growth flush was delayed for several years while the tree recovered from initial damage. This tree produced narrow annual rings from 1960 to 1963 before beginning a growth flush in 1964.

### LIMITATIONS OF TREE-RING ANALYSIS

Several factors limiting the use of tree-ring analysis to detect earthquake events became readily apparent in this study.

#### Severity of earthquake

The earthquake must be severe enough to damage the trees. Generally, without surface rupture (usually about magnitude 6.5 or greater) to damage the root system or enough ground shaking to tilt or top a tree, the earthquake would probably not be recorded in the tree-ring record.

#### Proximity to surface rupture

Trees must be close enough to the surface rupture to be damaged. For instance, in the Great Basin seemingly recent fault scarps are present along the base of many ranges. Unfortunately, these scarps are usually below treeline and are only rarely in areas inhabited by pinyon pines (*Pinus edulis*) and junipers (*Juniperus*). In this study, no evidence in the tree-ring record of trees #9 and #10, which were only 7 and 3 m, respectively, from the scarp, could be found of the 1959 Hebgen Lake earthquake (Table 1). In addition, tree #5, which was about 8 m from the



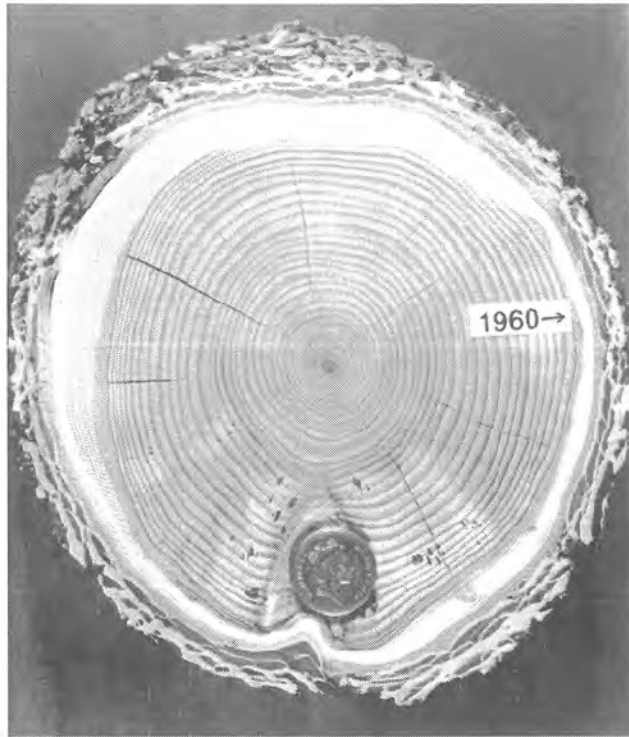


Figure 6- Photo of cross section of tree #14 showing an abrupt reduction in growth increment (tree-ring width) beginning in 1960. Coin is 20 mm in diameter.

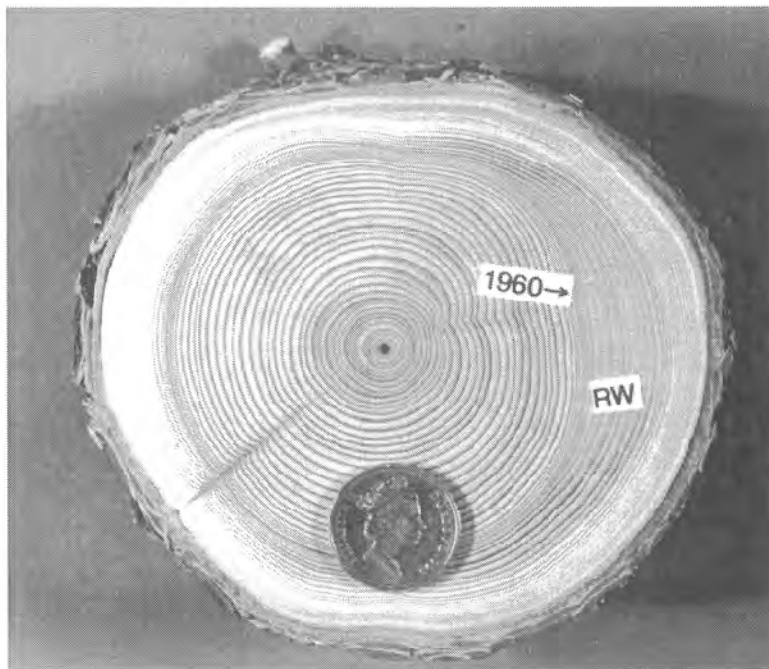
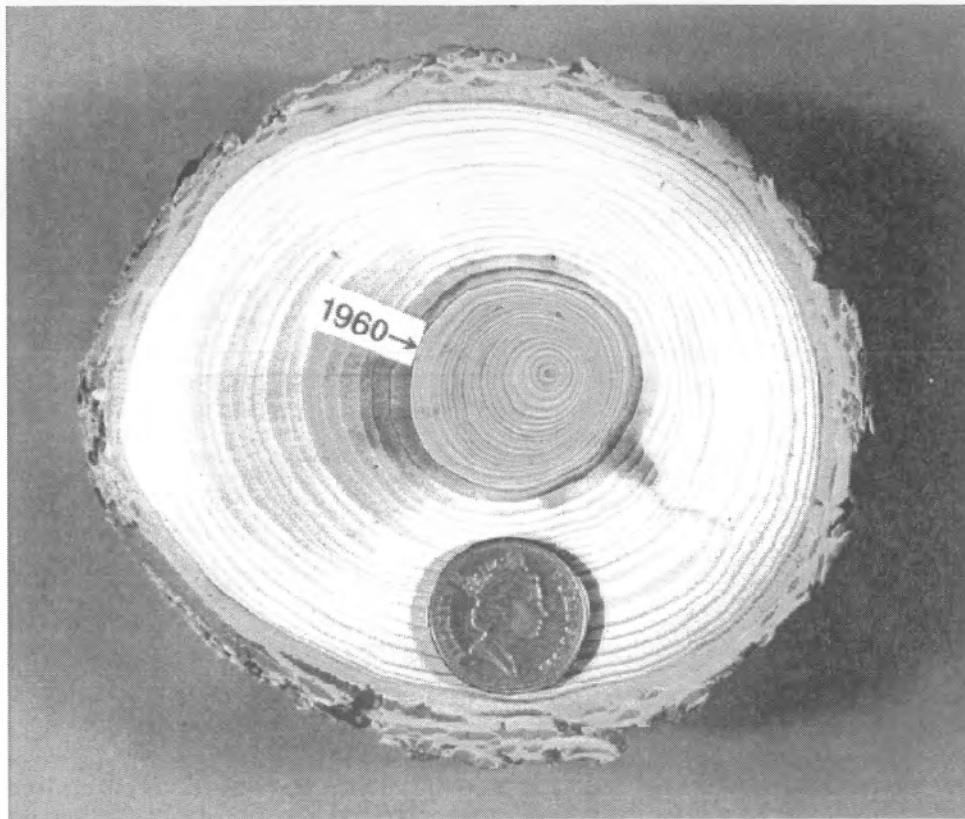


Figure 7- Photo of cross section of tree #16 showing the initiation of reaction wood in 1960. Coin is 20 mm in diameter.



**Figure 8-** Photo of cross section of tree #15 showing an abrupt increase in growth increment beginning in 1963. Coin is 20 mm in diameter.

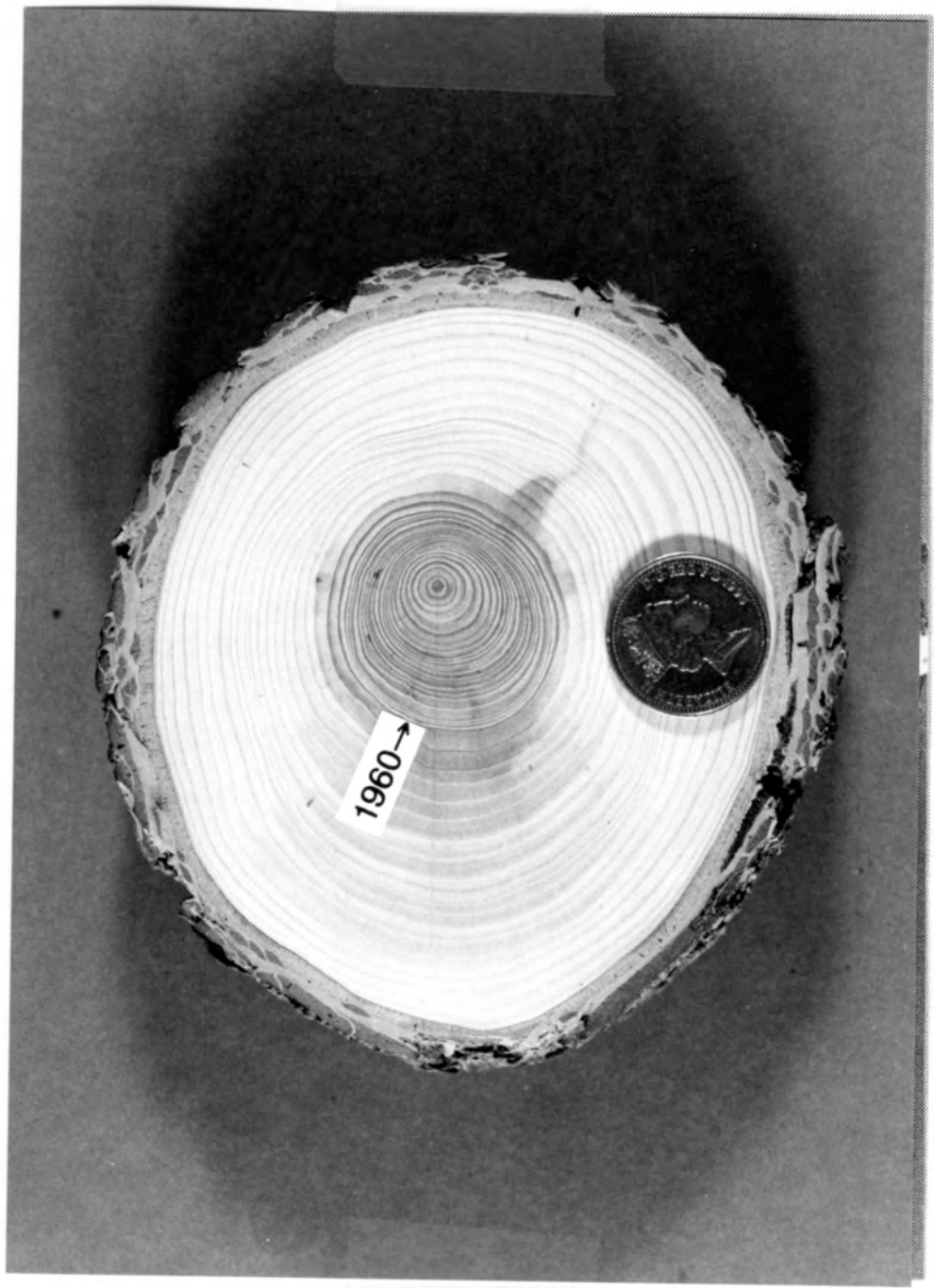


Figure 8

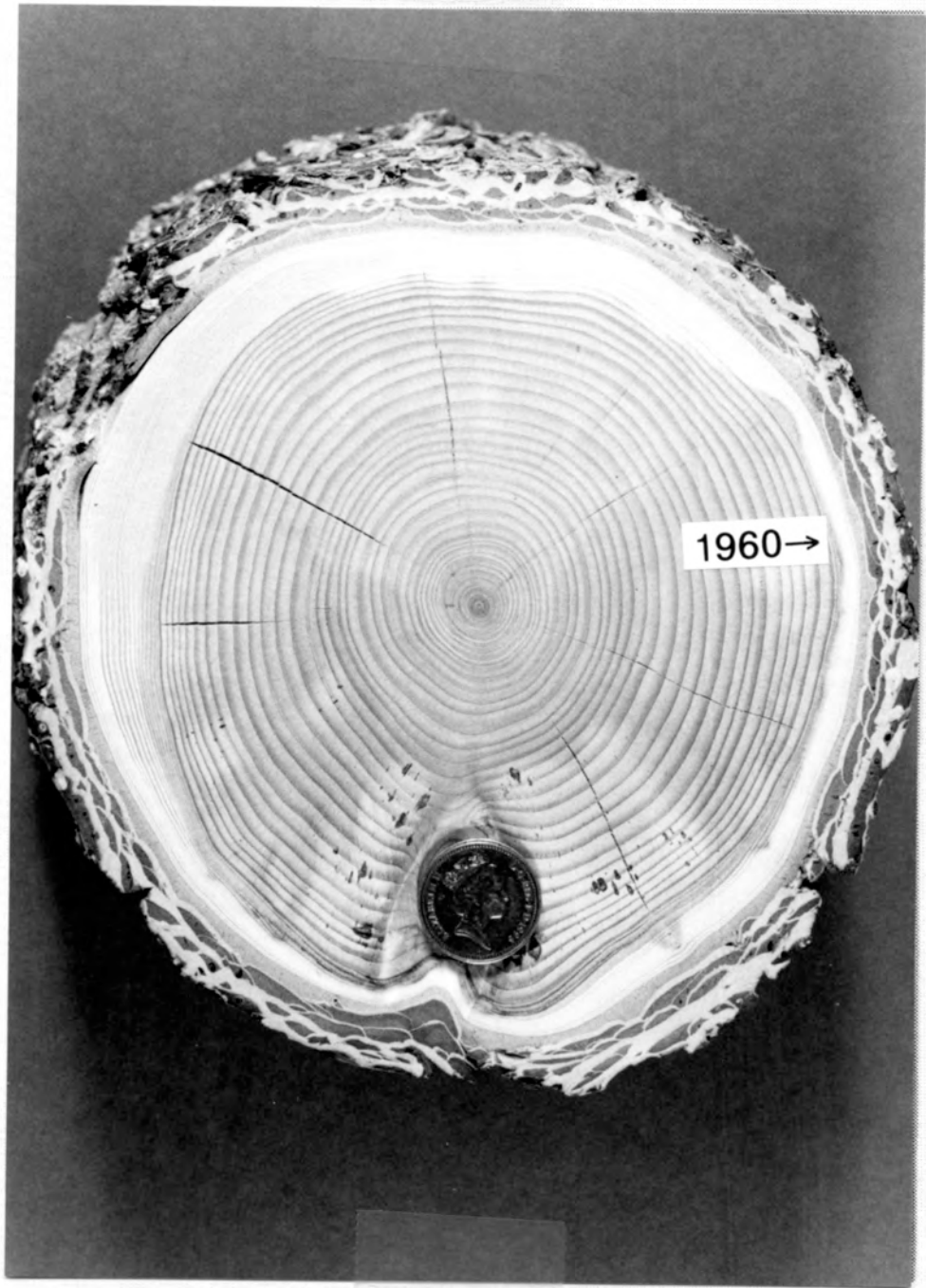


Figure 6

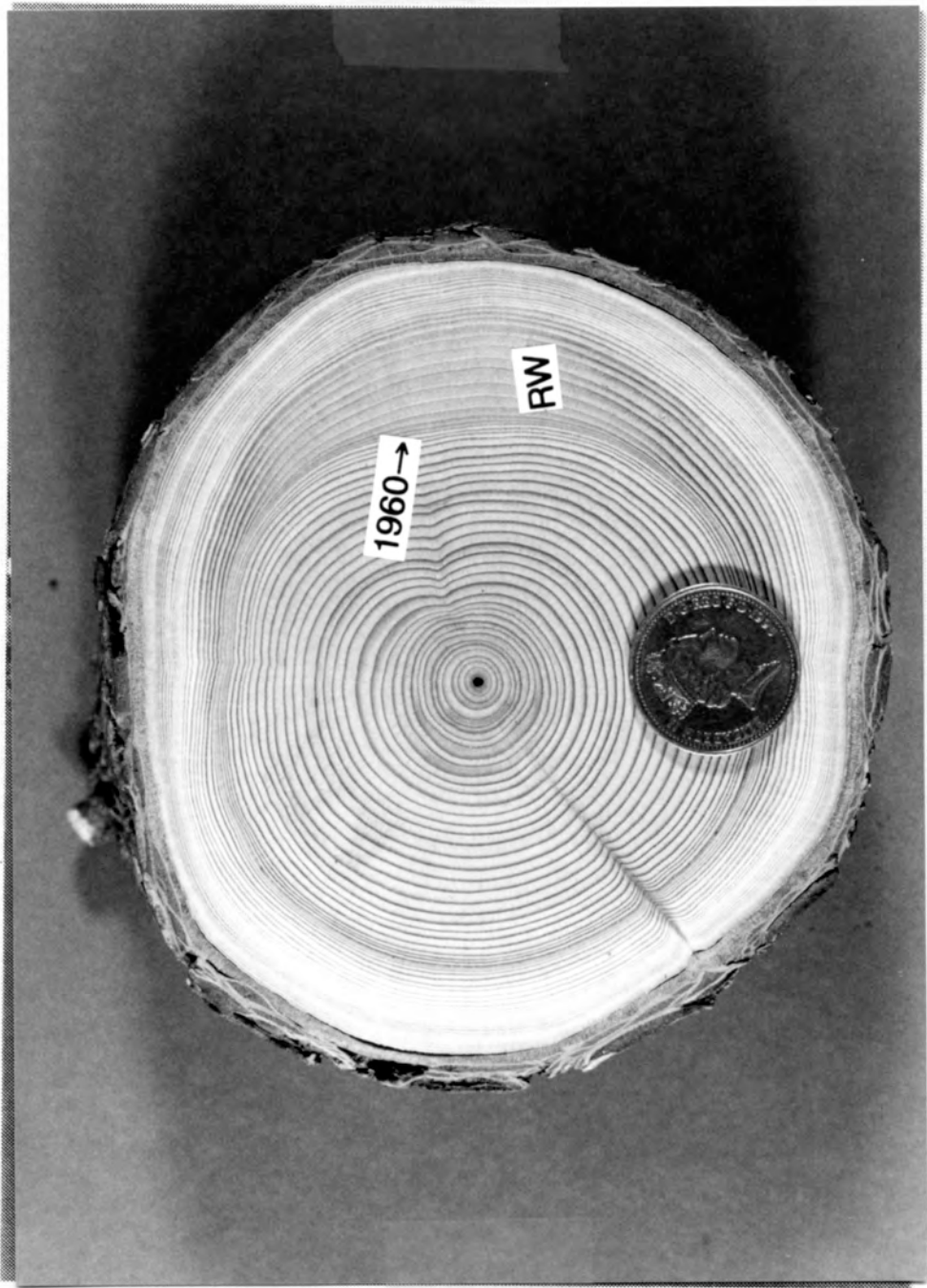


Figure 7

top edge of the scarp, recorded only slightly narrow rings in 1960 and 1961. Hence, trees sampled for earthquake information should be no more than several meters from an existing fault scarp.

### **Ages of the trees sampled**

The age of the trees themselves may be a limitation. Although ages of Douglas-firs can exceed 1000 years (Brown, 1996), the oldest tree in this study (#3) had an innermost ring of 1840 and only three trees had records extending back prior to 1850 (Table 1). Hence, information concerning possible earthquake events prior to the 1959 Hebgen Lake event could only be extended back to about 1850, about 20 or 30 years before white settlement of the region. No prior disturbance in the tree-ring record similar to that recorded by the 1959 Hebgen Lake earthquake is present in the trees sampled in this study. Hence, the only earthquake activity recorded at this site from 1850 until the sampling of the trees in 1984 is the 1959 Hebgen Lake earthquake.

The earthquake may cause an additional limitation on the age of the trees. Those trees damaged by an earthquake may suddenly be at a competitive disadvantage with other nearby trees that sustained little or no damage. This disadvantage may in time lead to an earlier than normal death, such that several decades after a major earthquake those trees that suffered the most damage and hence have the best evidence of the event in their tree-ring record, are no longer alive. At a site in the Gravelly Range, about 20 km to the west, 11 Douglas-firs, including one standing dead tree, were sampled for information concerning the relationship between landslide movement and earthquakes (O'Neill et al., 1994). Only the dead tree showed striking evidence of the 1925 Clarkson earthquake. None of the live trees showed any sign of disturbance of this event. The dead tree was heavily damaged and tilted by this event and formed wide annual rings of reaction wood for several years before entering a period of reduced growth rate (narrow annual rings). The tree died in 1932, yet remained standing for 60+ years before it was cross-sectioned for analysis.

Hence, it may be worthwhile to sample dead trees at a given site and cross-date them to the live trees at the same site.

### **Response to disturbance may mask subsequent disturbance**

While a tree is recovering from damage sustained by one event, such as forming very narrow annual rings, a subsequent event may not result in a notable disturbance in the tree-ring record. For instance in this study, tree #14 (Figs. 4a and 6) showed a marked reduction in annual ring width following the August 1959 Hebgen Lake earthquake that lasted for more than 20 years beginning in 1960. Hence, although this tree indicated a strong response to the Hebgen Lake event, subsequent earthquakes, if they had occurred, may not have been detected because this tree was already forming narrow annual rings. In addition, because older trees commonly grow at a slow rate (produce narrow annual rings), any reduction caused by earthquake damage might not be readily apparent in their tree-ring record.

### **Response recorded in tree-ring record can have number of possible causes**

Annual ring anomalies in trees disturbed by earthquakes (reduction in annual ring width, discontinuous and missing annual rings, reaction wood formation, abrupt increase in annual ring width) can be caused by a number of other damaging factors including landslides, snow avalanches, floods, windstorms, insect infestations, and fires. Hence, the investigator must be sure of the cause of the response recorded in the tree-ring record. It is important to determine the location of the sampled trees in relation to their geomorphic position; fault scarp, landslide, snow avalanche track, flood plain.

In addition to a tree that shows obvious physical damage, reductions in annual ring width due to damage can be separated from reductions due to climatic factors. In this study, reductions in annual ring width caused by the 1959 Hebgen Lake earthquake lasted from as little as two years to more than 20 years. Furthermore, the nearby control trees growing away from the

affected area (fault scarp in this case) did not display any reduction in annual ring width beginning in 1960 (Fig. 5b). Trees that exhibit a reduction in annual ring width caused by climatic factors should have an uniform response, hence, these trees should recover at about the same year, and such response should occur over a broader region (away from the scarp). Similar differences between earthquake disturbed trees and climatic responses were noted by Jacoby et al. (1988).

In this study, some of the sampled trees also displayed a reduction in annual ring width from 1917 to about 1924, and from 1933 to 1936. For the earlier period, most trees resumed normal annual ring widths by about 1924. For the latter period, the response was even more uniform and all trees resumed normal annual ring widths in 1937. This latter period also corresponds to a period of reduced annual ring widths recorded in Douglas-firs at a site near Gardner, Montana (Drew, 1975), about 55 km northeast of the Hebgen Lake area. Both periods of narrow annual rings correspond to periods of reduced spring and summer precipitation (Bradley, 1976). In addition, reaction wood is not associated with either period in trees sampled at the study site, hence these disturbances in the tree-ring record were caused by climatic factors.

## CONCLUSIONS

In this study the majority of Douglas-firs sampled along the fault scarp in this study displayed evidence of the 1959 Hebgen Lake earthquake in their tree-ring record. Because this earthquake occurred in mid-August, when the growing season was near its end, the 1959 annual ring appears normal and initial tree response is recorded in the 1960 annual ring. The most common response to earthquake damage was a marked reduction in annual growth increment, lasting from as little as two years to more than 20 years. Less commonly, the response of trees to the earthquake included discontinuous or missing annual rings, formation of reaction wood on the underside of tilted trees, and an abrupt increase in annual ring width.

Although the use of tree-ring analysis to date various geologic events has its limitations, the method can be a valuable tool to date events in regions lacking long historical records. In this study, because of the ages of the trees sampled, information concerning possible earthquake events prior to the 1959 Hebgen Lake event could only be extended back to about 1850. The only earthquake activity recorded in the tree-ring record at this site is that of the 1959 earthquake.

## ACKNOWLEDGMENTS

The author thanks K.M. Haller and S.F. Personius (U.S. Geological Survey, Denver) and K.L. Pierce (U.S. Geological Survey, Bozeman) whose knowledge and ideas contributed to this paper. This manuscript benefited substantially from reviews by F.C. Brunstein, T.K. Hinkley, L.E. Strickland (U.S. Geological Survey, Denver), and A.D. Barnosky (University of California, Berkeley).

## REFERENCES

- Bradley, R.S., 1976, Precipitation history of the Rocky Mountain states, Westview Press, Boulder, Colorado, 334 p.
- Brown, P.M., 1996, Oldlist: a database of maximum tree ages. In Dean, J.S., Meko, D.M., and Swetnam, T.W. eds., *Tree rings, environment, and humanity: Radiocarbon*, p. 727-731.
- Douglas, A.E., 1941, Crossdating in dendrochronology: *Journal of Forestry*, v. 39, p. 825-831.
- Doser, D.I., 1985, Source parameters and faulting processes of the 1959 Hebgen Lake, Montana, earthquake sequence: *Journal of Geophysical Research*, v. 90, p. 4537-4555.
- Drew, L.G., ed., 1975, *Tree-ring chronologies of western America, Washington, Oregon, Idaho, Montana, and Wyoming*: v. 5, Laboratory of Tree-Ring Research, University of Arizona, Tucson, 45 p.
- Jacoby, G.C., Jr., Sheppard, P.R., and K.E. Sieh, K.E., 1988, Irregular reoccurrence of large earthquakes along the San Andreas fault: evidence from trees: *Science*, v. 241, p. 196-199.
- Jacoby, G.C., Jr., and Ulan, L.D., 1983, Tree ring indications of uplift at Icy Cape, Alaska, related to 1899 earthquake: *Journal of Geophysical Research*, v. 88, no. B11, p. 9305-9313.

- Kienast, F., and Schweingruber, F.H., 1986, Dendroecological studies in the Front Range, Colorado, U.S.A: Arctic and Alpine Research, v. 18, p. 277-288.
- LaMarche, V.C., Jr., and Wallace, R.E., 1972, Evaluation of effects on trees of past movements on the San Andreas fault, northern California: Geological Society of America Bulletin, v. 83, p. 2665-2676.
- Meisling, K.E., and Sieh, K.E., 1980, Disturbance of trees by the 1857 Fort Tejon Earthquake, California: Journal of Geophysical Research, v. 85, no. B6, p. 3225-3238.
- O'Neill, J.M., LeRoy, T.H., and Carrara, P.E., 1994, Preliminary map showing Quaternary faults and landslides in the Cliff Lake Quadrangle, Madison County, Montana: U.S. Geological Survey Open-File Report 94-198, 1:24,000.
- Page, R., 1970, Dating episodes of faulting from tree-rings: effects of the 1958 rupture of the Fairweather fault on tree growth: Geological Society of America Bulletin, v. 81, p. 3085-3094.
- Panshin, A.J., and de Zeeuw, C., 1970, Textbook of wood technology (3rd ed., v. 1): McGraw-Hill, New York, 705 p.
- Sheppard, P.R., and Jacoby, G.C., 1989, Application of tree-ring analysis to paleoseismology: two case studies: Geology, v. 17, p. 226-229.
- Sheppard, P.R., and White, L.O., 1995, Tree-ring responses to the 1978 earthquake at Stephens Pass, northeastern California: Geology, v. 23, p. 109-112.
- Stokes, M.A., and Smiley, T.L., 1968, An introduction to tree-ring dating: University of Chicago, 73 p.
- Wallace, R.E., 1980, Degradation of the Hebgen Lake fault scarps of 1959: Geology, v. 8, p. 225-229.
- Wallace, R.E., and LaMarche, V.C., Jr., 1979, Trees as indicators of past movements on the San Andreas fault: Earthquake Information Bulletin, v. 11, p. 127-131.
- Witkind, I.J., 1964, Reactivated faults north of Hebgen Lake: U.S. Geological Survey Professional Paper 435-G, p. 37-50.
- Witkind, I.J., and Stickney, M.C., 1987, The Hebgen Lake earthquake area, *In* S.S. Beus, S.S., ed., Centennial Field Guide, Rocky Mountain Section: Boulder, Colorado, Geological Society of America, v. 2, p. 89-94.



# Geology of the Yellowstone Talc Mine

Mike Cerino, Luzenac America, Inc., Cameron, MT

---

## INTRODUCTION

The Yellowstone Mine is owned and operated by Luzenac America, Inc. part of Luzenac Group with talc mining, milling, and marketing organizations worldwide. Luzenac Group is 100% owned by Rio Tinto.

Yellowstone talc deposits are hosted in pre-Belt dolomitic marble located in the east foothills of the Gravelly range next to the Madison Valley, about 25 miles south of Ennis, Montana (**figure 1**). Pre-Beltian rocks in the Yellowstone Mine area are northeast striking metavolcanics and metasediments including dolomitic marble, phyllite, amphibolite, biotite-plagioclase schist, quartzite, and banded iron formation.

These rocks decrease in metamorphic grade from amphibolite grade in the Cherry Creek area north, of the Yellowstone mine to greenschist grade to the south (Vargo, 1990), (Heinrich and Rabbit, 1960). The lower grade greenschist rocks found adjacent to the Yellowstone mine include the central 1.5 by 3 mile body of marble that hosts talc deposits. Primary sedimentary structures present in the low-grade rocks, particularly cross bedding in the quartzites, indicate that stratigraphic up is to the northwest.

Differences in geochemistry, primary structure, and lithology between the lower grade rocks in the vicinity of the talc mine and the higher grade rocks to the north of the talc mine have led Vargo – (1990) to conclude that the lower grade greenschist rocks are a distinct suite of rocks,

separate from the Cherry Creek Metamorphic Suite. One of the more compelling pieces of evidence in support of this conclusion is the presence of primary sedimentary structures in the lower grade rocks. The primary aim of the selected field traverses for this trip is to observe documented sedimentary structures in the rock as well as some undocumented structures that may be sedimentary.

Traverses at three locations will cross pre-Beltian rock units in the vicinity of the Yellowstone Mine. Three additional stops will be made, in the open pits at the Yellowstone Mine to look at talc ore bodies in dolomitic marble. Leaders for this field trip will be Mike Cerino – Luzenac America, and Dick Berg – Montana Bureau of Mines and Geology.

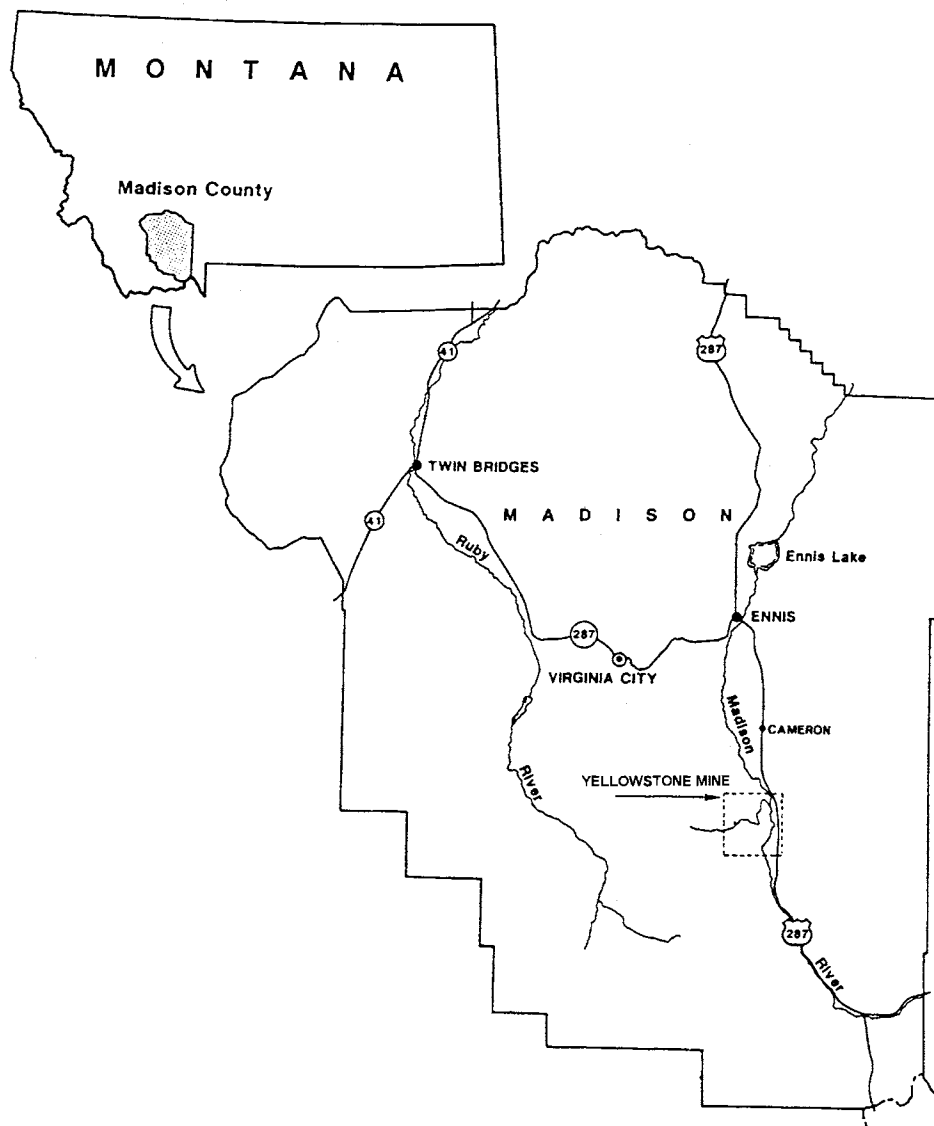
The Yellowstone Mine is located on private property. Permission from Luzenac America must be obtained before entering the property.

## Cumulative Mileage            Description

**0.0**     Meet at the parking lot just west of the Catholic church in Ennis, MT. Drive south on Main Street through town and continue south on US Hwy 287.

### **21.0**

**21.0**     Turn off US Hwy 287 just past the Indian Creek bridge (right) and proceed west on the gravel road.



General Location of the Yellowstone Talc Mine, Madison County, Montana.

FIGURE I

## 0.5

**21.5** Cross the Madison River at the McAtee bridge and follow the road up the river grade. Watch for semi-truck trailers hauling talc from the mine.

## 2.6

**24.1** Stop at the Yellowstone Mine office (**stop #1**), the large blue building on the right, to sign-in and pick-up a hardhat and safety glasses.

## 2.2

**26.3** Drive from the mine office back to the public road and continue up hill to **stop #2** (figure 2). The rock units along this traverse were mapped by Vargo-1990. Walk down the hogback ridge made up of northeast-striking units of banded iron formation, biotite plagioclase schist, quartzite, and phyllite (pCp). The banded iron formation (BIF) forms the backbone of the ridge top with outcrops of biotite plagioclase schist in contact to the northwest. A band of phyllite lies in contact to the southeast of the BIF. Layers of marble and quartzite lie within the phyllite map unit striking NE. Wedge set cross beds are visible in the quartzite along with discontinuous green coloration due to the presence of the chromium-rich muscovite, fuchsite. Vargo (1990) gave the following descriptions of these rock units:

- Banded iron formation (pCi)- alternating layers of magnetite and quartz with minor hematite, goethite, and hydrobiotite. Tight folds are locally abundant.
- Biotite plagioclase schist (pCbps) – Dark brown-gray to black, well foliated schist containing quartz, plagioclase, biotite, chlorite, magnetite, and muscovite. Abundant plagioclase porphyroblasts.
- Quartzite (pCq) – White, tan, gray, green, or black quartzite with variable amounts of

muscovite (fuchsite), biotite, and/or chlorite; black variety is actinolite bearing; tan variety is hematite and calcite bearing with minor micas. Tangential and trough crossbeds locally present. Occurs in phyllite unit as ridges or low outcrops where it is more micaceous.

- Phyllite (pCp) – Greenish-gray, greenish-red, gray-red, and dark gray phyllite containing quartz, biotite, chlorite, muscovite, hematite, and magnetite with rare garnet.

## 1.3

**27.6** Drive back down the public road to **stop #3** (figure 2). A long outcrop of quartzite with excellently preserved wedge set cross beds is exposed within a BIF unit here. The cross beds show that stratigraphic up is to the northwest.

## 0.4

**28.0** Continue down the public road to the gated entrance into the talc mine. **Stop #4** is a traverse across amphibolite, and phyllite in contact with the mass of dolomitic marble which hosts the Yellowstone Mine talc deposits.

- Amphibolite (pCa) – Green, fine-grained amphibolite containing actinolite, plagioclase, epidote, and quartz. Slightly foliated with local zones of chlorite-actinolite schist. Weathers to blocky outcrops (Vargo, 1990).
- Phyllite (pCp) – see description under stop #1.
- Dolomitic Marble (pCm) - Orange brown weathering surfaces, fine grained gray sucrosic marble composed primarily of dolomite with minor quartz mullion and rodding. Locally recrystallized into white to maroon coarse rhombohedral crystals. Contains talc deposits in commercial quantities.

Geologic Map of the  
Yellowstone Mine Area  
(Modified after Vargo - 1990)

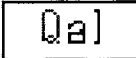


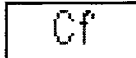


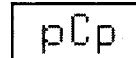
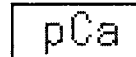








	Alluvium
	Gravels & Colluvium
	Rhyolite Ash and Tuff
	Flathead Quartzite
	Dolomitic Marble
	Talc Orebody
	Phyllite
	Amphibolite
	Banded Iron Formation
	Biotite Plagioclase Schist
	Reverse Fault
	Normal Fault
	Fold
	Tour Route
	Traverses
	Field Stops

Figure 2 a

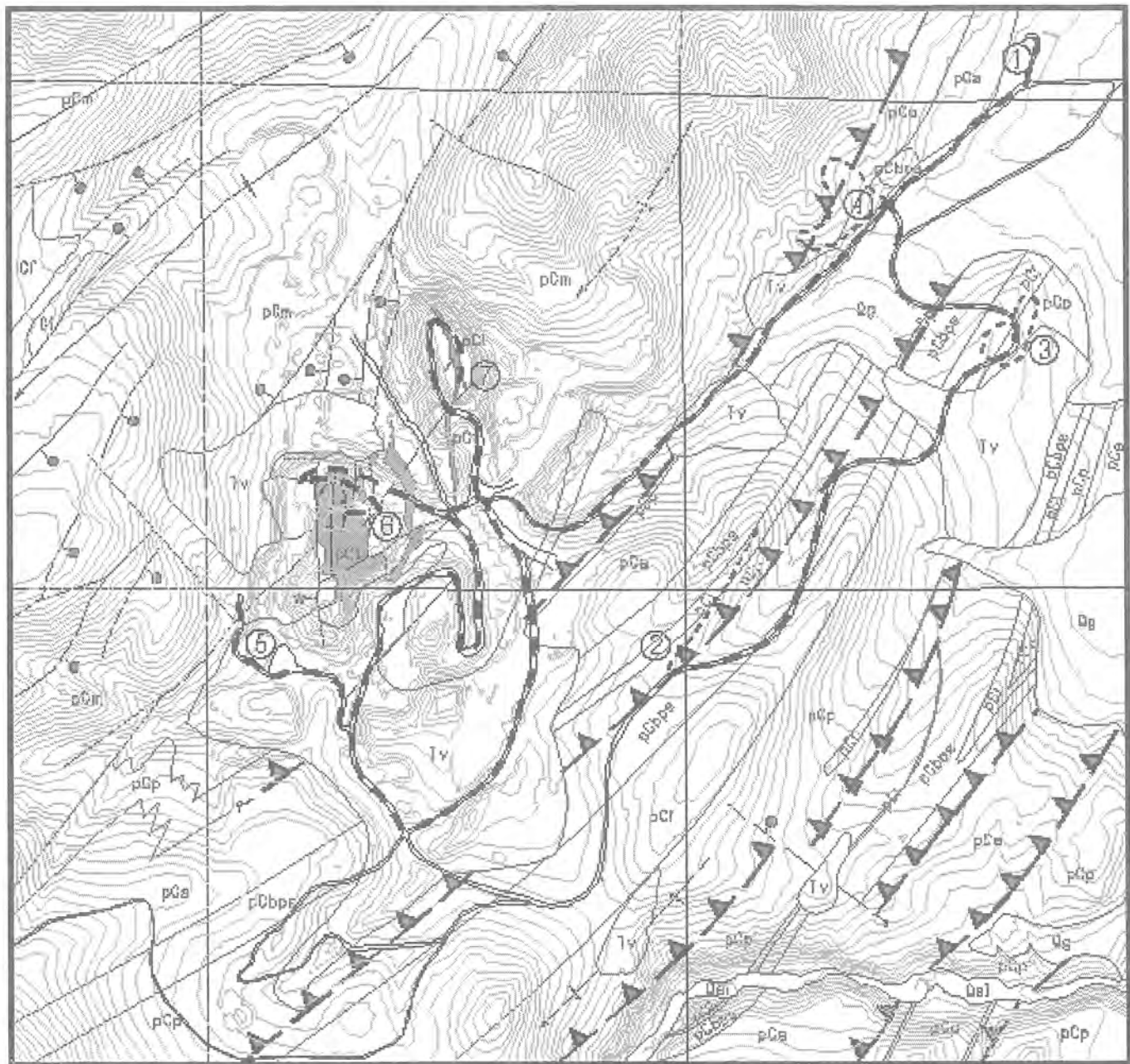


Figure 2 b

The amphibolite unit forms a continuous tabular layer parallel to the other northeast trending lithologic contacts in the area. The blocky outcrops described by Vargo appear as elongate masses defined by joint intersections plunging to the northwest. Cross sectional profiles of the elongate masses are ellipsoidal to lenticular. Heavy chloritization along joint surfaces give definition to the "log like" outcrops. Milholland – (1976), mentions the presence of relict pillow lavas within occurrences of amphibolite and phyllite on the north side of Johnny Gulch.

Further up slope, phyllite lies in fault contact with the overlying massive "central" dolomitic marble unit. The marble unit has been thrust over rocks lying to the southeast along a reverse fault. A "slice" of amphibolite lying at the marble – phyllite contact was most likely detached from the underlying mass of amphibolite and shoved intact into its current position.

Dolomitic marble core samples from near the phyllite-reverse fault contact show distinct cataclastic textures not found in marble around the talc mine area. Marbles close to the phyllite contact have prominent flaser texture with rounded to lensoid porphyroclasts of carbonate (dolomite/magnesite) and strongly foliated talc.

Up the hill there is a curious piece of float from the dolomitic marble unit that has been recrystallized into coarse-grained white and maroon rhombs of carbonate rock. The white and maroon coloration is separated into distinctive bands throughout the rock.

Hike back down the slope to the west into a draw with good exposures of marble and phyllite. The marble is full of quartz segregations that have been rolled into rod and mullion structures. Differential weathering of the quartz rods and dolomite along with the chocolate brown weathering surface of the marble give these outcrops the characteristic appearance of much of this marble. Down the draw close to the road are exposures of phyllite in large black slate-like sheets.

2.7

**30.7** Drive past the gate into the mine operations area to the observation point at **stop #5**. At this location the "South 40 Pit" can be viewed. This open pit mine was first started in 1986. Conventional surface mining methods are used: drilling and blasting 25 ft benches, loading with hydraulic shovels, and hauling with 65 ton Caterpillar trucks.

The talc orebody has been defined with over 1000 core and reverse circulation drill holes. Drilling data was used to generate a three-dimensional orebody model. Open pit designs are generated using the orebody configuration, slope stability data, and market demand for talc.

Talc mineralization is controlled by the original carbonate stratigraphy and a system of structural conduits that provided access for hydrothermal fluids that replaced dolomite. The three dimensional form of the orebody is that of a northward plunging antiform with satellite bodies of tabular talc that parallel both limbs. Talc mineralization is discordant to local foliation and the major structure of the marble host.

The 1.5 by 3 mile marble unit, which hosts the talc deposits is structurally thickened by isoclinal folds that plunge to the southwest as indicated by mullion and rodding structures (see stop #4). The marble unit is also cut by a series of normal faults which bound grabens and horsts at an average orientation of N35E. A secondary set of fractures seen primarily on aerial photos trends to the northwest.

Rhyolitic volcanics of the Huckleberry Ridge Tuff cap the South 40 talc deposit (Pritchett, 1993) and have to be stripped away prior to talc mining. The primary conduit for hydrothermal fluids is a north striking growth fault which over time has dragged volcanics from the surface deep into the interior of the fault. The "growth fault" controlled a V-shaped paleo-drainage surface that collected a thick accumulation of volcanic mudflows, and layers of unconsolidated ash, welded tuffs, and rhyodacite.

2.0

**32.7 Stop # 6** is in the bottom of the South 40 pit. It is mandatory that everyone wears a hardhat and safety glasses and takes the safety precautions discussed at the beginning of the trip.

Talc ore mined in the South 40 pit has a microcrystalline texture as opposed to lamellar varieties which have a visually macrocrystalline platy habit. This is important with respect to the chemical behavior of the talc in its end use. South 40 talc is also mineralogically pure talc without impurities like chlorite, quartz, and serpentine. Talc produced at the Yellowstone Mine contains no asbestos. Yellowstone talc contains approximately 1% ferrous iron that substitutes for magnesium in octahedral positions in the talc crystal lattice. This gives the talc its green coloration. Also present are small amounts of limonite and goethite, which are weathering products of pyrite. Also fluorine substitutes for OH in the talc to a minor extent. A minute amount of graphite, detectable only by TEM or microprobe, appears as gray colored bands present in both the talc and dolomite.

The South 40 orebody is heavily sheared allowing it to be mined without blasting. The presence of water perched in the talc mobilizes iron oxides with secondary deposition along fracture surfaces. Limonite and goethite create a wide range of variability in the whiteness of the pulverized talc powder sold into the market place. Great care is taken to selectively mine and sort the different talc grades by color to produce mill feeds that are specifically directed towards markets where color is extremely important and to those markets in which color is not as important (Berg, 1979).

### 1.3

**34.0** Drive out of the South 40 pit and on to the North Main pit (**Stop # 7**). Yellowstone talc mining operations originated in the area of the North Main pit with underground operations during WWII. Yellowstone talc was first mined to make electrical insulators for radios and radar sets. Its ease of milling into a desired shape and

low thermal expansion during firing made it a strategic mineral during the war.

The North Main deposit is a tabular vein of talc that averages 40 ft in width, strikes to the north, and dips 65 degrees east. This deposit differs from the South 40 deposit in several important ways. First, the talc is generally less sheared than the South 40 and must be blasted to mine. Also North Main talc is free of much of the iron oxide staining found in the South 40 deposit and can supply markets that demand products of higher brightness. However heavier concentrations of graphite are present as bands and swirls of gray coloration showing the classic "marbling" indicative of plastic deformation of the host carbonate.

Some of the graphite impurities visible in the North Main talc take on curious patterns of repeating dark and light banding in curved forms. This is reminiscent of the patterns in the marble float seen on the traverse at stop #4. A note of interest is the occurrence of stromatolites in a very similar dolomite hosted microcrystalline talc deposit at Three Springs Australia (Perriam, 1993).

Evidence for a later stage of talc formation exists in the North Main deposit. Pods and veinlets of clean apple green talc with botryoidal forms exist throughout the deposit as structures that cut across existing green to gray talc. This paragenetic relationship would indicate that not all of the talc in the Yellowstone deposits formed contemporaneously.

This concludes the field tour of the Yellowstone Mine and vicinity.

### ACKNOWLEDGEMENTS

I want to say thank you to Luzenac America, Inc. for permission to compile this field trip guide and for hosting the field trip. Also, thanks to Dick Berg for his valuable review of this field guide.

## REFERENCES

- Berg, R.B., 1979, Talc and Chlorite Deposits in Montana: Montana Bureau of Mines and Geology, Memoir No. 45, 66 p.
- Heinrich, E.W., & Rabbitt, J.C., 1960, Pre-Beltian Geology of the Cherry Creek and Ruby Mountains Areas, Southwestern, Montana: Montana Bureau of Mines and Geology, Memoir No. 38, 40 p.
- Millholland, M.,A., 1976, Mineralogy and petrology of Precambrian metamorphic rocks of the Gravelly Range, southwestern Montana: Bloomington, Indiana University, M.A. thesis, 134 p.
- Perriam, R.K.A., 1991, Draught Report: Petrological studies of the Three Springs talc deposit: unpublished report, 36 p.
- Pritchett, K., 1993, Huckleberry Ridge Tuff of the Madison Valley, southwest Montana: Northwest Geology, v. 22, p. 57-75
- Vargo, A.G., 1990, Structure and petrography of the Pre-Beltian rocks of the north-central Gravelly Range, Montana: Fort Collins, Colorado State University, M.S. thesis, 157 p.



# Laramide Contraction and Basin-and-Range Extension—Classic Examples from the Northwestern Madison Range and Madison Valley, Montana

**Karl S. Kellogg**, U.S. Geological Survey, Denver, CO 80225

**David R. Lageson**, Department of Earth Sciences, Montana State University, Bozeman, MT 59717-2470

**Chester A. Ruleman**, Department of Earth Sciences, Montana State University, Bozeman, MT 59717-2470

---

## INTRODUCTION

The Madison Valley is a prime example of an extensional structure in the Basin and Range province of western North America. The valley lies within the intermountain seismic belt (e.g., Smith and Sbar, 1974) and numerous historic earthquakes have been reported in the region (Qamar and Stickney, 1983). The valley is a north-striking, down-to-the-east half graben and the active normal faults of the Madison Range fault system of Pardee (1950), along the east side of the valley, are displayed as a series of prominent scarps. The large (magnitude 7.2) 1959 Hebgen Lake earthquake occurred along the Madison Range fault system about 40 km south of the fieldtrip area (U.S. Geological Survey, 1964), where fresh scarps and a huge landslide produced by the earthquake can be seen.

The northwestern Madison Range adjacent to the Madison Valley displays some of the most spectacular and well-exposed examples of Late Cretaceous and early Tertiary (Laramide) thrusting and reverse faulting anywhere in the Laramide structural province of North America. Two distinct types of basement-involved structures can be seen, both the result of generally east-directed contraction (Fig. 1). The first of these, the Spanish Peaks fault (Peale, 1896; Garihan and others, 1983), is a northwest-striking, southwest-directed, high-angle reverse fault with a minimum throw of 4,100 m. This structure is perhaps the largest single structure in southwestern Montana; it is prominently reflected in the topography and is easily visible on satellite imagery. The other major basement-involved structure is the Hilgard thrust system

(Tysdal, 1986), a complex array of generally north-striking, east-directed thrusts along the west side of the Madison Range. Net thrust displacement across the Hilgard thrust system decreases to zero northward along the Hilgard thrust system toward the impingement zone between the Hilgard and the Spanish Peaks systems. The Spanish Peaks fault is undeflected within this zone, indicating that significant movement had occurred along the Spanish Peaks fault prior to movement along the Hilgard thrust system (Kellogg and others, 1995). A dacite porphyry sill complex, dated by the  $^{40}\text{Ar}/^{39}\text{Ar}$  method at about 68-69 Ma, intrudes the thrusts of the Hilgard thrust system, indicating a minimum age for the initiation of Laramide deformation in the area (Tysdal and others, 1986).

The location of the Hilgard thrust system along the west side of the Madison Range adjacent to the Madison Valley mimics other thrust systems in southwestern Montana. For example, the Snowcrest thrust system lies along the northwest side of the Snowcrest Range adjacent to the Ruby River Valley and the Ruby thrust is along the northwest side of the Ruby Range adjacent to the Beaverhead Valley (Fig. 1). This geometry does not appear to be fortuitous; it is likely that the position of Tertiary normal faults was inherited from the older Laramide thrusts (Schmidt and others, 1984, 1993; Kellogg and others, 1995). A model for this inheritance is outlined in Fig. 2 and is explained briefly as follows (refer to Kellogg and others [1995] for a more complete discussion). During Laramide thrusting, the Hilgard thrust system occupied the leading edge of a large basement arch, the Gravelly arch (Scholten, 1967). As the leading

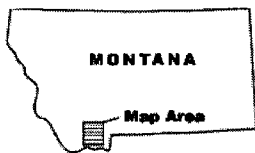
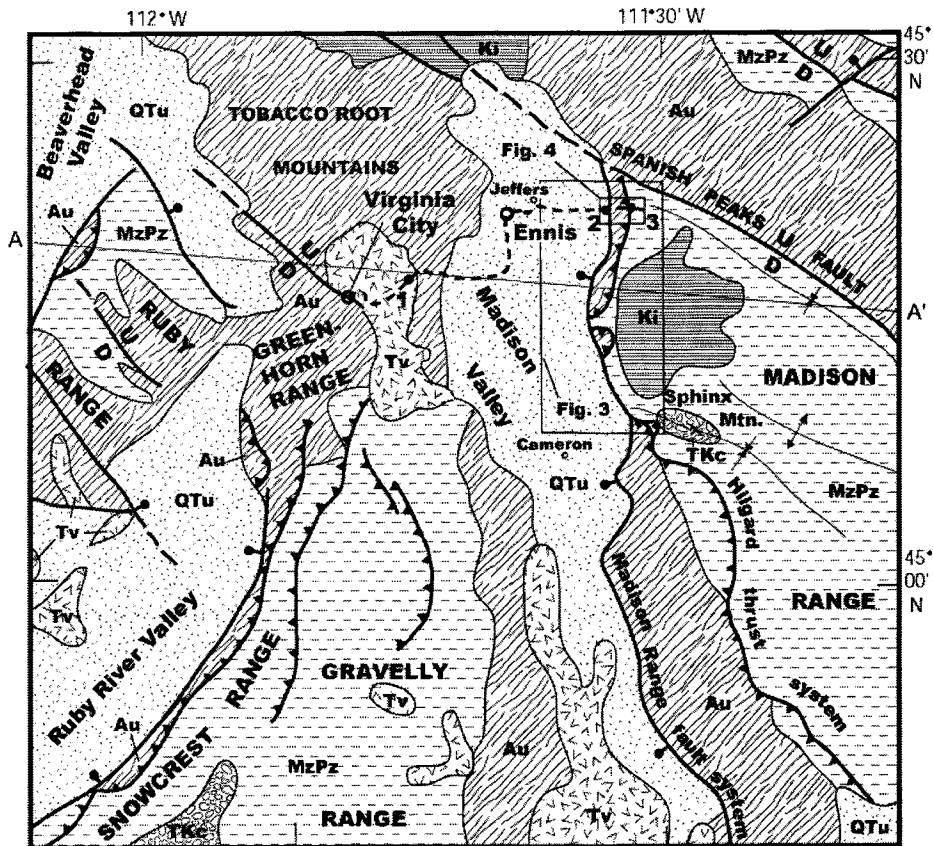
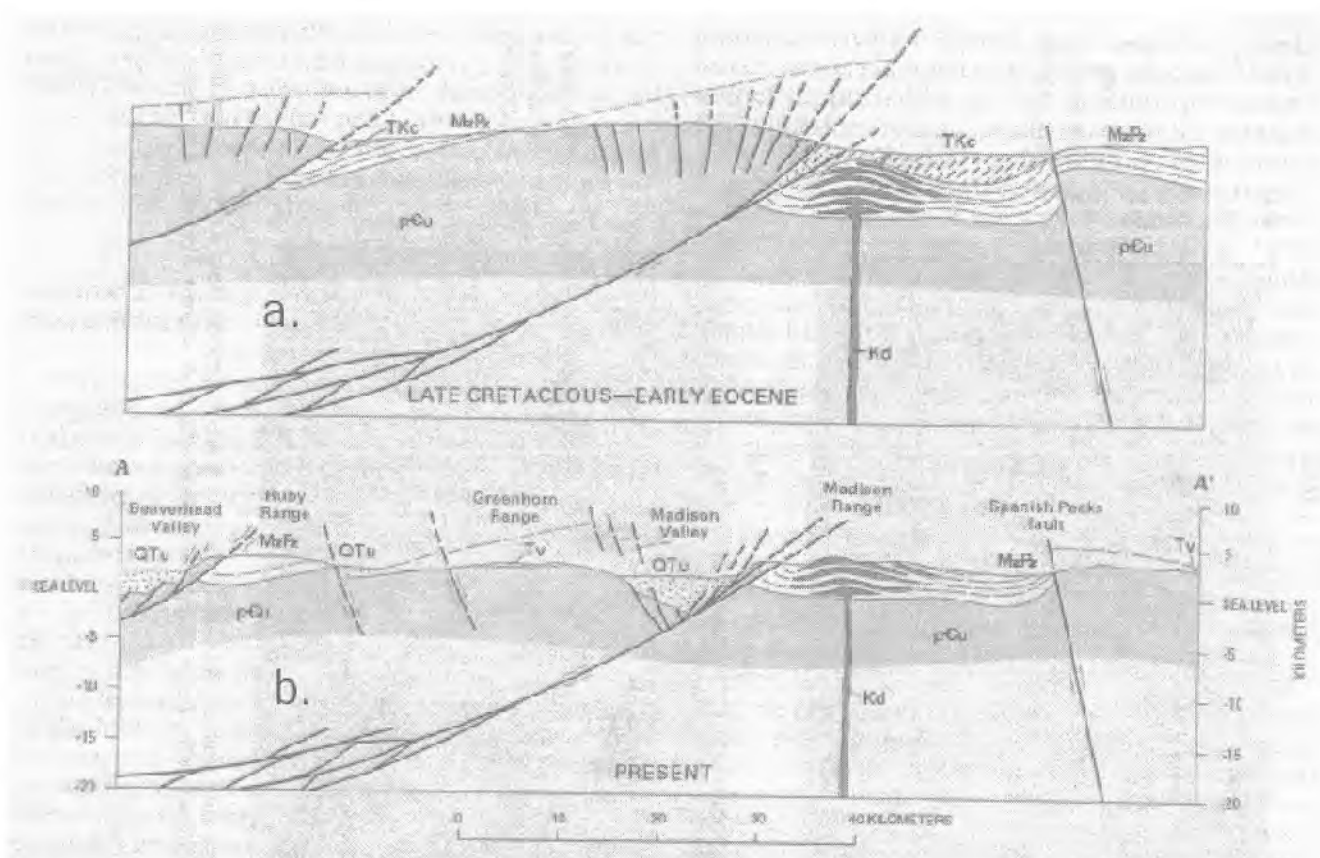


Figure 1: Simplified tectonic map of parts of the Greenhorn Range (northern Gravelly Range), southern Tobacco Root Mountains, the Madison Valley, and the northwestern Madison Range, showing the route of the fieldtrip. Cross-section line A-A' is shown approximately in Fig. 2a. Adapted from Kellogg and others (1995).

**EXPLANATION**

- Quaternary and Tertiary basin deposits
  - Tertiary volcanic rocks
  - Upper Cretaceous intrusive rocks
  - Lower Tertiary and Upper Cretaceous synorogenic sedimentary rocks
  - Mesozoic and Paleozoic rocks
  - Archean (mostly) rocks
  - Normal fault—Dashed where inferred
  - Thrust fault—Teeth on upper plate
  - Reverse fault—Dashed where concealed
  - Syncline
  - Anticline
  - Fieldtrip route
  - 1, 2, 3 Fieldtrip stops
- 0 10 20 30 KM

edge of the basement uplift was thrust over the Mesozoic section, the eastward-tapering thrust tip of the uplift underwent rotational sagging above the basin sediments, thereby producing extension and normal faulting in the arched basement block of the thrust tip. During subsequent generally east-west Tertiary crustal extension, the north-striking normal faults were exploited to form the prominent north-trending valleys; i.e., the crests of the former basement arches collapsed, producing a “structural inversion” (Schmidt and Dresser, 1984) or reversal of topography. The thrusts are preserved along the west side of the range and form the eastern side of a “perched basement wedge” (Lageson and Zim, 1985); valley-bounding normal faults form the western side of the wedge.



**Figure 2:** Schematic east-west cross sections across a portion of southwest Montana showing major tectonic elements for (a) the close of Laramide deformation, and (b) the present. The symbols are the same as those on Fig. 1. Line of cross section A-A' (Fig. 2b) shown on Fig. 1. From Kellogg and others (1995).

This field trip will examine the Madison Valley graben and the normal faults that define the eastern side of the valley. We will then drive up Jack Creek, through the “perched basement wedge,” to observe some spectacular thrusts of the Hilgard thrust system and the tight, overturned footwall syncline that underlies the system. In Jack Creek we can also see (from a distance) the intersection of the Hilgard thrust system and Spanish Peaks fault.

### Field trip route

We start in the old gold-mining town of Virginia City, the former Territorial Capitol of Montana. All the features we will see today are on the recently published Ennis 1:100,000 quadrangle (Kellogg and Williams, 2000). Virginia City lies mostly on Archean gneiss at the edge of the Oligocene and Eocene Virginia City volcanic field, composed mostly of andesite and basalt flows, although rocks as felsic as rhyolite are also present. Three localities in the volcanic field give the following potassium-argon dates: (1) 49.3±2.5 and 51.1±1.9 Ma (biotite) and

51.0±3.8 Ma (plagioclase); this flow is just north of Virginia City and overlies Archean basement; (2) 34.4±3.0 Ma (whole rock); and (3) 32.7±1.4 Ma (whole rock) (Marvin and others, 1974).

A major placer discovery was made on Alder Creek, just west of Virginia City, in 1863 and over 2.5 million oz of gold were recovered from dredging operations between 1863 and the start of World War II (Edward T. Ruppel, personal commun., 2002). Subsequent to the discovery of the rich placer deposits, lode quartz gold deposits were discovered in the northern Gravelly Range and southern Tobacco Root Mountains, although the production from these bedrock deposits paled in comparison to the placer deposits.

We proceed east on Highway 287 towards the Madison Valley. Our first stop is 6.5 miles from Virginia City at a prominent turnout on the right with a magnificent view over the valley.

### Stop 1.

There are a number of features we can see from here.

**The Madison Valley.** The valley is a relatively simple half graben, downfaulted on the east along the Madison Range normal fault zone (MRNFZ). The valley formed along the axial zone of the Laramide Madison-Gravelly arch; the east side of the arch is now represented by the Hilgard thrust system, exposed on the west side of the Madison Range. Regional extension began during the late Eocene following a protracted period of erosion and peneplanation (Kuenzi and Fields, 1971; Hanneman and Wideman, 1991), but the present narrow extensional basins of southwestern Montana, such as the Madison Valley, began forming in the middle Miocene during more rapid extension. These basins were filled with both clastic (commonly conglomeratic) and lacustrine sediments (Fields and others, 1985). Seismic evidence (Canadian Hunter, Ltd., written commun., 1994) indicates that the basin-fill deposits dip progressively steeper with depth against the MRNFZ, a growth fault relationship. The maximum depth of the valley is 4,500 m (14,500 ft) near the small town of Cameron (Rasmussen and Fields, 1983), and this rather remarkable depth has prompted some past petroleum industry exploration in hopes of discovering another Railroad Valley (Nevada)-type oil field (D.A. Lopez, personal communication, 1994). To date, two dry wells have been drilled in the basin, a disappointment to industry, although the seismic profiles made during exploration have been extremely useful in interpreting basin structure (Kellogg and others, 1995). We'll examine one profile across the valley.

Note the huge alluvial fan emanating from Cedar Creek, which formed during Bull Lake glaciation (about 140-100 ka) (Schneider and Ritter, 1987). This fan underscores that as the east side of the valley subsided the predominant sedimentation came from the Madison Range, as compared to the Gravellys and Tobacco Roots. This eastern-source influx pushed the Madison River to the west side of the Valley. Curiously, these features contrast with those at Jack Creek, which is about 5 km north. The discharge from

Jack Creek is similar to that in Cedar Creek and the MRNFZ traverses the mouths of both creeks. Yet, no fan emanates from Jack Creek. Rather, the mouth of Jack Creek is about 300 m lower than the mouth of Cedar Creek and the valley of Jack Creek is incised into the basin fill and contains as many as 11 terrace levels (Bearzi, 1987). We'll discuss some possible reasons for these vastly contrasting geomorphic styles.

**Sphinx Mountain and the Hilgard thrust system (HTS).** The prominent peak to the southeast is Sphinx Mountain, with its satellite peak, The Helmet. Both these peaks are underlain by the late Cretaceous Sphinx Conglomerate, which was shed from the Scarface thrust, the trace of which is only about 1 km west of The Helmet (someone conveniently left a block of the conglomerate here in the parking area). Hanging-wall rocks of the Scarface thrust, one of the major thrusts of the Hilgard thrust system, are highly fractured Archean gneiss (Schmidt and others, 1993). A traverse up Sphinx Mountain reveals a classic unroofing sequence through the Sphinx Conglomerate. Predominantly Cretaceous clasts comprise the base of the sequence and the maximum clast age increases as one traverses up the mountain; a few Precambrian clasts are found at the summit (DeCelles and others, 1987).

The prominent, steeply-dipping to overturned rocks that form the jagged ridges along the west side of the Madison Range are predominantly those of Mississippian Madison Group limestones. The younging direction is to the east and these rocks form parts of footwall synclines beneath one or more thrusts of the Hilgard thrust system. In the background is Fan Mountain, underlain by Late Cretaceous rocks intruded by a Late Cretaceous dacite sill complex (Kellogg, 1992). The obvious white stripe across the face of Fan Mountain is a 20-m-thick tuffaceous sand and siltstone marker bed in the Telegraph Creek Formation.

A combined paleomagnetic and geochronologic study of the dacite sills suggest that Laramide deformation was about 75 percent completed at the end of the Cretaceous (Kellogg and Harlan,

1991); the difference in paleomagnetic direction between sills intruding overturned fold limbs and upright limbs is about 25 percent of the interlimb angle. Several of these sills, dated at about 68-69 Ma (Tysdal and others, 1986; S.S. Harlan, unpublished data, 1992), intrude overturned limbs of folds.

From here, we proceed down the hill towards Ennis, the largest town in the Madison Valley. Drive east down Ennis' main street, cross the Madison River, and almost immediately turn left toward the community of Jeffers. Take the first gravel road that ascends the terrace (Cameron bench) east of Jeffers and, with one jog, proceed due east toward the mouth of Jack Creek. Stop 2 is on the Cameron bench, just southwest of the mouth of Jack Creek.

### Stop 2.

**Scarps of the Madison Range normal fault zone.** Five sections of Quaternary normal faulting having differing structural control and morphological expression have been identified along the western base of the Madison Range (Schneider, 1990; Ruleman, 2002). (The term "section" rather than "segment" is used here because the latter term has acquired a specific meaning in neotectonic studies not necessarily implied here). Jack Creek, our destination on this field trip, lies at the north end of the Cameron section (section 4) and the south end of the Spanish Peaks section (section 5). Along the Cameron and Spanish Peaks sections, from Cedar Creek north to Watkins Creek (Fig. 3), the Hilgard thrust system is exposed along the range front in the footwall of the Madison normal fault. The Hilgard thrust system and the Madison normal fault bound a perched basement wedge, with Archean metamorphic rocks in thrust contact with Phanerozoic strata on the east side of the basement wedge and in normal fault contact with basin-fill sediments on the west side of the wedge. As a result, the range front consists of a typical Archean assemblage of quartzo-feldspathic gneiss and amphibolite. Between Cedar and Jack Creek, a complex system of normal faults results from normal-slip reactivation of multiple thrust splays that collectively correspond to frontal and lateral

ramps of the Hilgard thrust system. The range front is relatively linear and trends subparallel to the Hilgard thrust system. At approximately Jourdain Creek (Fig. 3), the trend of the range front changes northward from approximately due north to N25W. This change coincides with the zone of interaction of the west- to southwest-dipping Hilgard thrust system and the northeast-dipping Spanish Peaks fault.

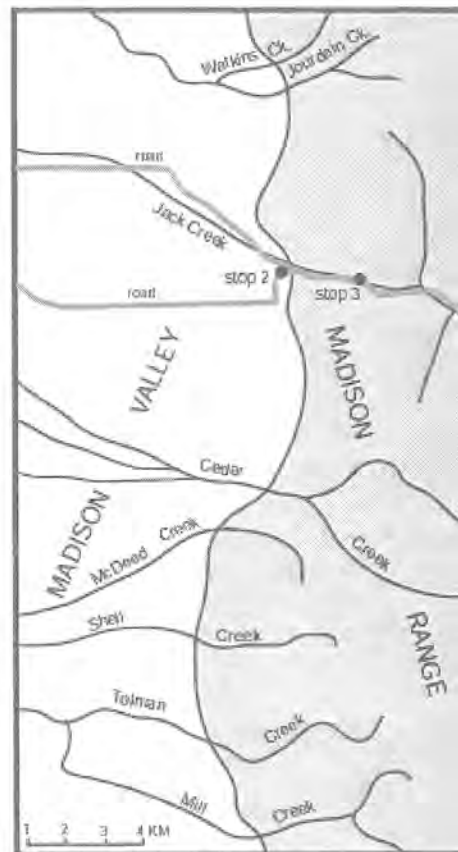


**Figure 3:** Sketch geographic map showing features referred to in the text. Stops 2 and 3 are also shown. Refer to Kellogg and Williams (2000) and Schneider (1990) for description and portrayal of faults.

Just south of Jack Creek the Madison normal fault is expressed as a fault-line scarp at the bedrock-colluvium contact. Fault scarps appear to have been fluvially trimmed and steepened by Holocene erosion along this section. Late Pleistocene fans were deposited on the downthrown, west side of a larger mid-Pleistocene fault scarp and Late Pleistocene

deposits are inset approximately 1.0 m into older colluvium and alluvium.

From Jourdain Creek south to Mill Creek (Fig. 3), fault scarps on Late Pleistocene fan alluvium and undivided colluvium/alluvium have surface offsets ranging from 1.3 m to 8.8m, generally increasing southward (Ruleman, 2002). A small single-event fault scarp (surface offset = 1.3 m) exists between Jack and Jourdain Creeks. At McDeed Creek, a Late Pleistocene fan is offset 2.4 m. To the south, older range-front colluvium/alluvium is offset 4.9 m. From McDeed Creek south to Tolman Creek, the Madison fault scarp is right at the

bedrock/colluvium interface and is expressed as *nastri di faglia*, or bedrock fault scarps with freshly exposed surfaces. South of Shell Creek, a Late Pleistocene fan deposit is offset 8.8 m. Thus, surface offset increases in a southward direction along the northern reach of the Madison normal fault (Ruleman, 2002).

From Stop 2, we proceed east up Jack Creek, passing through highly fractured and locally brecciated Archean gneiss in the perched basement wedge between the MRNFZ and the structurally highest thrust (Jack Creek thrust) of the Hilgard thrust system (Fig. 4).

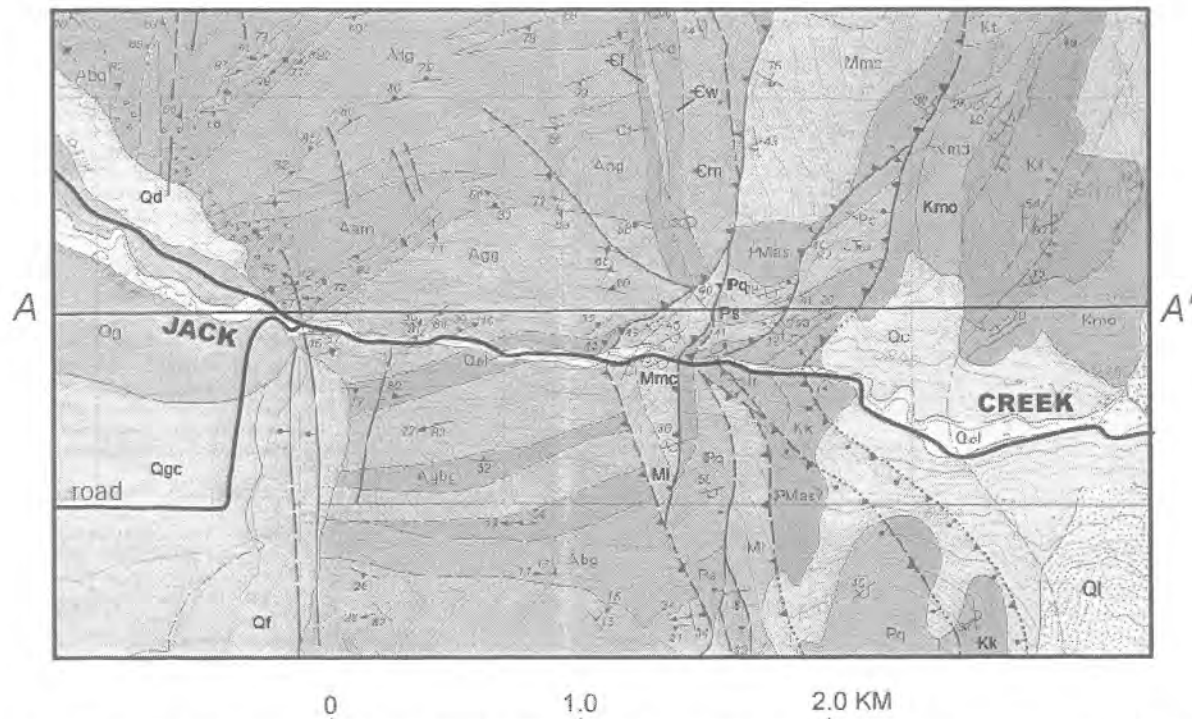


**Figure 4:** Geologic map of the area around Jack Creek, from part of the Fan Mountain 7 1/2' quadrangle (Kellogg, 1992). The symbols of Phanerozoic rocks and deposits are: ef – Flathead Sandstone; ew - Woolsey Shale; em - Meagher Limestone; MI – Lodgepole Limestone; Mmc – Mission Canyon Limestone; hMas – Amsden and Snowcrest Range Groups; hq – Quadrant Sandstone; Ps – Shedhorn Sandstone; Jdu – Morrison formation, Ellis Group, and Dinwoody formation; Kk – Kootenai formation; Kt – Thermopolis Shale; Kmd – Muddy Sandstone; Kmo – Mowry Shale; Kf – Frontier Formation; Qal – alluvium; Ql – landslide deposits; Qf – fan deposits; Qgc – terrace gravels of the Cameron bench; Qg – terrace gravel deposits. Various Archean rocks are prefaced by the letter A. Fig. 5 shows a simplified cross-section along A-A'.

A long-standing paradox of Laramide tectonics has been how the basement can apparently rotate so dramatically if the commonly overturned cover rocks above the basement are in depositional contact, as appears to be the case on

the ridges above us where overturned Middle Cambrian Flathead Quartzite lies depositionally on basement. *En masse* block rotations by an amount comparable to the attitude of the basement-cover contact lead to a major “space

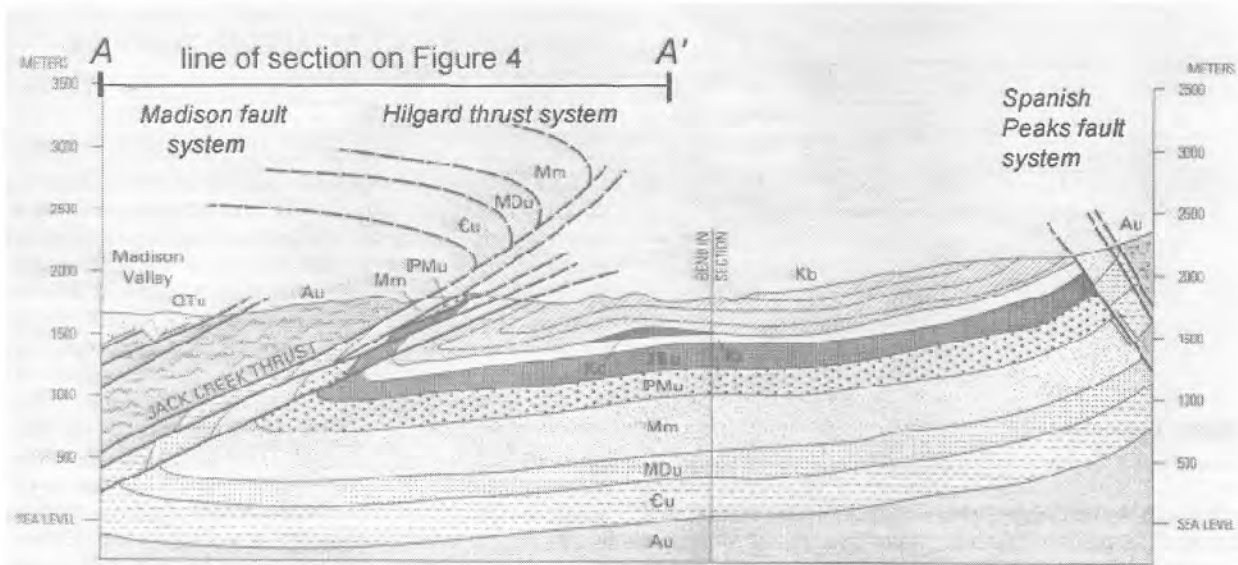


**Figure 5:** Cross section A-A' (Fig. 4) along Jack Creek showing the thrust relationships and the geometry of the thrust-imbricated footwall syncline. The units are simplified from those in Fig. 4, and are: Au – Archean rocks; eu – Cambrian, undifferentiated; Mm – Madison Group; hMu – Shedhorn and Quadrant sandstones, and Amsden and Snowcrest Range groups; Jdu – Morrison formation, Ellis Group, and Dinwoody Formation; Kb – Frontier Formation, Mowry Shale, Muddy Sandstone, and Thermopolis Shale; Kd – dacite porphyry. From Kellogg and others (1995); refer to Fig. 2 of Kellogg and others (1995) for the trace of the complete line of section.



**Figure 6:** View of Jack Creek from the air showing the regional relationships. Symbols are: e undiff. – Cambrian rocks, undifferentiated; MDu – Three Forks and Jefferson Formations; Mm – Madison Group: Mission Canyon and Lodgepole Limestones; hMu – Shedhorn and Quadrant Sandstones, and Amsden and Snowcrest Range Groups; hq – Quadrant Sandstone; Ps – Shedhorn Sandstone; Jdu – Morrison Formation, Ellis Group, and Dinwoody Formation; Kk – Kootenai Formation; Kt – Thermopolis Shale; Kmd – Muddy Sandstone; Kmo – Mowry Shale; and Kf – Frontier Formation.

problem.” A model by which rotation is accomplished by domino-style rotation of tabular slabs of basement, bounded by Reidel shears or extension fractures between two or more major thrusts, accounts for both rotation of the basement and observed north-striking breccia zones within the thrustured basement block (Kellogg and others, 1995).

Our first stop will be at the Jack Creek thrust. From here we will walk about a mile east through the Hilgard thrust system.

### Stop 3.

**A walk through the footwall of the Hilgard thrust system.** We will stop at the first major thrust (thrust 1, the Jack Creek thrust), which juxtaposes basement above overturned Lower Mississippian Lodgepole Limestone. From here, we will walk up the road, passing across 4 additional thrusts (thrusts 2-5; Figs. 4 and 5). All the sedimentary rocks for the next kilometer are in the overturned limb of a thrust-imbricated footwall syncline, the Mill Creek syncline. Unfortunately, not all thrusts are exposed along the road, but the relationships are clearly visible on the hillside to the north. Thrust 2 places Upper and Lower Mississippian Mission Canyon Limestone above Pennsylvanian and Mississippian Amsden Group rocks; thrust 3 juxtaposes Amsden Group rocks above Upper and Middle Jurassic Rierdon Limestone; thrust 4 places Rierdon over Lower Cretaceous Kootenai Formation; and thrust 5 places Kootenai over Lower Cretaceous Muddy Sandstone. An annotated photo taken from the air (Fig. 6) helps to show the relationships in Jack Creek.

When we get to the good exposure of the Muddy Sandstone, examine it carefully and determine if you can tell the stratigraphic “up” direction. This outcrop, like all those we walked through, was interpreted as overturned (Kellogg, 1992) in the overturned limb of the tight Mill Creek syncline. The trace of the hinge of the Mill Creek syncline lies in the Upper Cretaceous Frontier Formation across the creek (it’s covered along the road). Extensive slip along bedding planes was clearly necessary to accommodate this type of tight folding, and slickensided

surfaces are common on some beds, particularly at shale-sandstone interfaces.

A spectacular zone of small thrust faults that accommodate tight folding is exposed at Shell Creek, a few km south of here (a rugged 2-hour hike is necessary to view these structures). At that locality, the Shell Creek thrust is interpreted as an out-of-syncline thrust related to synclinal crowding in the hinge zone of the tight Mill Creek syncline (Kellogg and others, 1995).

If time permits, we might walk on Diamond-J ranch land to examine the good exposure across the creek. However, reasonably good views of the well-exposed structural relationships can be achieved from the road.

We’ll return to Virginia City via the valley of lower Jack Creek. Notice the many terraces along the valley and ponder the dramatic geomorphic difference between Jack Creek and Cedar Creek.

### **REFERENCES**

- Bearzi, J.P., 1987, Soil development, morphometry, and scarp morphology of fluvial terraces at Jack Creek, southwestern Montana: Bozeman, Montana State University, M.S. thesis, 131 p.
- DeCelles, P.G., Tolson, R.B., Graham, S.A., Smith, G.A., Ingersoll, R.V., White, J., Schmidt, C.J., Rice, R., Moxon, I., Lemke, L., Handschy, J.W., Follo, M.F., Edwards, D.P., Cavazza, W., Caldwell, M., and Bargar, E., 1987, Laramide thrust-generated alluvial-fan sedimentation, Sphinx Conglomerate, southwestern Montana, American Association of Petroleum Geologists, v. 71, p. 135-155.
- Fields, R.W., Rasmussen, D.L., Tabrum, A.R., and Nichols, Ralph, 1985, Cenozoic rocks of the intermontane basins of western Montana and eastern Idaho--a summary, in Flores, R.M., and Kaplan, S.S., eds., Cenozoic paleogeography of west-central United States: Society of Economic Paleontologists and Mineralogists, Rocky Mountain Section, p. 9-36.
- Garihan, J.M., Schmidt, C.J., Young, S.W., and Williams, M.A., 1983, Geology and recurrent movement history of the Bismark-Spanish Peaks-Gardiner fault systems, southwest Montana, in Lowell, J.D., and Gries, Robbie, eds., Rocky Mountain Foreland Basins and



- uplifts: Rocky Mountain Association of Geologists, p. 295-314.
- Hanneman, D.L., and Wideman, D.J., 1991, Sequence stratigraphy of Cenozoic continental rocks, southwestern Montana: Geological Society of America Bulletin, v. 103, p. 1335-1345.
- Kellogg, K.S., 1992, Geologic map of the Fan Mountain quadrangle, Madison County, Montana: U.S. Geological Survey Quadrangle Map GQ-1706, scale 1:24,000.
- Kellogg, K.S., and Harlan, S.S., 1991, Style and timing of deformation in the northwestern Madison Range, southwestern Montana: Geological Society of America Abstracts with Programs, v. 23, no. 4, p. 38.
- Kellogg, K.S., Schmidt, C.J., and Young, S.W., 1995, Basement and cover-rock deformation during Laramide contraction in the northern Madison Range (Montana) and its influence on Cenozoic basin formation: American Association of Petroleum Geologists Bulletin, v. 79, no. 8, p. 1117-1137.
- Kellogg, K.S., and Williams, V.S., 2000, Geologic map of the Ennis 30' x 60' quadrangle, Madison and Gallatin Counties, Montana, and Park County, Wyoming: U.S. Geological Survey Geologic Investigations Series I-2690, scale 1:100,000.
- Kuenzi, W.D., and Fields, R.W., 1971, Tertiary stratigraphy, structure, and geologic history, Jefferson Basin, Montana: Geological Society of America Bulletin, v. 82, p. 3373-3394.
- Lageson, D.R., and Zim, J.C., 1985, Uplifted basement wedges in the northern Rocky Mountain foreland: Geological Society of America Abstracts with Programs, v. 7, no. 4, p. 250-251.
- Marvin, R.F., Wier, K.L., Mehnert, H.H., and Merritt, V.M., 1974, K-Ar ages of selected Tertiary igneous rocks in southwestern Montana: Isochron/West, no. 10, p. 17-20.
- Pardee, J.T., 1950, Late Cenozoic block faulting in western Montana: Geological Society of America Bulletin, v. 61, p. 359-406.
- Peale, A.C., 1896, Description of the Three Forks Sheet, Montana: U.S. Geological Survey Geologic Atlas Folio 24, 5 p.
- Qamar, A.I., and Stickney, M.C., 1983, Montana earthquakes, 1869-1979--historical seismicity and earthquake hazard: Montana Bureau of Mines and Geology Memoir 51, 79 p.
- Rasmussen, D.L., and Fields, R.W., 1983, Structural and depositional history, Jefferson and Madison basins, southwestern Montana: American Association of Petroleum Geologists Bulletin, v. 67, p. 1352.
- Ruleman, C.A., III, 2002, Quaternary tectonic activity within the northern arm of the Yellowstone tectonic parabola and associated seismic hazards, southwest Montana [M.S. Thesis]: Bozeman, Montana, Montana State University, 157 p.
- Schmidt, C.J., and Dresser, H., 1984, Late Cenozoic structural inversion in a region of small extensional strain, SW Montana: Geological Society of America Abstracts with Programs, v. 16, no. 6, p. 646-647.
- Schmidt, C.J., Evans, J.P., Harlan, S.S., Weberg, E.D., Brown, J.S., Batatian, D., Deer, D.N., Malizzi, L., McDowell, R.J., Nelson, G.C., Parke, M., and Genovese, P.W., 1993, Mechanical behavior of basement rocks during movement of the Scarface thrust, central Madison Range, Montana, *in* Schmidt, C.J., Chase, R., and Erslev, E.A., eds., Laramide basement deformation in the Rocky Mountain foreland of the western United States: Boulder, Colorado, Geological Society of America Special Paper 280, p. 89-105.
- Schmidt, C.J., Sheedlo, Mark, and Werkema, Michael, 1984, Control of range-bounding normal faults by earlier structures, southwestern Montana: Geological Society of America Abstracts with Programs, v. 16, no. 4, p. 253.
- Schneider, N.P., 1990, Four-dimensional segmentation of the Madison Range and Valley, southwest Montana, *in* Hall, R.D., ed., Quaternary geology of the western Madison Range, Madison Valley, Tobacco Root Range, and Jefferson Valley: Rocky Mountain Friends of the Pleistocene field trip guidebook, Indiana University, p. 58-88.
- Schnieder, N.P., and Ritter, D.F., 1987, Late Pleistocene response of the Madison River to regional base level change for the Madison Valley, southwest Montana: Geological Society of America Abstracts with Programs, v. 19, no. 5, p. 332.
- Scholten, Robert, 1967, Structural framework and oil potential of extreme southwestern Montana, *in* Henderson, L.B., ed., Montana Geological Society 18th Annual Field Conference Guidebook: Billings, Montana, Montana Geological Society, p. 7-19.
- Smith, R.B., and Sbar, M.L., 1974, Contemporary tectonics and seismicity of the western United States, with emphasis on the intermountain seismic belt: Geological Society of America Bulletin, v. 85, p. 1205-1218.

- Tysdal, R.G., 1986, Thrust faults and back thrusts in Madison Range of southwest Montana foreland: American Association of Petroleum Geologists Bulletin, v. 70, p. 360-376.
- Tysdal, R.G., Marvin, R.F., and DeWitt, E.H., 1986, Late Cretaceous stratigraphy, deformation, and intrusion in the Madison Range of southwestern Montana: Geological Society of America Bulletin, v. 97, p. 859-868.
- U.S. Geological Survey, 1964, The Hebgen Lake, Montana, earthquake of August 17, 1959: U.S. Geological Survey Professional Paper 435, p. 37-50.

# Digital Maps of Igneous and Tectonic Features, USGS Headwaters Project Area, Northern Rocky Mountains of Idaho, Western Montana, and Eastern Washington

Arthur A. Bookstrom, David Cleveland, Reed S. Lewis, and Michael L. Zientek

---

Preliminary digital maps of significant igneous and tectonic features of the regional Headwaters Project area will be available for inspection at a poster session, during which we hope to elicit comments and suggestions from conference participants. These maps and their accompanying databases derive from a digital geologic map of the Headwaters Project area in preparation for the U.S. Forest Service. The maps are based on available geologic maps at 1:100,000 to 1:250,000 scales, which are being made into digital databases by the U.S. Geological Survey, the Idaho Geological Survey, the Montana Bureau of Mines and Geology, and the Washington Department of Natural Resources.

Significant igneous features are classified by age, lithologic composition (according to the IUGS classification), and by place-based formal or informal geologic names. The database also includes mineralogical and textural information on color index, alumina saturation, alkalinity, redox conditions, and levels of emplacement. Some plutonic suites include multiple lithologies that are spatially, temporally and compositionally related but span multiple compositional fields. Formal or informal geologic names from the literature are associated with igneous features such as volcanic fields, cauldron complexes and calderas, dike swarms, sill swarms, batholiths, stocks, and other plutons.

Significant tectonic features include litho-tectonic terranes, rifts, depositional basins, accreted terranes, suture zones, tectonic lineaments with long and varied tectonic histories, strike-slip fault zones and associated trans-pressure and trans-tensional zones, fold and thrust belts, metamorphic core complexes, detachment faults, horsts, grabens, and tilted

blocks. We have identified and named these features by comparing features shown on the source maps with features identified and described in the literature, or by experts involved in ongoing research. We intend to classify tectonic features by age, and will attempt to discriminate between different types of deformation at different times along features that have undergone multiple episodes of deformation.

Digital maps of geology, lithology, igneous and tectonic features, litho-tectonic terranes, significant mineral deposits, mines and prospects of various types will be combined with maps of deep crustal structural features inferred from gravity and magnetic data to provide background information for estimation of undiscovered mineral deposits of selected types. Economic trends for mineral commodities present in the region will guide selection of deposit types for which estimates of undiscovered resources will be made. These estimates, along with records of past and present mineral-related activities will be used to identify areas where mineral-related activities can be expected in National Forests of the region during the next 15 years. In addition to supporting studies of mineral-resources, these digital maps and databases will provide the Forest Service with a wealth of geologic information, which they will be able to access, query, and apply a variety of scientific problems and land-management issues and problems of regional to local scale.

# Digital Geologic Map Data Model v. 4.3 Implementation, USGS Headwaters Project Area, Northern Rocky Mountains of Idaho, Western Montana, and Eastern Washington

J. Douglas Causey, Michael L. Zientek, Arthur A. Bookstrom, Thomas P. Frost, David E. Boleneus, Bradley S. Van Gosen, Anna B. Wilson, and Karl V. Evans

---

Preliminary coding of geologic information in a Microsoft Access database for 46 geologic maps in Idaho, Montana, and Washington provides a mechanism to examine variations in geology over large regions while maintaining details that commonly are lost in regional compilations. The Headwaters Project has obtained or produced digital geologic maps at scales of 1:100,000 and 1:250,000 for parts of Idaho, Montana, and Washington. U.S. Geological Survey geologists in Spokane and Denver coded information about the geologic map units into the database.

The database was created based on version 4.3 of a draft digital geologic map data model (<http://geology.usgs.gov/dm>) being designed by the USGS, Geologic Survey of Canada, and State Geological Surveys. Modifications made in the database design were necessary in order to capture information deemed important to mineral resource assessment as well as some factors of interest to colleagues at the U.S. Forest Service. These modifications involved creation of a unique list of lithology terms and addition of special tables.

Geologic descriptions from published maps or associated documents were converted to digital format and incorporated into the database. This information as well as descriptions in other publications was used by geologists to code fields in the database. Some coding was based on interpretation of geologic data. Guidelines were developed to minimize personal differences in interpretation.

Methods were developed to handle several problems encountered in the process of creating and coding the database. Detailed coding of map units was prohibitive given time and money

available. The major (dominant or most common) lithology and a unit (encompassing the entire range) lithology term were coded. For these purposes, it was necessary to interpret the geologic description or talk to experts as to what lithology was most important. If there was no information to the contrary, the first mentioned rock names were accepted as representative of the dominant lithology.

A major hurdle in coding the database was the variety of lithologic terms and their inconsistent application in the geologic literature. We desired a hierarchical classification that emphasized rock composition. In our attempt to develop a system that would be consistent across the major rock divisions, we developed a list of 604 lithologic terms arranged in a hierarchical system that represents our best solution.

Plutonic rocks are of particular interest because of their association with many important mineral deposits. A table was constructed to capture information about depth of emplacement, intrusion type and form, and alumina saturation. This information is not explicitly stated on most map descriptions; the geologists attributing the database had to interpret available data to code these fields.

The development of data entry forms was of great assistance to people involved in coding information. Forms were designed such that appropriate terms could be selected from drop-down lists. While the lists can easily be modified, they do restrict the user and minimize spelling errors. The result is that data is more consistent and derivative maps are easier to create. Examples of types of maps that can be produced and analyses that are possible will be demonstrated

# GEOLOGIC MAPS FOR MONTANA

## Montana Bureau of Mines and Geology's Geologic Mapping Program

Karen W. Porter, Edmond G. Deal, and Patrick J. Kennelly

---

Montana Bureau of Mines and Geology's (MBMG) geologic mapping program is directed at completion of a 1:100,000-scale bedrock geologic base, in digital form, for the State. This scale is the minimum scale useful to geologic problem solving, and is the optimum scale for a state-wide data base. In 1996, MBMG initiated map completions in GIS, and began bringing older maps into digital form. As of July, 2002, geologic maps are completed for 66 of Montana's 94 1:100,000-scale quadrangles. Digital coverage is available for 92% of the state: 70% at the 1:100,000 scale from MBMG, and an additional 22% at the 1:250,000 scale from the U.S. Geological Survey (USGS) or from MBMG.

Simultaneously, larger-scale (1:48,000; 1:50,000), more detailed maps are being produced for the State's primary population centers, including both urban areas and the intermontane valleys of western Montana. State and local agencies' daily work is focused on establishing and balancing land- and resource-use patterns for these areas that are experiencing rapid growth of both permanent and seasonal populations. To date, maps are complete for the Metropolitan Billings area, Bitterroot Valley, and part of the Gallatin Valley. FY 2002 work will complete the Gallatin Valley and initiate the Upper Yellowstone (Paradise Valley) areas.

A new Geologic Map of Montana is also progressing. Each new 1:100,000-scale quadrangle becomes a part of the developing data base that will become the new State map. Parallel efforts include continuous edge-matching to produce a seamless coverage, and continuous development of a standard list of stratigraphic names and letter symbols. The plan

and time frame for completion of the new Geologic Map of Montana are closely dependent upon adequate funding for both the field and GIS aspects of the work. Specific stages are: (a) completion of seamless data east of 112° west longitude; (b) completion of seamless data west of 112° west longitude; (c) completion of correlation charts and other text elements; and (d) formal publication of the map. We anticipate that the digital data will be made available ahead of the formal publication.

Since passage of the National Geologic Mapping Act in 1992, the STATEMAP element of the U.S.GS's National Cooperative Geologic Mapping Program has been the primary source of outside funding for MBMG's new maps. MBMG has matched these dollars on a 1:1 basis. Other funding sources have included other USGS contracts, the Montana Department of Transportation, and the U. S. Forest Service. Although MBMG's mapping program is directed internally, all work funded by the STATEMAP program is under advisement by a STATEMAP Advisory Committee representing State and Federal agencies, industry, and academia.

At MBMG's web site, <http://www.mbmgt.mtech.edu>, one may view the periodically updated status of the mapping program, the availability of digital data, and linkage to the Publications Office for ordering maps.

# The October 28, 1998 Waterloo, Montana Earthquake

**Michael Stickney**, Montana Bureau of Mines and Geology, Montana Tech of the University of Montana, 1300 West Park Street, Butte, MT 59701  
[mstickney@mtech.edu](mailto:mstickney@mtech.edu)

---

On the evening of October 27, 1998 at 8:11 p.m., a magnitude 4.1 earthquake shook the northern Jefferson Valley and surrounding areas. The Earthquake Studies Office of the Montana Bureau of Mines and Geology received approximately 100 reports from residents that felt the earthquake. From those reports with sufficient information, Modified Mercalli Intensities were assigned and plotted on a map. Maximum intensities of IV were observed at four locations within 12 km of the epicenter, including the towns of Waterloo and Silver Star. Only three reports consistent with intensity III shaking were received, including one from the town of Whitehall. The area of intensity II shaking was much larger, extending east to Manhattan, north to Helena, and northwest to Gold Creek. Eight reports of intensity I shaking came from Missoula and the Bitterroot Valley. Curiously, no reports of shaking came from areas south of the epicenter, including the towns of Twin Bridges, Sheridan, Virginia City and Dillon.

The Waterloo earthquake occurred in the Montana seismograph network within 28 km of the two closest seismograph stations. A total of 50 P arrival times and one S arrival time were used to determine a hypocenter location. The computed horizontal uncertainty of only 600 m indicates that the epicenter position is well determined. The computed hypocenter depth of  $5.4 \pm 1.9$  km is not as well constrained because the closest seismograph station lies nearly five times as far away as the computed hypocenter depth. An analysis of the stability and uniqueness of the hypocenter depth indicates that was between 4 and 6 km.

An anemic aftershock sequence followed the Waterloo earthquake that included 20 locatable earthquakes during the first month. A magnitude 2.3 aftershock that occurred 64 minutes after the main shock was reported felt by some residents

within 12 km of the epicenter. The largest aftershock occurred 18 days later with a magnitude of 2.5. No other aftershocks exceeded magnitude 2.0 and only five aftershocks exceeded magnitude 1.5. No foreshocks were observed.

A main shock-fault plane solution constructed from 36 P wave first motions is virtually identical to a moment tensor solution derived from regional broadband waveforms by Oregon State University. The focal mechanism reveals normal faulting with the nodal plane striking N25W and dipping 61W interpreted as the fault plane.

The epicenter of the Waterloo earthquake falls on the Tobacco Root range-front fault near a prominent bend where the fault changes strike from northeast to north. However, the Waterloo earthquake did not result from slip on the Tobacco Root fault. The hypocentral depth of 5.4 km places the seismic source within the footwall block of the Tobacco Root fault. Also the N25W trend of the slipped fault inferred from the focal mechanism does not match the northeast to north strike of the adjacent Tobacco Root fault.

A seven-month hiatus in seismicity followed the Waterloo aftershock sequence. In late 1999, low-magnitude seismicity resumed in the area. Approximately 40 earthquakes with magnitudes less than 2.0 occurred through September 2001. In early October 2001, vigorous seismicity resumed with approximately 230 earthquakes through May 2002. The most recent seismicity is clustered about 2 km northeast of the 1998 Waterloo epicenter and is typical of an earthquake swarm in contrast to the Waterloo main shock/aftershock sequence. Seven earthquakes have magnitudes within one unit of the largest event (a magnitude 3.6 on February

2, 2002) and the largest event occurred 4 months after the sequence began. Fault plane solutions of the seven largest 2001-2002 events all show normal faulting, but on faults ranging in strike from NW to ENE. Such variability in focal mechanisms is another characteristic of earthquake swarms in the region.

Recent earthquakes in the Waterloo area form part of a larger pattern of seismicity in the Tobacco Root region. Earthquakes are common and are widely distributed in the northeastern half of the Tobacco Root mountain range, but virtually absent in the southeastern part of the range. Although not sharply defined by the seismicity pattern over the past 20 years, the boundary between the active and inactive parts of the mountain range seems to generally coincide with the NW-trending Bismark fault. This fault is not known to have any Quaternary expression but may serve as a boundary between an actively deforming northeastern block and a quiescent southwestern block.



**Northwest Geology**  
**Montana State University**  
**Volume 31**  
**Summer 2002**

**PAPERS**

<b>Author</b>	<b>Page</b>	<b>Title</b>
Murphy, Julia G., Foster, D.A., Kalakay, T.J., John, B.E., and Hamilton, M.	1	U-Pb Zircon Geochronology of the Eastern Pioneer Igneous Complex, SW Montana: Magmatism in the Foreland of the Cordilleran Fold and Thrust Belt
Hammarstrom, Jane M., Van Gosen, B.S., Kunk, M.J., and Herring, J.R.	12	Gold-Bearing Quartz Veins in the Virginia City Mining District, Madison County, Montana
Gammons, Christopher H. and Matt, D.O.	44	Using Fluid Inclusions to Help Unravel the Origin of Hydrothermal Talc Deposits in Southwest Montana
Carrara, Paul E.	54	Response of Douglas Firs Along the Fault Scarp of the 1959 Hebgen Lake Earthquake, Southwestern Montana

**ROAD LOGS**

Cerino, Mike	66	Geology of the Yellowstone Talc Mine
Kellogg, Karl S., Lageson, D.R., and Ruleman, C.A.	74	Laramide Contraction and Basin-and-Range Extension – Classic Examples from the Northwestern Madison Range and Madison Valley, Montana

**ABSTRACTS**

Bookstrom,, Aurthur A., Cleveland, D., Lewis, R.S., and Zientek, M.L.	84	Digital Maps of Igneous and Tectonic Features, USGS Headwaters Project Area, Northern Rocky Mountains of Idaho, Western Montana, and Eastern Washington
Causey, J. Douglas, Zientek, M.L., Bookstrom, A.A., Frost, T.P., Boleneus, D.E., Van Gosen, B.S., Wilson, A.B., and Evans, K.V.	85	Digital Geologic Map Data Model v 4.3 Implementation, USGS Headwaters Project Area, Northern Rocky Mountains of Idaho, Western Montana, and Eastern Washington
Porter, Karen W., Deal, E.G., and Kennelly P.J.	86	GEOLOGIC MAPS FOR MONTANA: Montana Bureau of Mines and Geology's Geologic mapping Program
Stickney, Michael	87	The October 28, 1998, Waterloo, Montana Earthquake